

Cooling history and relief evolution  
of Corsica (France) as constrained by  
fission track and (U-Th)/He thermochronology

Dissertation

zur Erlangung des Grades eines Doktors der Naturwissenschaften

der Geowissenschaftlichen Fakultät  
der Eberhard-Karls-Universität Tübingen

vorgelegt von  
Martin Danišík  
aus Malacky (Slowakei)

2005

Tag der mündlichen Prüfung: 15. Juli 2005

Dekan: Prof. Klaus G. Nickel, Ph.D.

1. Berichterstatter: PD Dr. Joachim Kuhlemann

2. Berichterstatter: Prof. Wolfgang Frisch

Tübinger Geowissenschaftliche Arbeiten	A	72	130 S.	52 Abb. 5 Tab.	Tübingen, Juli 2005
--	---	----	--------	-------------------	---------------------------

## **Band 72**

# **COOLING HISTORY AND RELIEF EVOLUTION OF CORSICA (FRANCE) AS CONSTRAINED BY FISSION TRACK AND (U-TH)/HE THERMOCHRONOLOGY**

**Martin Danišík**

Tübingen

2005

**Key words:** Corsica, thermochronology, relief, paleorelief, Alpine wedge, Variscan basement, fission track dating, (U-Th)/He dating, helium, paleosurface, exhumation, burial, uplift, peneplain, thermal modeling, Western Mediterranean, passive margin, apatite, Ligurian-Provençal Basin, rifting, geomorphology, extension, denudation.

Copyright © Martin Danišik 2005. All rights reserved. Alle Rechte vorbehalten.

Copyright © Universität Tübingen 2005 (TGA Series A, ISSN 0953-4921).

Citations of this volume should take the form:

Danišik, M. (2005): Cooling history and relief evolution of Corsica (France) as constrained by fission track and (U-Th)/He thermochronology. *Tübinger Geowiss. Arb., Reihe A*, **72**, 1-130.

Please note that according to German transcription rules, 'Tübingen' transcribes to 'Tuebingen' in case of lack of the character 'ü'.

***Library of Congress Cataloging-in-Publication Data***

**Cooling history and relief evolution of Corsica (France) as constrained by fission track and (U-Th)/He thermochronology.** / Danišik, Martin

p. cm. — (Publication / Geological and Palaeontological Institute, University of Tuebingen, Germany; no. 72)

Includes bibliographical references.

ISSN 0953-4921

1. Geology, Geophysics

I. Title. II. Series.

551.8—dc21

This work is subject to copyright. All rights are reserved, whether the whole or part of the material is concerned, specifically the right of translation, reprinting, re-use of illustrations, recitation, broadcasting, reproduction on microfilms or in other ways, and storage in data banks including publication via the internet or other computer network.

The storage of the abstract of the volume in its entirety together with the name(s) of the author(s) and the title of the volume is allowed for citation purposes provided that the copyright notice appears.

[www.uni-tuebingen.de](http://www.uni-tuebingen.de)

Printed in Germany

Bisher erschienen in dieser Reihe:

- Nr. 1 RING, U. (1989): Tectogenesis of the Penninic/Austroalpine boundary zone: the Arosa Zone (Grisons-Rätikon area, Swiss-Austrian Alps).
- Nr. 2 BETZLER, C. (1989): The Upper Paleocene to Middle Eocene between the Rio Segre and the Rio Llobregat (eastern South Pyrenees): facies, stratigraphy and structural evolution.
- Nr. 3 HEINZ, W. (1989): Vulkanoklastische Komponenten und deren geodynamische Bedeutung für die Entwicklung der Southern Uplands von Schottland.
- Nr. 4 SICK, M. (1989): Paleomagnetism of ophiolite complexes from the southern Middle American Landbridge (Costa Rica and western Panama).
- Nr. 5 BRÜCKMANN, W. (1989): Typische Kompaktionsabläufe mariner Sedimente und ihre Modifikation in einem rezenten Akkretionskeil (Barbados Ridge).
- Nr. 6 VAVRA, G. (1989): Die Entwicklung des penninischen Grundgebirges im östlichen und zentralen Tauernfenster der Ostalpen — Geochemie, Zirkonmorphologie, U/Pb-Radiometrie.
- Nr. 7 SCHWENTKE, W. (1990): Upper Cretaceous tectono-sedimentary and facies evolution of the Basque Pyrenees (Spain).
- Nr. 8 RICHTER, C. (1990): The anisotropy of magnetic susceptibility — Numeric models, deformation experiments, and practical application in structural geology.
- Nr. 9 HEINZLER-JONCZYK, G. (1992): PTt-Paths in the southeast Tauern Window (Eastern Alps).
- Nr. 10 HAIß, N. (1992): Untersuchungen zur Genese von Plagioklasgneisen im Basiskristallin der Ostalpen (Gleinalm- Ötztal- und Silvrettakristallin).
- Nr. 11 KRAUS, S. (1992): Stratigraphy and facies of the "Garumnian" — Late Cretaceous to Early Paleogene — in the Treppe region, central southern Pyrenees.
- Nr. 12 SFEIKOS, A. (1992): Geology, analysis of deformation and kinematics of the Pelagonian nappe system, Kamvounia mountains (North Thessaly, Greece).
- Nr. 13 LIU, G. (1992): Permian to Eocene sediments and Indian passive margin evolution in the Tibet Himalayas.
- Nr. 14 BECKER, B. (1993): The Structural Evolution of the Radstadt Thrust System, Eastern Alps, Austria — Kinematics, Thrust Geometries, Strain Analysis.
- \* Nr. 15 DÜRR, S.B. (1993): The Mid- to Early-Late Cretaceous Xigaze forearc basin (south Tibet); Sedimentary evolution and provenance of clastic sediments. [13 EUR]
- \* Nr. 16 MICHEL, G. (1993): Neokinematics along the North Anatolian Fault. [15 EUR]
- \* Nr. 17 HERRMANN, U.R. (1993): The origin of a „Terrane“: U/Pb zircon systematics, geochemistry and tectonics of the Xolapa complex (southern Mexico). [12 EUR]
- Nr. 18 GRÄFE, K.-U. (1994): Sequence Stratigraphy in the Cretaceous and Paleogene (Aptian to Eocene) of the Basco-Cantabrian Basin (N. Spain).
- Nr. 19 PROKOPH, A. (1994): Zyklische Sedimentation im Oberalb des Norddeutschen Beckens.

- \* Nr. 20 REICHERTER, K. (1994): The Mesozoic tectono-sedimentary evolution of the Central Betic seaway (external Betic Cordillera, Southern Spain). [15 EUR]
- \* Nr. 21 RATSCHBACHER, L., SPERNER, B., MESCHEDE, M. & FRISCH, W. (1994): Computer techniques and applications: A program library for stress and strain analysis. [10 EUR]
- \* Nr. 22 MESCHEDE, M. (1994): Tectonic evolution of the northwestern margin of the Caribbean Plate in the light of the "terrane concept": Structural and geochemical studies in southern Mexico and Costa Rica. [13 EUR]
- \* Nr. 23 KÖLBL-EBERT, M. (1995): Paläozoische Ganggesteine (Rhyodazite/Dazite und Lamprophyre) des Südschwarzwaldes. [14 EUR]
- Nr. 24 JIN, J. (1995): Dynamic stratigraphic analysis and modeling in the south-eastern German molasse basin.
- Nr. 25 PATZELT, A. (1996): Palaeo- and rockmagnetism of Cretaceous to Tertiary sediments from the Tethyan Himalaya: evidence for crustal shortening and deformation of the northern Indian margin due to the collision with Eurasia.
- \* Nr. 26 LÄUFER, A.L. (1996): Variscan and Alpine tectonometamorphic evolution of the Carnic Alps (Southern Alps) — Structural analysis, illite crystallinity, K-Ar and Ar-Ar geochronology. [13 EUR]
- \* Nr. 27 SPERNER, B. (1996): Computer programs for the kinematic analysis of brittle deformation structures and the Tertiary tectonic evolution of the Western Carpathians (Slovakia). [13 EUR]
- Nr. 28 MAYER, H. (1996): Magnetostratigraphic and Cyclostratigraphic Investigations of the Early Cretaceous Biancone Formation at Cison and Pra da Stua (Southern Alps, Italy) with Palaeoclimatical, Geochronological and Geomathematical Implications.
- \* Nr. 29 PFÄNDER, Jörg (1996): TWIST — Ein Computerprogramm zur Strainberechnung aus Calcit-Zwillingsdaten und seine Anwendung in der Deformationsanalyse des alpinen Vorlandes. [10 EUR]
- \* Nr. 30 WINKLER, M. (1996): Genese und geodynamische Stellung der Zentralgneise im Tauernfenster. [13 EUR]
- Nr. 31 SCHUSTER, F. (1996): Paleoecology of Paleocene and Eocene Corals from the Kharga and Farafra Oases (Western Desert, Egypt) and the Depositional History of the Abu Tartur Carbonate Platform, Kharga Oasis.
- Nr. 32 GÜLDENPFENNIG, M. (1997): Geologische Neuaufnahme der Zone von Badenweiler-Lenzkirch (Südschwarzwald) unter besonderer Berücksichtigung unterkarbonischer Vulkanite und Grauwacken.
- \* Nr. 33 ZWEIGEL, P. (1997): The Tertiary tectonic evolution of the Eastern Carpathians (Romania): Orogenic arc formation in response to microplate movements. [13 EUR]
- \* Nr. 34 NOUFAL, A.W. (1997): Geology and tectonic evolution of the Gulf of Suez, West-Central Sinai, Egypt. [15 EUR]
- \* Nr. 35 GÎRBACEA, R.A. (1997): The Pliocene to Recent Tectonic Evolution of the Eastern Carpathians (Romania) [13 EUR]
- Nr. 36 SCHAUER, M. (1998): Dynamische Stratigraphie, Diagenese, und Rohstoffpotential des Oberjura (Kimmeridge 1-5) der mittleren Schwäbischen Alb.

- Nr. 37 LEHMANN, J. (1998): Systematic palaeontology of the ammonites of the Cenomanian-Lower Turonian (Upper Cretaceous) of northern Westphalia, North Germany.
- Nr. 38 RÖSLER, W. (1998): Magnetostratigraphy of Neogene fluvial sediments: results from a high resolution study and several new sections in the Nepalese Siwaliks.
- \* Nr. 39 GRÄFE, K. (1998): Exhumation and thermal evolution of the Cordillera de Talamanca (Costa Rica): constraints from fission track analysis,  $^{40}\text{Ar}$ - $^{39}\text{Ar}$ , and  $^{87}\text{Rb}$ - $^{87}\text{Sr}$  chronology. [13 EUR]
- \* Nr. 40 BRÜGEL, A. (1998): Provenances of alluvial conglomerates from the Eastalpine foreland: Oligo-/Miocene denudation history and drainage evolution of the Eastern Alps. [15 EUR]
- Nr. 41 HU, S. (1998): A magnetic study on lacustrine sediments from Zoigê Basin, Eastern Tibetan Plateau, China.
- \* Nr. 42 ELIAS, J. (1998): The thermal history of the Ötztal-Stubai-complex (Tirol; Austria/Italy) in the light of the lateral extrusion model. [15 EUR]
- Nr. 43 ASPRION, U. (1998): Ground-penetrating Radar (GPR) analysis in aquifer-sedimentology: Case studies, with an emphasis on glacial systems of SW Germany.
- \* Nr. 44 FETSCHER, M. (1998): Strukturelle und petrologische Entwicklung des Terraba-Forearcs im zentralen Bereich des flach subduzierten Cocos-Rückens, Süd-Costa Rica.  
MORITZ, E. (1998): Interpretation von LWD-Daten mit Hilfe von künstlichen neuronalen Netzen und genetischen Algorithmen (unter Anwendung auf Daten des ODP Leg 170, Costa Rica Convergent Margin). [15 EUR]
- \* Nr. 45 WALDHÖR, M. (1999): The Small-circle reconstruction in paleomagnetism and its application to paleomagnetic data from the Pamirs. [13 EUR]
- \* Nr. 46 ABD EL-NABY, H.H. (1999): Geology, petrochemistry and tectogenesis of the Wadi Um Ghalaga area, eastern desert, Egypt. [14 EUR]
- Nr. 47 RÖHL, H.-J. (1999): Hochauflösende palökologische und sedimentologische Untersuchungen im Posidonien-schiefer (Lias  $\epsilon$ ) von SW-Deutschland.
- Nr. 48 SCHMID-RÖHL, A. (1999): Hochauflösende geochemische Untersuchungen im Posidonienschiefer (Lias  $\epsilon$ ) von SW-Deutschland.
- \* Nr. 49 CHINCHILLA CHAVES, A.L. (1999): Geologie und Struktur des Ophiolith-Komplexes der Nicoya-Halbinsel (Costa Rica). [13 EUR]
- \* Nr. 50 HUSSIEN MOHAMMED, B. (1999): The geology, structure and geochemistry of the crystalline rocks of the Moyale area, Southern Ethiopia: Implications for the tectogenesis of the Precambrian basement. [13 EUR]
- Nr. 51 PÖPPELREITER, M. (1999): Controls on epeiric successions exemplified with the mixed siliciclastic-carbonate Lower Keuper (Ladinian, German Basin).
- \* Nr. 52 SZÉKELY, B., FRISCH, W., KUHLEMANN, J., & DUNKL, I. (1999): 4th Workshop on Alpine Geological Studies. 21-24 September 1999, Tübingen (Germany). [20 EUR]

- \* Nr. 53 LÓPEZ, A. (1999): Neo- and paleostress partitioning in the SW corner of the Caribbean plate and its fault reactivation potential. [20 EUR]
- Nr. 54 LÖFFLER, S.-B. (1999): Systematische Neubearbeitung und paläoökologische Aspekte der unteroligozänen Molluskenfauna aus den Zementmergeln von Bad Häring (Unterinntal, Tirol).
- \* Nr. 55 REINECKER, J. (2000): Stress and deformation: Miocene to present-day tectonics in the Eastern Alps. [13 EUR]
- Nr. 56 HORNING, J. (1999): Dynamische Stratigraphie, Reservoir- und Aquifer-Sedimentologie einer alluvialen Ebene: Der Stubensandstein in Baden-Württemberg (Obere Trias, mittlerer Keuper).
- \* Nr. 57 SCHNEIDERMEIER, T. (2000): Paläolithische Fundschichten in quartären Lockersedimenten (Südwestdeutschland): Prospektionsmethoden, Stratigraphie und Paläoökologie. [15 EUR]
- \* Nr. 58 HUBICH, D. (2000): Geodynamische Entwicklung der Karnischen Alpen. [13 EUR]
- \* Nr. 59 TRAUTWEIN, B. (2000): Detritus provenance and thermal history of the Rhenodanubian flysch zone: mosaic stones for the reconstruction of the Eastern Alps. [13 EUR]
- \* Nr. 60 SZÉKELY, B. (2001): On the surface of the Eastern Alps — a DEM study. [13 EUR]
- \* Nr. 61 PAWELLEK, T. (2001): Fazies-, Sequenz- und Gamma-Ray-Analyse im höheren Malm der Schwäbischen Alb (SW-Deutschland) mit Bemerkungen zur Rohstoffgeologie (hochreine Kalke). [30 EUR]
- \* Nr. 62 CAMPOS BEJARANO, L. (2001): Geology and basins history of Middle Costa Rica: an intraoceanic island arc in the convergence between the Caribbean and the Central Pacific plates. [13 EUR]
- \* Nr. 63 MOSER, F. (2001): Tertiäre Deformation in den Rumänischen Südkarpaten: Strukturelle Analyse eines Blattverschiebungskorridors am Westrand der Moesischen Plattform. [13 EUR]
- \* Nr. 64 DAKRORY, A.M. (2002): Biostratigraphy, paleoenvironment and tectonic evolution of the Late Cretaceous-Early Paleogene succession on the North African plate (Sinai, Egypt) and a comparison with some European and Asian sections. [20 EUR]
- \* Nr. 65 DÜNKEL, I. (2002): The genesis of East Elba iron ore deposits and their interrelation with Messinian tectonics. [15 EUR]
- Nr. 66 MOST, T. (2003): Geodynamic evolution of the Eastern Pelagonian Zone in north-western Greece and the Republic of Macedonia. Implications from U/Pb, Rb/Sr, K/Ar, <sup>40</sup>Ar/<sup>39</sup>Ar geochronology and fission track thermochronology. TOBIAS LIB online
- Nr. 67 MOST, P. (2003): Late Alpine cooling histories of tectonic blocks along the central part of the TRANSALP- traverse (Inntal-Gardertal): Constraints from geochronology. *Tübinger Geowiss. Arb., Reihe A* **67**, 1-97.
- \* Nr. 68 HELBING, H. (2003): No suture in the Sardinian Variscides: A structural, petrological, and geochronological analysis. [15 EUR]
- Nr. 69 JUNGHANS, W.-D. (2003): Fazies, Zyklizität, Petrophysik und Paläomagnetik im Buntsandstein der Bohrung Kraichgau 1002 (SW-Deutschland).

- \* Nr. 70 SCHULLER, F. (2004): Evolution and geodynamic significance of the Upper Cretaceous Gosau basin in the Apuseni Mountains (Romania). [15 EUR]
- \* Nr. 71 SCHWAB, M. (2004): The amalgamation of the Pamirs and their subsequent evolution in the far field of the India-Asia collision. [15 EUR]
- \* Nr. 72 DANIŠÍK, M. (2005): Cooling history and relief evolution of Corsica (France) as constrained by fission track and (U-Th)/He thermochronology. [15 EUR]

Herausgeber: Institut für Geowissenschaften, Universität Tübingen

Sigwartstraße 10, D-72076 Tübingen

ISSN 0953-4921

\* zu beziehen über: Dr. Joachim KUHLEMANN, Institut für Geowissenschaften der Universität Tübingen, Sigwartstraße 10, D-72076 Tübingen, Fax: ++49 7071 5059, e-mail: [kuhlemann@uni-tuebingen.de](mailto:kuhlemann@uni-tuebingen.de)

Aktueller Stand erschienener Bände über: [http://www.uni-tuebingen.de/geo/gpi/tga/reihe\\_a.html](http://www.uni-tuebingen.de/geo/gpi/tga/reihe_a.html)

Preise sind ohne Gewähr. Prices are subject to change.

# CONTENTS

Abstract .....	XI
Zusammenfassung .....	XIV
Introduction	
1.1 Scope of the study .....	1
1.2 Aims of the study .....	3
2 Geological setting	
2.1 Introduction .....	4
2.2 Variscan Corsica .....	6
2.3 Alpine Corsica .....	6
2.4 Sedimentary successions .....	7
2.4.1 Eocene sediments .....	7
2.4.2 Oligocene sediments .....	9
2.4.3 Miocene sediments .....	9
2.4.3.1 Bonifacio Basin .....	9
2.4.3.2 Saint Florent Basin .....	10
2.4.3.3 Francardo-Ponte Leccia Basin .....	10
2.4.3.4 Oriental Plain .....	10
2.5 Geodynamic evolution of Corsica within the plate tectonic history of the Western Mediterranean .....	11
2.6 Previous thermochronological studies in Corsica .....	14
3 Geomorphological setting	
3.1 Introduction .....	17
3.2 Characteristics of the paleorelief .....	18
4 Fission track and (U-Th)/He dating techniques	
4.1 Fission track thermochronology .....	21
4.1.1 Introduction .....	21
4.1.2 Fission track formation .....	21
4.1.3 Age calculation .....	22
4.1.4 Fission track annealing and modeling .....	24
4.2 Apatite (U-Th)/He thermochronology .....	26
4.2.1 Introduction .....	26
4.2.2 He ingrowth .....	26
4.2.3 Alpha recoil correction .....	27
4.2.4 Sensitivity of the apatite (U-Th)/He thermochronometer .....	29

5	Dating procedure	
5.1	Sampling	32
5.2	Mineral separation	33
5.3	Fission track analysis	33
5.4	(U-Th)/He analysis	33
5.4.1	Apatite grain selection	33
5.4.2	The $^4\text{He}$ analysis	34
5.4.3	U and Th analysis	35
5.4.3.1	Apatite dissolution and isotopic dilution	35
5.4.3.2	ICP-MS analysis	35
5.4.4	Results of mineral standard	36
5.4.5	Error calculation	37
6	Results	
6.1	Zircon fission track results	39
6.2	Apatite fission track results	39
6.3	Apatite (U-Th)/He results	45
7	Interpretation and discussion	
7.1	Zircon fission track data	48
7.1.1	Introduction	48
7.1.2	ZFT domains	48
7.1.3	Conclusions	51
7.2	Apatite fission track data	52
7.2.1	Elevation profiles and exhumation rates derived from AFT data	52
7.2.1.1	Terminology	52
7.2.1.2	Theory	53
7.2.1.3	Results	55
7.2.1.4	Age-elevation pattern in regional scale	56
7.2.1.5	Conclusions	57
7.2.2	Trends and patterns in apatite fission track data	58
7.2.2.1	Treatment procedure on AFT datasets of previous studies	58
7.2.2.2	Spatial distribution of AFT ages	58
7.2.2.3	Trends and pattern in track length data	61
7.2.2.4	Chemical composition of the apatites	62
7.2.2.5	Conclusions	63
7.2.3	Subdivision into AFT domains	64
7.2.3.1	Domain I	64
7.2.3.1.1	Classification according to passive margin models	68
7.2.3.2	Domain II	70
7.2.3.3	Domain III	73
7.2.3.3.1	Tentative reconstruction of the Alpine accretionary wedge and foreland basin	76

7.2.3.4 Domain IV .....	77
7.2.3.5 Conclusions.....	79
7.3 (U-Th)/He data .....	80
7.3.1 Introduction.....	80
7.3.2 Paleosurfaces in Corsica and available constraints .....	81
7.3.3 Interpretation and discussion of (U-Th)/He data.....	82
7.3.4 Conclusions.....	86
8 Synthesis and conclusions	
8.1 A comprehensive model.....	88
8.2 Final conclusions.....	93
Acknowledgements .....	94
References .....	96
Appendices .....	i
Appendix A	
Mineral separation.....	i
Appendix B	
Fission track methodology .....	ii
Appendix C	
Description of the He extraction line .....	vi

## ABSTRACT

The island of Corsica in the Western Mediterranean represents a natural laboratory for studying the processes of cooling, exhumation, and relief formation, since there are several advantageous features that make Corsica an excellent study area. In a relatively small territory, two distinct principal domains are distinguished: (i) Alpine Corsica, a complex nappe stack dominated by metamorphic rocks of oceanic origin metamorphosed during the Alpine orogeny; and (ii) Variscan Corsica, a well-exposed Variscan crystalline basement made up mainly of unmetamorphosed granitoid rocks. Geodynamic evolution is characterized by Mesozoic extension and opening of the Ligurian-Piedmont Ocean, followed by middle Late Cretaceous to Eocene shortening, resulting in Alpine collision when the Alpine nappes were thrust onto the Variscan basement. In the Oligocene, the tectonic regime changed from a compressional to an extensional one, and continuous rollback of a newly evolved Apenninic subduction zone led to collapse of the Alpine wedge, rift inception merging to ocean spreading, and drifting of the Corsica-Sardinia block away from the European mainland. At present, the Corsica-Sardinia block is a micro-continent surrounded by two oceanic domains. From the geomorphological standpoint, Variscan Corsica represents an outstanding ridge-and-valley structure with peaks exceeding 2000 m in elevation, where the most spectacular features are paleosurface remnants of unknown age preserved at elevations between 200 and 2300 m.

The aim of this study is to investigate the thermal and exhumation history and relief evolution of Corsica, and to constrain the age of paleosurface remnants through the use of three low-temperature dating techniques: zircon fission track (ZFT), apatite fission track (AFT) and (U-Th)/He thermochronology. Each of these methods has a characteristic temperature sensitivity of between  $\sim 200\text{-}300^\circ\text{C}$ ,  $\sim 60\text{-}120^\circ\text{C}$ , and  $\sim 40\text{-}75^\circ\text{C}$ , respectively, which makes it possible to detect temperature changes in uppermost crust that can be induced by deposition or removal of rock masses by erosion or tectonic processes, or by changes in topographic relief. Previous thermochronological studies primarily focused on investigating the inversion of the Alpine wedge in NE Corsica, whereas the major part of Variscan Corsica is virtually unexplored. This study concentrates specifically on these regions with the highest relief and paleosurface remnants.

Altogether 3 ZFT, 67 AFT and 40 (U-Th)/He analyses were performed on samples from the Variscan basement and Eocene flysch sediments. The data published in other studies were carefully revised according to strictly defined criteria and fully integrated into the actual dataset.

ZFT analyses from the central part of the Variscan basement yield ages between  $144.6 \pm 10$  and  $159.2 \pm 9.8$  Ma. These ages record a thermal event related to the Jurassic opening of the Ligurian-

Piedmont Ocean. Inferring from the data of other studies it can be concluded that the ZFT system in the eastern margin of Variscan Corsica was partially reset during Eocene metamorphism, and that during the Cretaceous there was no thermal event affecting Variscan Corsica. In Alpine Corsica, ZFT data together with  $^{40}\text{Ar}/^{39}\text{Ar}$  data bracket the time of tectonic denudation of Alpine units between ~33 and 19 Ma.

AFT data range from  $16.4 \pm 1.4$  to  $105.3 \pm 7.2$  Ma, AFT ages from Eocene flysch are all completely reset. Based on the AFT data and thermal modeling results the cooling history of Corsica can be reconstructed as follows: after the Jurassic thermal event related to opening of the Ligurian-Piedmont Ocean, the basement was cooling to near-surface conditions where it remained until the Early Paleocene. Since the Late Paleocene, the basement was progressively buried below sediments of the foreland basin, and later during Eocene collision it was partly covered by Alpine nappes. At the end of the Eocene, all of Variscan Corsica had been covered by a thick pile of rocks, leading to a total reset of the AFT system in the major part of the basement. In the Oligocene, after tectonic reorganization, the basement started to exhume, which led to the removal of the thick cover from the top of the basement. The removal of the cover occurred by erosional denudation in the major part of Variscan Corsica, as well as by tectonic denudation in the NE part of the island. AFT ages from the NW part of the basement record an Early Miocene thermal event associated with the opening of the Ligurian-Provençal Ocean.

(U-Th)/He analysis was performed on 12 samples from nine different paleosurface remnants, and yield ages between  $16.0 \pm 2.3$  and  $22.1 \pm 0.9$  Ma. There are no obvious differences in He age between different paleosurface remnants, although the vertical distance in some cases is more than 1600 m. This indicates that all paleosurface remnants in Corsica have their origin in one single paleosurface. Segmentation of the paleosurface and differential uplift of individual blocks happened after the time of cooling through the temperature zone sensitive to the (U-Th)/He system. The age of the paleosurface formation is bracketed on the basis of FT data, thermal modeling results and consideration of stratigraphic and structural data, between ~120 and 60 Ma. During Eocene collision, the paleosurface was buried by a thick flysch pile and was thus protected from destruction. In the Oligocene, the paleosurface started to exhume and the cover was removed. During the Miocene rotation, the paleosurface was cut by faults, and at ~17 Ma the region was uplifted by differential block movements, creating relief and inducing valley incision. This event can be understood as an onset of peneplain destruction that occurred mainly by fault-induced valley incision and widening.

The data presented in this study bring new light to the understanding of the thermal, tectonic and morphological evolution of Corsica and provide new insight on the geodynamic evolution of the Western Mediterranean realm. Moreover, the results demonstrate that different low-temperature dating techniques used in tandem have great potential for unraveling the thermal history of rocks at shallow depth, and can significantly reduce the number of "acceptable solutions" obtained when using only one

method. Furthermore, it is shown that after proper revision, it is possible to integrate several, otherwise contradicting, FT datasets.

## ZUSAMMENFASSUNG

Die Insel Korsika im westlichen Mittelmeer stellt ein natürliches Labor dar, um Prozesse wie Abkühlung, Exhumierung und Reliefbildung zu studieren. Es gibt mehrere Vorteile, die Korsika zu einem guten Forschungsobjekt machen. Auf relativ engem Raum finden sich zwei deutlich unterschiedliche Bereiche: (i) Alpines Korsika: ein komplexer Deckenstapel aus Metamorphiten ozeanischen Ursprungs, welche während der alpidischen Orogenese metamorphisiert wurden; (ii) Variszisches Korsika: Grundgebirge, welches hauptsächlich aus unmetamorphen Granitoiden besteht. Die geodynamische Entwicklung von Korsika lässt sich folgendermaßen darstellen: mesozoische Extensionstektonik. Bei der Öffnung des Ligurisch-Penninischen Ozeans, gefolgt von mittelkretazischer bis eozäner Einengung, mit der daraus resultierenden Kollision wurden die alpinen Decken auf das variszische Grundgebirge aufgeschoben. Im Oligozän änderte sich das tektonische Regime von Kompression zu Extension. Zurückrollen der jungen apenninischen Subduktionszone führte zu einem Kollaps des alpinen Orogens Korsikas, und beginnendes Rifting zur Abspaltung des korsisch-sardischen Blocks vom europäischen Festland. Der heutige korsisch-sardische Block stellt einen Mikrokontinent dar, der von zwei ozeanischen Bereichen umgeben ist. Aus geomorphologischer Sicht ist das Variszische Korsika eine Struktur mit parallel angeordneten Rücken und Tälern mit Gipfeln von mehr als 2000 m Höhe. Hier finden sich, zwischen 200 und 2300 m Seehöhe, Reste von Altflächen unbekanntes Alters.

Ziel dieser Arbeit ist es, die thermische Geschichte sowie die Exhumierung und Reliefentwicklung von Korsika zu erforschen. Hierzu sollten die Alter der Altflächen mittels drei Methoden der Niedrigtemperatur-Thermochronologie ermittelt werden: Datierung mit Hilfe der Zirkon-Spaltspuren-Methode (ZFT), der Apatit-Spaltspuren-Methode (AFT) und der (U-Th)/He-Methode. Jedes dieser Mineralsysteme hat unterschiedliche Intervalle für die Schließungstemperatur: ~200-300°C, ~60-120°C beziehungsweise ~40-75°C. Diese Temperaturspektren machen es möglich, Veränderungen in der oberen Kruste zu bestimmen, die z. B. auf die Ablagerung von Gesteinen, oder deren Entfernung durch Erosion oder tektonische Prozesse sowie durch Veränderungen der Topografie zurückzuführen sind. Frühere thermochronologische Untersuchungen konzentrierten sich auf die Inversionstektonik des alpinen Deckenkeils in NE-Korsika, wohingegen der größte Teil des Variszischen Korsikas unerforscht blieb. Diese Arbeit konzentriert sich speziell auf diesen variszischen Teil mit seinem höheren Relief und größeren Anteil an Altflächen.

Insgesamt wurden 3 ZFT-, 67 AFT- und 40 (U-Th)/He-Analysen vom variszischen Grundgebirge und vom eozänen Flysch gemacht. Daten von anderen Publikationen wurden sorgfältig recherchiert, um sie in den aktuellen Datensatz einzubauen.

ZFT-Analysen vom zentralen Teil des variszischen Grundgebirges führen zu Altern zwischen  $144.6 \pm 10$  und  $159.2 \pm 9.8$  Ma. Diese Daten zeigen ein thermisches Ereignis, welches mit der Öffnung des Ligurischen-Penninischen Ozeans im Jura zusammenhängt. Zusammen mit Daten von anderen Publikationen kann die Schlußfolgerung gezogen werden, dass das ZFT-System im östlichen Teil des Variszischen Korsikas durch Metamorphose im Eozän teilweise zurückgesetzt wurde, und dass während der Kreide keine thermische Beeinflussung erfolgte. Im Alpen Korsika zeigen ZFT-Analysen und  $^{40}\text{Ar}/^{39}\text{Ar}$ -Daten, dass die tektonische Denudation dieser Einheiten zwischen  $\sim 33$  und 19 Ma erfolgte.

AFT-Alter erstrecken sich zwischen  $16.4 \pm 1.4$  Ma und  $105.3 \pm 7.2$  Ma, wobei die Alter im eozänen Flysch vollständig zurückgesetzt wurden. Aufgrund der AFT-Alter und einer thermischen Modellierung kann die Abkühlgeschichte von Korsika folgendermaßen rekonstruiert werden: nach der Öffnung des Ligurisch-Penninischen Ozeans im Jura kühlte das Grundgebirge bis zu oberflächennahen Bedingungen ab, unter denen es bis ins frühe Paläozän verblieb. Seit dem späten Paläozän wurden die Grundgebirgseinheiten von Sedimenten bedeckt und später bei der eozänen Kollision teilweise von alpinen Decken überlagert. Gegen Ende des Eozäns wurde das gesamte Variszische Korsika von mächtigen Sedimenten bzw. den alpinen Decken überlagert, was zur totalen Umstellung des AFT-Systems führte. Im Oligozän begann die Exhumierung des Grundgebirges und die damit verbundene Abtragung der Bedeckung. Die Abtragung erfolgte durch Erosion im Hauptteil des Variszischen Korsikas und durch tektonische Denudation im NE-Teil der Insel. AFT-Alter vom NW-Teil des Grundgebirges zeigen ein frühmiozänes thermisches Ereignis, welches mit der Öffnung des Ligurisch-Provençalischen Ozeans zusammenhängt.

(U-Th)/He-Analysen wurden an 12 Proben von 9 verschiedenen Altflächen vorgenommen. Sie ergaben Alter zwischen  $16.0 \pm 2.3$  und  $22.1 \pm 0.9$  Ma. Es bestehen keine ersichtlichen Unterschiede in den He-Altern zwischen den verschiedenen Altflächen, obwohl in manchen Fällen der Höhenunterschied mehr als 1600 m beträgt. Das bedeutet, dass alle Altflächen in Korsika ihren Ursprung in einer einzigen Altfläche haben. Die Zerlegung bzw. Segmentierung der Altflächen und die differentielle Hebung individueller Blöcke erfolgte nach der Abkühlung unter die Schließungstemperatur des (U-Th)/He-Systems. Das Bildungsalter der Altflächen wird durch FT Daten, thermische Modellierung und unter Berücksichtigung von Stratigraphie und Strukturdaten auf  $\sim 120$  bis 60 Ma eingegrenzt. Während der eozänen Kollision waren die Altflächen von einem mächtigen Flyschstapel überdeckt und so vor Erosion geschützt. Im Oligozän begann die Exhumierung der Altflächen und die aufliegenden Schichten wurden erodiert. Während der Rotation Korsikas im Miozän wurde die Rumpffläche von Störungen durchschnitten. Vor etwa 17 Ma wurde

die Region gehoben, differentielle Blocktektonik gestaltete ein neues Relief und induzierte die Bildung von Flusstälern. Dieses Ereignis kann als Beginn der Zerstörung der Rumpffläche verstanden werden, die hauptsächlich durch das störungsinduzierte Einschneiden von Tälern und deren Aufweitung vor sich ging.

Die Daten, die in der vorliegenden Studie präsentiert werden, bringen neue Erkenntnisse über die thermische, tektonische und morphologische Entwicklung von Korsika und den gesamten westmediterranen Raum. Außerdem zeigen die Daten, dass die Kombination verschiedener Datierungsmethoden der Niedertemperatur-Thermochronologie großes Potential zur Entschlüsselung der Geschichte von Gesteinen in seichten Krustenbereichen haben. Die Zahl „akzeptabler Lösungen“ wird signifikant reduziert, sobald man mehrere Methoden anwenden kann. Schließlich kann gezeigt werden, dass es nach sachgerechter Korrektur der Daten durchaus möglich ist, verschiedene, ansonsten unvereinbare FT-Datensätze zu integrieren.

# INTRODUCTION

## 1.1 SCOPE OF THE STUDY

For this study, Corsica has been chosen as a natural laboratory for investigation of the tectonic and surface processes by means of low temperature thermochronology. There are several advantageous features that make Corsica an excellent study area, for instance:

1. On a relatively small territory two distinct domains are distinguished – Alpine Corsica (complex nappe stack dominated by metamorphic rocks) and Variscan Corsica (well-preserved Variscan crystalline basement);

2. The succession of the major compressional and extensional events is more or less well established: since the Mesozoic, the area has experienced a series of compressional and extensional episodes, leading to Alpine collision and emplacement of the Alpine nappes onto the continental Variscan basement, and subsequent extensional collapse, rifting, oceanic spreading and basin formation;

3. The island exhibits an outstanding morphological framework with moderate to rugged relief, altitudes exceeding 2000 m, and paleosurface remnants preserved at levels of local summits.

All these attributes have attracted the attention of geologists for a long time. Despite relatively intensive research on Corsica in the last decades on subjects such as the kinematics of the Alpine collision (e.g., Mattauer et al., 1981; Malavieille, 1983; Durand-Delga, 1984; Harris, 1984; Warburton, 1986; Malavieille et al., 1998), extension, inversion of the orogenic front, basin formation (Fournier et al., 1991; Jolivet et al., 1991; Jolivet and Faccenna, 2000), rotation of the Corsica-Sardinia block (e.g., Vigliotti and Kent, 1990; Vigliotti et al., 1990; Vigliotti and Langheim, 1995), or the high pressure - low temperature (HP/LT) metamorphism event (Caron et al., 1981; Gibbons and Horák, 1984; Lahondère, 1988; Lahondère and Guerrot, 1997), the issue of the low-temperature thermal evolution has not yet been adequately resolved. Although a relatively large database of low-temperature chronological data exists on Corsica, the data are restricted mainly to the NE part (Carpéna et al., 1979; Lucazeau and Mailhé, 1986; Mailhé et al., 1986; Cavazza et al., 2001; Fellin, 2003; Fellin et al., 2005) and western coast of the island (Jakni, 2000; Jakni et al., 2000; Zarki-Jakni et al., 2004). The central part, with the highest relief and paleosurface remnants, is virtually unexplored in this respect and is the main target for this study.

Several open questions still exist concerning the tectonothermal evolution of Corsica, such as:

1. Which processes governed the thermal history of Corsica? This question is still a matter of debate. There are several opinions presented, each having its pros and cons. For instance, exhumation related to erosional denudation and passive margin uplift linked to the rifting of the Ligurian-Provençal basin (Jakni, 2000; Jakni et al., 2000), tectonic denudation from below the Alpine nappes (Jolivet et al., 1990, 1991; Brunet et al., 1997, 2000), maybe linked to the Tyrrhenian rifting (Cavazza et al., 2001), or cooling related to migration of the locus of extension from west to east, isostatic rebound following the inversion of Alpine compressional front (Zarki-Jakni, 2004) are discussed. Certainly, a combination of some or all of these processes is an option for all authors.

2. What was the timing of final cooling? To date, a wide range of apatite fission track ages is presented from Corsica (between ~55 and 12 Ma), which suggests quite a long-lasting cooling process, however there are also periods of reheating detected by thermal modeling. So it is not clear whether the cooling process was continuous or periodic in space and time.

3. How did the relief evolve and how old are the remnants of the paleosurface? Already Rondeau (1961) recognized several paleosurfaces in Corsica and tried to reconstruct an episodic uplift scenario on the base of river terraces especially in the Gravona Valley. Young episodic uplift scenarios are also favored by Seidl (1974) on the base of terraces in the lower Golo Valley in Alpine Corsica. Kuhlemann et al. (2005a) proposed a scenario with two generations of paleosurfaces, based on the digital elevation model analysis, published thermochronological data, and structural and morphological observations. The latter scenario provides a unique case to be tested and justified or rejected by low-temperature thermochronometers, and the question of the age of the paleosurfaces can be possibly answered.

4. How was the pre-Tertiary thermal evolution of the Variscan crystalline basement? Mailhé et al. (1986) argued for Mesozoic partial reset of Variscan zircon fission track ages caused by thrusting of Alpine units of various thickness. In contrast, Vance (1999) interpreted the data of Mailhé et al. (1986) as related to the opening of the Jurassic Tethys Ocean.

In order to resolve these issues, two dating methods have been used in this study: the fission track (FT) method, applied both on apatite and zircon, and the (U-Th)/He method, applied on apatite. Each of these isotopic systems has a distinct sensitivity to temperature, and therefore a characteristic "closure temperature" (Dodson, 1973):  $245 \pm 50^\circ\text{C}$  for the zircon fission track (ZFT),  $110 \pm 10^\circ\text{C}$  for the apatite fission track (AFT), and  $\sim 75^\circ\text{C}$  for the (U-Th)/He system (Hurford, 1986; Laslett et al., 1987; Wolf et al., 1996a,b; Farley, 2000). A combination of all these methods can provide essential information on temperature changes in the upper crustal levels in the course of time, generally caused by the deposition or removal of excess material as a result of tectonic, sedimentary, erosive and magmatic processes, which is crucial in the context of this study.

The new thermochronological data presented here will be combined with previous properly revised thermochronological data and published structural, sedimentological, and geomorphologic data in order to constrain the thermotectonic and geodynamic evolution of Corsica.

## **1.2 AIMS OF THE STUDY**

The aims of the study are:

1. To understand the processes controlling the exhumation of Corsica;
2. To provide further constraints on the exhumation history of Corsica in the low-temperature domain by means of ZFT, AFT and (U-Th)/He thermochronology, in order to improve our understanding of thermal, tectonic and morphological response of continental crust to the processes controlling the exhumation of Corsica;
3. To gain a better understanding of the timing, rate and amount of vertical movements that have occurred in Corsica;
4. To date and bracket the time of paleosurface formation;
5. To constrain the mode of geodynamic and landscape evolution of Corsica.

## 2 GEOLOGICAL SETTING

### 2.1 INTRODUCTION

Corsica is an island up to 180 km long and 84 km wide, situated in the northern part of the Western Mediterranean Sea (Fig. 2-1). It is located between 43°01' and 41°22' northern latitude and 8°33' and 9°34' eastern longitude, 180 km from the French and 82 km from the Italian mainland. The coastline extends to over ~950 km. It is bounded by the Western Mediterranean Sea in the west, the Ligurian Sea in the north, the Tyrrhenian Sea in the east, and accompanied by the island of Sardinia in the south (12 km distance). With 8 682 km<sup>2</sup>, it is the third largest island in the Western Mediterranean (after Sicily - 25 706 km<sup>2</sup> and Sardinia - 24 090 km<sup>2</sup>). Owing to a spectacular relief, Corsica is often referred to as the "Mountain in the Sea": with 20 peaks over 2000 m and average altitude of 565 m, is by far the highest island in the entire Mediterranean. The highest point (Monte Cinto) culminates at 2706 m, at a distance of only 24 km from the coast.

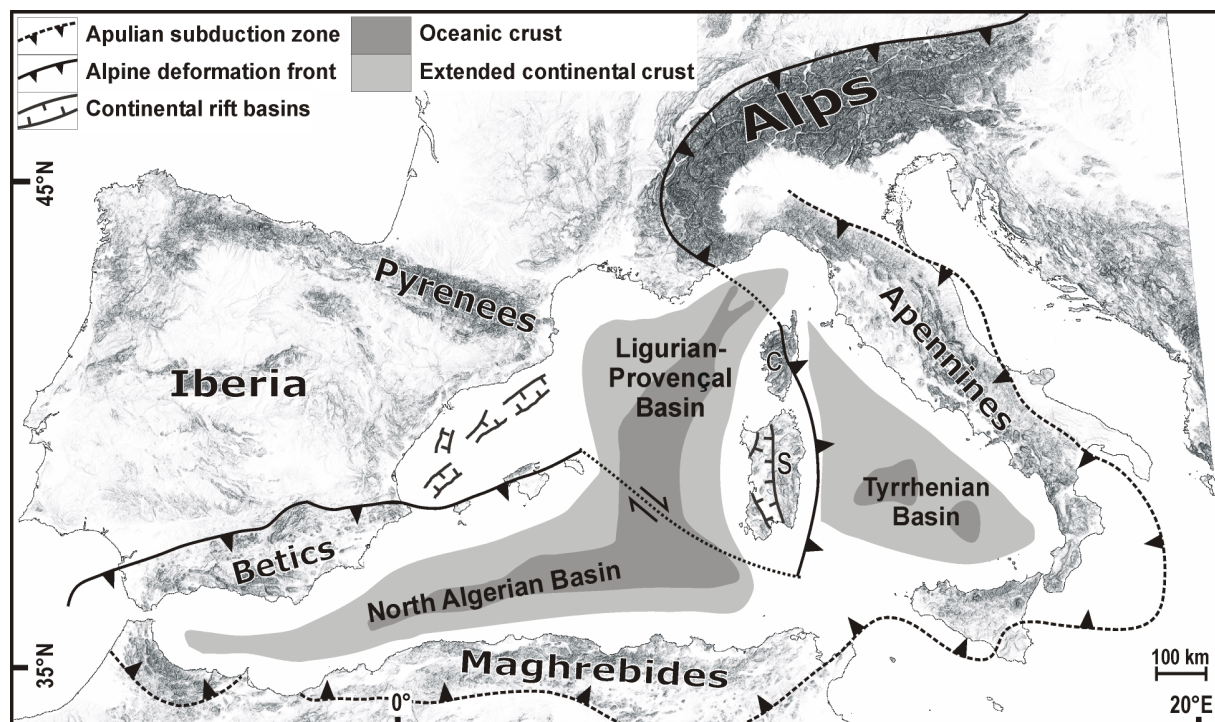
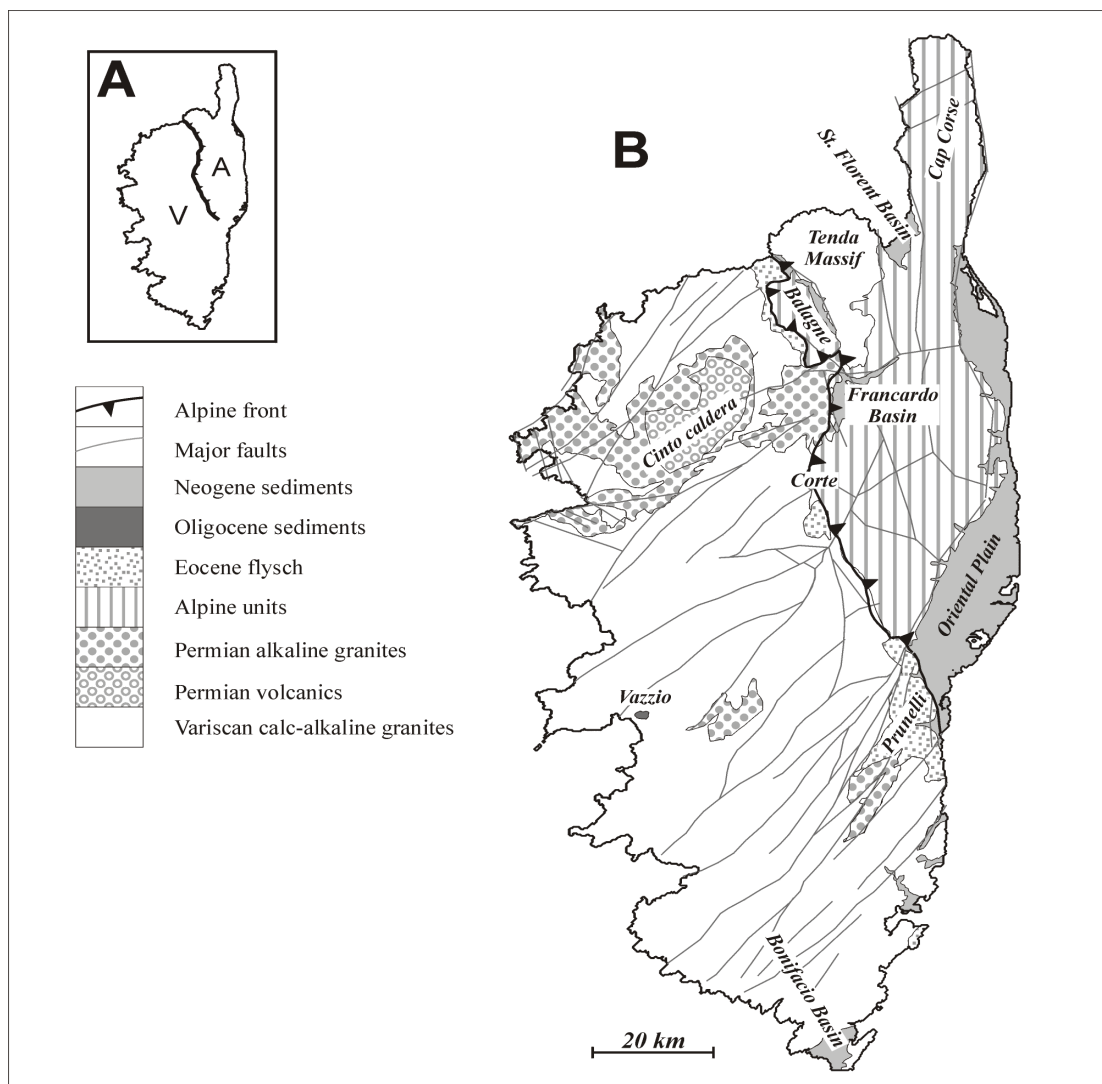


Fig. 2-1: Digital elevation model of the Western Mediterranean region with major, simplified geological structures (modified after Gueguen et al., 1998). C - Corsica, S - Sardinia.

Geologically, Corsica and Sardinia form a micro-continent, surrounded by two oceanic domains - the Ligurian-Provençal Basin in the west and the Tyrrhenian Basin in the east (Fig. 2-1). Corsica is traditionally divided into two parts (Fig. 2-2): (i) the larger western part, called Variscan Corsica, is Variscan crystalline basement composed mainly of unmetamorphosed granitoid rocks; (ii) the eastern part, called Alpine Corsica, is a southern extension of the continental Alpine chain comprising nappe slices mostly of oceanic crust and its sedimentary cover metamorphosed during the Alpine orogeny (Boccaletti et al., 1971; Mattauer and Proust, 1976; Durand-Delga, 1978; Durand-Delga, 1984). The dividing line between these two main parts runs roughly from St. Florent in the north, southwards to Corte, then southeastward to Solenzara and the eastern coast. Besides the two principal domains mentioned above, there are also several post-tectonic Tertiary basins filled with Miocene to Quaternary sediments, which rest unconformably upon the Variscan and Alpine domains.



**Fig. 2-2:** A: illustration showing two principal domains in Corsica, V - Variscan Corsica; A - Alpine Corsica. B: schematic map of major lithotectonic units (modified after Rossi et al., 1980).

In the following paragraphs, the geological settings of the Variscan part, the Alpine part and the Tertiary sedimentary successions are briefly described. Then an abridged description of the geodynamic evolution of Corsica is provided, and finally all relevant thermochronological data are reviewed.

## 2.2 VARISCAN CORSICA

Variscan Corsica is a continental block of Variscan basement (Fig. 2-2), which was rifted and drifted off from the European plate. The oldest lithologies are represented by sparse remnants of Upper Precambrian – Lower Paleozoic polymetamorphic rocks (Biotite-Muscovite-Garnet-gneisses, Biotite-gneisses, and migmatites). Locally, a low-grade metamorphic Upper Precambrian unit is unconformably overlain by Paleozoic sediments (conglomerates, lydites, quartzites). Most of Variscan Corsica is built up of various granitoid and volcanic rocks with intrusion ages between 340 and 260 Ma, related to the Variscan orogeny (Cocherie et al., 1984). They formed in two cycles of syn-orogenic magmatism with calc-alkaline affinity during the Carboniferous (producing mostly granodiorites and monzogranites), and post-orogenic magmatism with alkaline affinity during the Permian (producing mostly alkaline granites and rhyolites). The crystalline basement is locally covered by Upper Carboniferous conglomerates and sandstones, Permian arkoses and greywackes. Mesozoic rocks are represented by sparse occurrences of Upper Triassic and Lower Jurassic shallow water carbonates.

## 2.3 ALPINE CORSICA

Alpine Corsica, located in the north-eastern part of the island (Fig. 2-2A), consists of various nappes, which were deformed, metamorphosed and emplaced during the Alpine orogeny. The nappes comprise abundant ophiolitic fragments, local granitic or gneissic slices and large masses of sediments, which were mostly deposited upon oceanic crust. The ophiolites were derived from the Ligurian-Piedmont Ocean. This basin, which separated the European and African plates, developed during Jurassic and Cretaceous times (trondhjemitic associated with the ophiolites have been dated at  $161 \pm 3$  Ma; Ohnenstetter et al., 1981).

The Alpine nappe stack can be divided into three main units, from base to top (Daniel et al., 1996): 1. the external units (referred as "paraautochthon"), 2. the Schistes Lustrés Nappe sensu lato, and 3. the Upper Unit (or "Nappe Supérieur").

The external units comprise the Tenda Massif and the Corte slices. The Tenda Massif consists of Variscan granitic basement belonging to the European margin. The Corte slices are a nappe stack containing Variscan crystalline basement with an Upper Paleozoic to Eocene sedimentary cover (Amaudric du Chaffaut, 1982; Egal, 1992). According to Lahondère (1991), both units were deformed and metamorphosed under middle pressure - low temperature (MP/LT) conditions (pressure to 0.5 GPa and temperature of  $300 \pm 50^\circ\text{C}$ ), during Eocene collision and thrusting of the Schistes Lustrés nappes (Mattauer et al., 1981; Gibbons and Horák, 1984; Warburton, 1986; Jourdan, 1988).

The Schistes Lustrés Nappe *sensu lato* comprises several oceanic and continental units, which were thrust onto the European continental margin and metamorphosed in MP/LT to high pressure - middle temperature (HP/LT) conditions (blueschist and eclogite facies). Oceanic units contain all members of the ophiolite suite (ultramafics, gabbros, sheeted dikes, pillow basalts, and red radiolarian pelagic cherts), monotonous calc-schists and flysch of Cretaceous age, lithologically similar to the Schistes Lustrés Nappe of the Western Alps (Caron, 1977). Continental units contain para- and orthogneisses of continental affinity with their sedimentary cover (marbles and quartzites).

The upper unit (or "Nappe Supérieure") is the topmost structural unit of Alpine Corsica and is constituted mainly of ophiolitic material and oceanic sediments of Upper Jurassic age as well as Upper Cretaceous flysch (Durand-Delga, 1984). The upper unit can be subdivided into the Balagne, Nebbio and Macinaggio nappes. They rest tectonically upon the basement of Variscan Corsica, Schistes Lustrés Nappe, Tenda massif, and Eocene foreland basin (Egal, 1992). The emplacement took place during the Middle Eocene, as attested by the presence of olistostrome deposits with Lutetian nummulites below the Balagne Nappe (Nardi et al., 1978; Durand-Delga, 1984; Jourdan, 1988). Unlike in the Schistes Lustrés Nappe, the upper unit was affected only by very low- to low-grade metamorphism, no HP/LT mineral assemblages have been found.

## **2.4 SEDIMENTARY SUCCESSIONS**

### **2.4.1 Eocene sediments**

Eocene (locally also Paleocene but mainly Lower and Middle Eocene) flysch sediments are widely distributed along the border zone between Alpine and Variscan Corsica (Fig. 2-3). The successions are composed of conglomerates with components of basement, quartzites, arkoses, and pelites; thickness varies from tens to hundreds meters.

The Eocene flysch was initially deposited in the trough (or "foreland basin") in front of the approaching Alpine nappes during collision (e.g., Egal, 1992). The relationship of Eocene sediments to the autochthonous continental basement and allochthonous Alpine nappes is complex and is interpreted as recording a diachronic emplacement of nappes (Egal, 1992).

In the southeastern part of Corsica, in the Prunelli region, the Eocene sediments (Prunelli

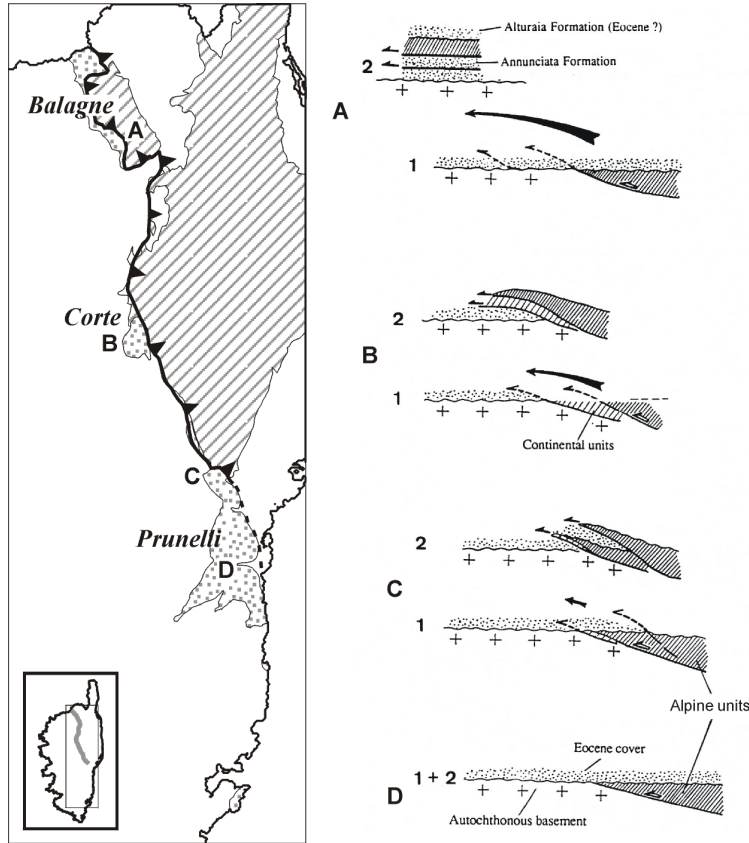


**Fig. 2-3:** Left: present-day position of Eocene flysch (dotted fill) in Corsica. Right: schematic illustration of the position of the flysch and structural setting of the autochthonous and allochthonous units before (1) and after (2) the Eocene thrusting. The displacement associated with the thrusts, represented by large arrows, increases from the south to the north (modified after Egal, 1992).

flysch) transgressively overlie autochthonous basement as well as Schistes Lustrés, implying that Alpine nappes were tectonically emplaced before the deposition of latest Eocene flysches (see Fig. 2-3D; Amaudric du Chaffaut, 1982).

Further to the north, the Eocene flysch is involved in a tectonic imbrication, where Schistes Lustrés and serpentinites are in the superposition on the Eocene flysch (Fig. 2-3B,C). This implies that tectonic imbrication postdates the deposition of Eocene sediments.

In the northern parts of Corsica, Upper Paleocene to Lower Eocene carbonates and Lower to Middle Eocene flysch transgressively overlie Variscan basement (Fig. 2-3A), which is indicative of slow subsidence at shallow marine conditions followed

by rapid subsidence and sedimentation in the trench (Durand-Delga, 1978). The Paleocene and Eocene formations are overlain by the Balagne nappe, indicating that thrusting of the Ligurian nappes in a very high position must have happened after the deposition of the Eocene sediments (Nardi et al., 1978; Durand-Delga, 1984; Jourdan, 1988).

## 2.4.2 Oligocene sediments

Oligocene deposits, described as Vazzio formation by Ferrandini et al. (1999), are preserved only in the WSW part of the island in the area of Ajaccio (Fig. 2-2B). The succession is composed of a continental sedimentary sequence, mainly conglomerate, with a thickness of 250-300 m. The age was determined as Late Chattian (24-25 Ma) on the basis of pollen and mammal findings. The conglomerates were deposited in torrential and lacustrine environment within a depression or paleo-thalweg. The fact that most of the pebbles come from Variscan basement suggests that part of the Variscan basement near Ajaccio was eroded in the Late Oligocene. From the structural standpoint, the Vazzio formation was deposited in a half-graben structure related to the Ligurian-Provençal rift system (Ferrandini et al., 1999).

## 2.4.3 Miocene sediments

The Miocene sediments of Corsica have been deposited in basins bordered by extensional faults. They transgressively overlie all pre-Neogene formations and are exposed in four major basins (Francardo-Ponte Leccia, Bonifacio, Saint Florent, and Oriental Plain), which are located exclusively along the eastern margins of Variscan and Alpine Corsica (Fig. 2-2). Basin formation is related to the extensional tectonic regime from Oligocene to present, controlled by eastward migration of the Apenninic subduction zone. In general, sedimentary cycles consist of Upper Burdigalian terrestrial conglomerates, followed by marine sandstones, calcarenites, and marls, of Upper Burdigalian to Lower Serravallian age, indicating subsidence below sea-level (Orszag-Sperber and Pilot, 1976).

### 2.4.3.1 BONIFACIO BASIN

The Miocene succession of the Bonifacio Basin in southernmost Corsica is ca. 600 m thick and rests on the Variscan basement (Orszag-Sperber and Pilot, 1976). The sequence starts with the Upper Aquitanian (20.6-21.3 Ma) ignimbrite deposits dated by the  $^{40}\text{Ar}/^{39}\text{Ar}$  method on plagioclase (Ferrandini et al., 2003). The ignimbrites are overlain by Upper Burdigalian terrestrial conglomerates and marine deposits (coral reefs, silts, and sandy limestones). The succession ends with Lower Langhian cross-bedded calcarenites indicating regression. The absence of Lower Burdigalian strata indicates emersion of the region at that time.

### **2.4.3.2 SAINT FLORENT BASIN**

The Saint Florent Basin in the NE part of the island contains a ca. 500 m thick sequence lying upon the Nebbio and Tenda units. The sedimentary sequence consists of three marine formations lying between two continental ones (Ferrandini et al., 1998). At the base, probably Burdigalian continental conglomerates with clasts from the underlying Nebbio and Tenda units are found. Overlying marine series are of Upper Burdigalian to Lower Serravallian age and contain clayey sandstones, silts, limestones, marls, and calcarenites. The marine deposits are overlain by fluvial coarse conglomerates of probably Tortonian age with clasts from the Variscan basement.

### **2.4.3.3 FRANCARDO-PONTE LECCIA BASIN**

Francardo-Ponte Leccia Basin is an intramontane halfgraben in the center of Corsica, bounded to the west by Variscan basement, and to the east by Alpine units. The succession is around 600 m thick and consists of conglomerates derived from the basin shoulders. The conglomerates are ca. 150 m thick, poorly sorted, and massive, and were deposited as mass-flow fans (Ferrandini and Loÿe-Pilot, 1992). The conglomerates are transgressively covered by ca. 125 m thick marls and mudstones (Taverna Formation), documenting a change to marine environment during Late Burdigalian times. The subsequent regression is documented by the overlying Francardo Formation, a 300 m thick conglomerate unit, consisting of well rounded pebbles mostly derived from the Variscan basement. The unit is interpreted as deltaic sediments of the Golo paleoriver, draining the Variscan basement in the west (Orszag-Sperber and Pilot, 1976; Ferrandini and Loÿe-Pilot, 1992; Kuhlemann et al., 2005a).

### **2.4.3.4 ORIENTAL PLAIN**

The most complete sedimentary succession is preserved below the Oriental Plain, where over 2 km of Upper Burdigalian to Pliocene sediments have been deposited (Orszag-Sperber and Pilot, 1976; Orszag-Sperber, 1978). The Oriental Plain represents the margin of the offshore Corsica Basin with up to 8 km of sediments (Mauffret et al., 1999).

The sediments are largely marine sandstones, marls and limestones, whereas continental formations are preserved only sporadically. The sequence is formed by an Upper Burdigalian basal breccia lying above the Schistes Lustrés Nappe, followed by Upper Burdigalian to Serravallian marine marls, sandstones and conglomerates containing clasts from the Variscan basement, and Upper Serravallian continental conglomerates. The sequence continues with Tortonian limestones interbedded with siliciclastic material interpreted as a carbonate platform with material supplied from the Variscan basement. Clasts from the Schistes Lustrés first appear in the Lower Messinian deltaic

conglomerates. The youngest marine deposits of onshore Corsica are the sandy marls attributed to the Lower Pliocene (Loÿe-Pilot and Magné, 1989). The sequence ends with fluvial conglomerates of probably Upper Pliocene age (Loÿe-Pilot and Magné, 1978).

## 2.5 GEODYNAMIC EVOLUTION OF CORSICA WITHIN THE PLATE TECTONIC HISTORY OF THE WESTERN MEDITERRANEAN

During the Carboniferous (~360-320 Ma), convergence between the Gondwana and Laurasia continents led to the consumption of the intervening Paleotethys Ocean and to continental collision of both plates (Variscan orogeny), giving rise to Pangea continent (Stampfli et al., 2002). Continental collision induced syn-orogenic magmatic activity with calc-alkaline affinity, generating numerous granitoid intrusions, for instance the Corsica-Sardinia batholith, which at present forms a major part of Variscan Corsica and parts of Sardinia. Variscan convergence ended within the Late Carboniferous. The Permian to middle Triassic evolution of Pangea (Fig. 2-4) was characterized by an extensional tectonic regime with widespread post-orogenic plutonic and volcanic activity with alkaline affinity. The Carboniferous Corsica-Sardinia batholith was intruded by alkaline granites and overlain by alkali-rhyolitic complexes (e.g., Monte Cinto caldera).

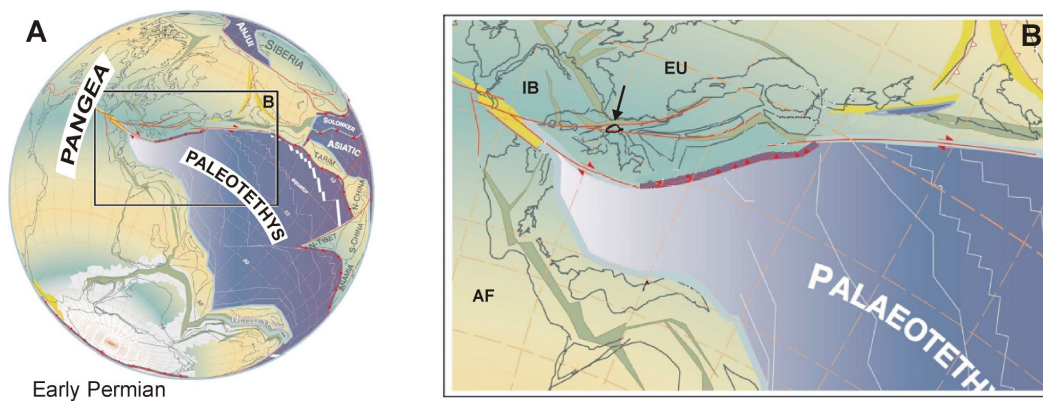


**Fig. 2-4:** Paleogeographic reconstruction of Paleotethys during the Late Permian (modified after Stampfli et al., 2002). Position of Corsica is indicated by an arrow in the figure B. AF - Africa, EU - Eurasia; IB - Iberia.

During Late Triassic to Jurassic times, rifting started (Frisch, 1981; Loup, 1992; Borel, 1995), and opening of the central Atlantic and the Ligurian-Penninic Ocean led to the final break-up of Pangea (Fig. 2-5). The Corsica-Sardinia block along with several other microplates (e.g., Calabria, Rif, Kabylies, Peloritani) formed the south-eastern margin of the Iberian plate at that time. To the west, the Iberian plate was separated from North America by the Atlantic Ocean, to the south from Africa by the

Ligurian-Piedmont Ocean. From the European plate the Iberian plate was detached in the Late Jurassic, when the Pyrenean rift system started to open and Valais Ocean developed.

Oceanic spreading continued until Cenomanian/Turonian times, when the African plate movement changed in a northward direction with respect to the Eurasian plate, resulting in a change from an extensional setting to convergence (Dewey et al., 1989). The Ligurian-Piedmont Ocean started to close and the European plate was subducted under the African plate (Fig. 2-5). During Late Cretaceous - Paleocene times, the Iberian plate collided with Europe, resulting in the Pyrenean thrust and fold belt (Olivet, 1996).

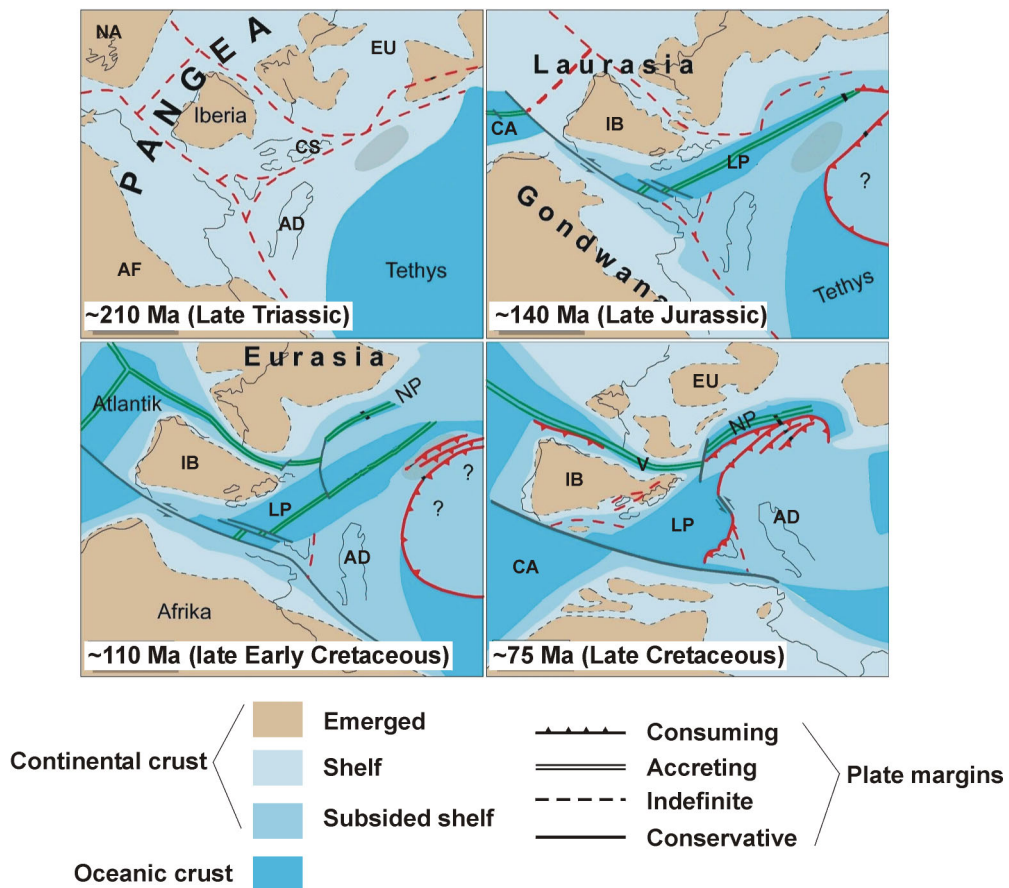


**Fig. 2-5:** Paleogeographic reconstruction of the Western Mediterranean region from the Late Triassic until the Late Cretaceous (modified after Frisch and Meschede, 2005). AD - Adria, AF - Africa, CA - Central Atlantic, CS - Sardinia-Corsica, EU - Eurasia, IB - Iberia, LP - Ligurian-Piedmont Ocean, NA - North America, NP - North Penninic Ocean, V - Valais Ocean.

The ongoing northward movement of the African plate (resp. the Apulian microplate) resulted in the emplacement of the ophiolitic successions derived from the Ligurian-Piedmont ocean (Alpine nappes) onto the Variscan basement of Corsica (Fig. 2-6). During the collision, flysch was deposited in the foreland basin in front of the approaching Alpine nappes. Thrusting of the Alpine nappes had polyphase character, lasting from the Late Cretaceous to the Late Eocene.

In the Early Oligocene, a "flip" of the subduction from SSE to NNW occurred, and the Apenninic subduction zone evolved, resulting in the transition from the compressional tectonic regime to an extensional one in the western Mediterranean region at ~33 Ma (R hault et al., 1984; Brunet et al., 2000). The Corsica-Sardinia block was still attached to the Iberian plate and formed its NE promontory (Gorini et al., 1993). In the Rupelian (~30 Ma), continental rifting commenced between southern France and Corsica-Sardinia in the zone of the future Gulf of Lion in response to the pull by

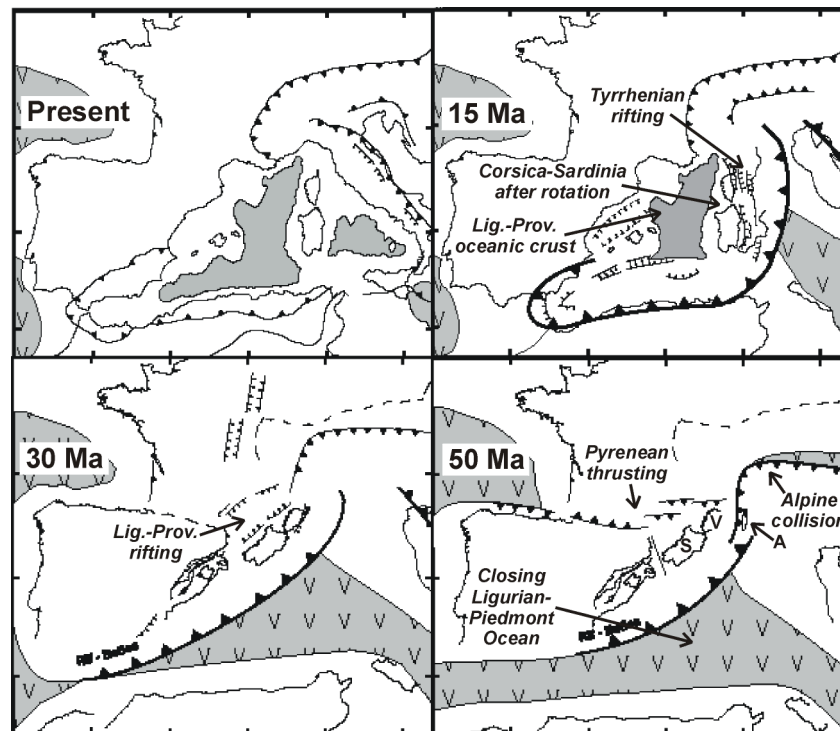


**Fig. 2-6:** Paleotectonic reconstruction of the Western Mediterranean region from the Eocene to present (modified after Lacombe and Jolivet, 2005). Gray shaded areas represent oceanic crust, V - Variscan Corsica, A - Alpine Corsica, S - Sardinia.

the eastward retreating Apenninic subduction zone (Bellaiche et al., 1976; Cherchi and Montadert, 1982; S eranne, 1999). The rifting resulted in the opening of the Ligurian-Proven al basin, splitting off the Corsica-Sardinia block from the European mainland (Fig. 2-6). From ~21 to 16 Ma, rifting was followed by oceanic spreading in the Ligurian-Proven al Basin, resulting in a ~30  counter-clockwise rotation of the Corsica-Sardinia block around a rotation pole located in the Gulf of Genoa (Montigny et al., 1981; Vigliotti and Langheim, 1995). At ~18 Ma, rifting moved to the east, initiating formation of extensional basins in central and eastern Corsica (Carmignani et al., 1995; Mauffret et al., 1999). During the Late Miocene, ongoing subduction rollback gave way to extension in the Tyrrhenian basin (presently separating Corsica-Sardinia from the Italian mainland; Fig. 2-6). In this framework, the Corsica-Sardinia block forms a microcontinent surrounded by two back-arc basins with respect to the westward dipping Apenninic subduction zone (Figs. 2-1 and 2-6; Doglioni et al., 1999; Zeck 1999).

The Western Mediterranean rifting phase is evidenced also by onshore and offshore occurrences of magmatic rocks in Sardinia, Corsica, Provence, the Ligurian-Provençal and the Tyrrhenian Basins since the Early Oligocene. Magmatic activity appears as (i) subduction-related calc-alkaline magmatism, indicating NW-dipping subduction of the Apulian plate beneath the Corsica-Sardinia block, and (ii) rift-related intraplate alkaline volcanism, which were both connected in space and time (Bellon, 1976; Coulon, 1977; Réhault et al., 1984; Pecerrillo, 2003).

## 2.6 PREVIOUS THERMOCHRONOLOGICAL STUDIES IN CORSICA

Several apatite fission track studies have been carried out in Corsica during the last decades, providing information on the Tertiary tectonothermal evolution of this region. However, older studies (Carpéna et al., 1979; Lucazeau and Mailhé, 1986; Mailhé et al., 1986), based on the population dating method, reported AFT ages older than  $^{40}\text{Ar}/^{39}\text{Ar}$  white mica ages (Brunet et al., 2000) and ZFT ages from the same samples, both indicating higher temperatures. Therefore they were considered to be inaccurate by some other authors (see discussion in Cavazza et al., 2001; Zarki-Jakni et al., 2004). More recent studies (Jakni, 2000; Jakni et al., 2000; Cavazza et al., 2001; Fellin, 2003; Zarki-Jakni et al., 2004; Fellin et al., 2005), based on the meanwhile preferred external detector dating method, report substantially younger AFT ages, in line with the higher-temperature thermochronometers.

Most studies focused on the investigation of the tectonothermal processes on the Alpine orogenic wedge in the NE part of Corsica, where the Alpine-Variscan contact is best exposed.

The study of Cavazza et al. (2001) reports AFT ages between  $19.6 \pm 3.5$  and  $13.8 \pm 1.6$  Ma from a W-E trending profile across the Variscan basement, the Alpine foreland and the Alpine wedge along the NE margin of the island. The data record an episode of exhumation during late Early Miocene times. No obvious difference in age among the structural units implies synchronous Neogene exhumation and absence of significant differential vertical displacement between footwall (Variscan Corsica) and hanging-wall (Alpine Corsica) in the study area. Inferring from the complete reset of foreland sedimentary samples, the authors also proposed that prior to the late Early Miocene, northern Corsica was covered by either the Alpine nappes or the foreland deposits.

Studies of Jakni (2000), Jakni et al. (2000) and Zarki-Jakni et al. (2004) report AFT data both from Alpine and Variscan Corsica. The AFT cooling ages from Alpine Corsica, ranging from  $22.5 \pm 1.2$  to  $12.3 \pm 2.9$  Ma, are coherent with those of Cavazza et al. (2001). From Variscan Corsica, a relatively wide AFT age spectrum is presented (from  $53.8 \pm 4.1$  to  $10.5 \pm 0.8$  Ma), forming a clear spatial pattern (Fig. 2-7): older AFT ages ( $> 30$  Ma) show broad track length distributions and occur in the SW part of the island. Younger AFT ages ( $< 30$  Ma) with narrow track length distributions form a

crescent-shaped pattern running from the NW to the SE, where ages become younger with decreasing distance to the Alpine thrust front. The ages from the W and NW coast are interpreted to record cooling related to erosional denudation, which is attributed to the rifting in the Ligurian-Provençal Basin and passive margin uplift of Variscan Corsica. The younger ages close to the Alpine front are interpreted as recording a cooling related to eastward migration of the locus of extension from the Ligurian-Provençal to the Tyrrhenian Basin.



**Fig. 2-7:** Distribution of AFT ages proposed by Zarki-Jakni et al. (2004).

Studies of Fellin (2003) and Fellin et al. (2005) report AFT data (in range from  $30.5 \pm 3.2$  to  $12.7 \pm 2$  Ma) integrated with detailed structural and sedimentological analyses from the Neogene basins of central and NE Corsica. The results indicate rapid cooling related to exhumation of the pre-Neogene basement (Variscan and Alpine units) during the Early to Middle Miocene. The exhumation was accompanied by normal faulting, leading to subsidence and formation of a narrow basin in central and eastern Corsica since the Burdigalian. This basin was inverted during the Tortonian, in the course of final exhumation.

In order to evaluate the thermotectonic evolution of Corsica in higher temperature levels than the apatite FT system can provide, relevant results obtained by high-temperature thermochronometers are briefly reviewed.

The first zircon FT study from Corsica was presented by Mailhé et al. (1986), however as in the case of AFT data from the same study, the ZFT results were not considered by later authors (see Cavazza et al., 2001; Fellin, 2003; Zarki-Jakni et al., 2004; Fellin et al., 2005) although their accuracy has never been disproven. The ZFT ages, ranging between 225 and 36 Ma, show a

clear trend of decreasing age from west to east. This is interpreted as partial reset of Variscan ages due to varying thicknesses of the Alpine nappe pile during collision. More recently, some additional ZFT ages (19, 21, 74, 69 Ma) were reported from Alpine Corsica (Zattin et al., 2001; Fellin et al., 2005). These ages do not conflict with the data of Mailhé et al. (1986) and provide new constraints on the timing of Alpine metamorphism.

In contrast to ZFT data, a quite large number of  $^{39}\text{Ar}/^{40}\text{Ar}$  mica ages is reported from NE Corsica (Maluski, 1977; Amaudric du Chaffaut and Saliot, 1979; Mailhé, 1982; Jourdan, 1988; Lahondère, 1991; Brunet et al., 1997; Brunet et al., 2000), ranging between ~65 and 25 Ma. A summarizing interpretation was presented by Brunet et al. (2000) who argued for the thrusting of

Alpine nappes onto the Variscan basement lasting from ~45 to 32 Ma, followed by inversion of shear sense and reactivation of thrust planes as extensional shear zones resulting in the tectonic denudation of metamorphic rocks from below the Alpine nappes starting at 33 and lasting to 25 Ma.

An important constraint on the age of HP/LT metamorphism was provided by Lahondère and Guerrot (1997), who reported a Sm/Nd age of  $\sim 83.8 \pm 4.9$  Ma (isochron defined on a whole rock-garnet-glaucophane-clinopyroxene assemblage) from an eclogitic lens in the gneissic rocks of Serra di Pigno - Farinole unit (later referred to as SPF unit, for location see Fig. 7-1-1), pointing to a Cretaceous age of HP metamorphism in the Schistes Lustrés Nappe s. l.

### 3 GEOMORPHOLOGICAL SETTING

#### 3.1 INTRODUCTION

Corsica exhibits some spectacular geomorphological features. For instance, the highest point (Monte Cinto), reaching 2706 m a.s.l., is located only in 24 km from the coast and 50 km from the toe of the continental margin; there are 20 peaks of over 2000 meters; both the maximum and mean elevation, as well as the mean relief of Corsica, is substantially higher than those of any other Western Mediterranean island.

From the morphological standpoint, there are substantial differences between Alpine and Variscan Corsica (Fig. 3-1).

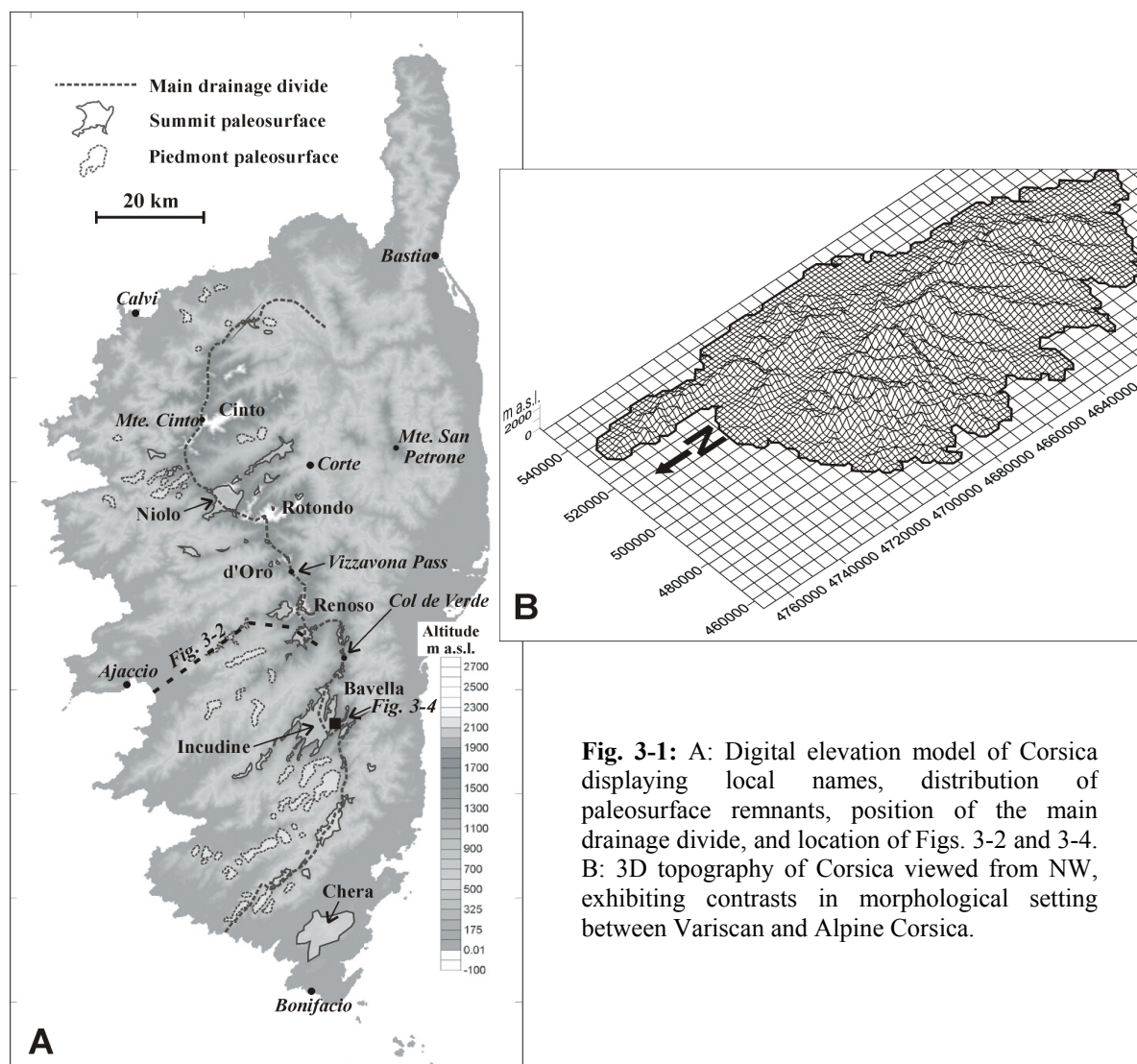


**Fig. 3-1:** A: Digital elevation model of Corsica displaying local names, distribution of paleosurface remnants, position of the main drainage divide, and location of Figs. 3-2 and 3-4. B: 3D topography of Corsica viewed from NW, exhibiting contrasts in morphological setting between Variscan and Alpine Corsica.

Alpine Corsica is characterized by a moderate relief with the large Oriental Plain in the east. The maximum altitude of 1767 m (Mte. San Petrone), and the mean elevation and relief are significantly lower than in Variscan Corsica.

Variscan Corsica is characterized by a rugged mountainous relief with altitudes exceeding 2000 m, where the peak and mean elevations increase from the S to the N. In map view, the most prominent morphologic features are SW-NE trending ridges, deeply incised by fault-controlled linear gorges (Fig. 3-1B). According to bathymetric maps, the relief character continues offshore, where the ridges and valleys form narrow peninsulas and deep submarine canyons, respectively.

The S-shaped main drainage divide clearly shows an asymmetry with respect to distribution of the highest central peaks (Fig. 3-1A). The Vizzavona Pass (1163 m a.s.l., the lowest pass of the main drainage divide situated in the central part of the island), separates two different morphological domains within the Variscan Corsica. North of this pass, the main drainage divide is located several km west of the highest peaks on the SW-NE trending ridges, and reaches its minimum distance to the west coast SE of Calvi. South of the Vizzavona Pass, all the highest peaks are aligned along the main drainage divide. Further to south, the main drainage divide is shifted to the east: south of Col de Verde it is located less than 15 km from the east coast and more than 40 km from the west coast. Such an asymmetrical drainage divide pattern indicates differential uplift and tilting.

The tectonic boundary between Variscan and Alpine Corsica is morphologically accentuated by the deep longitudinal valleys of the Ostriconi and Golo rivers, as well as by the steep eastern margin of Variscan Corsica with triangular facets, which are typical for active normal faults.

## 3.2 CHARACTERISTICS OF THE PALEORELIEF

On a smaller scale, paleorelief remnants, forming flat plateaus with slightly undulating relief, are the most striking features (Fig. 3-1A). Paleorelief can be discriminated from the "recent" relief by analyzing the slope angles along hypsometric profiles. The term "recent" relief is referred here to areas without breaks in the slopes in hypsometric river profiles, equilibrated to the recent sea-level. Typically, the slope angles of the "recent" relief increase from the coast landward up to an edge (Fig. 3-2). Above this edge much lower slope angles, again increasing inland, are observed. These edges basically represent breaks in slopes and border the paleorelief areas. Calculated slope angle distribution shows differentiation between recent and paleorelief (see Fig. 3-3): paleorelief areas display a median of 14 degrees, whereas areas of recent relief display a median of 23 degrees (Kuhlemann et al., 2005a). Kuhlemann et al. (2005a), based on the field observation and analysis of a digital elevation model (DEM) and topographic maps (at a scale of 1:25000, IGN France), identified

two levels of paleorelief in Corsica: (i) a summit paleosurface and (ii) a piedmont-type planation paleosurface.

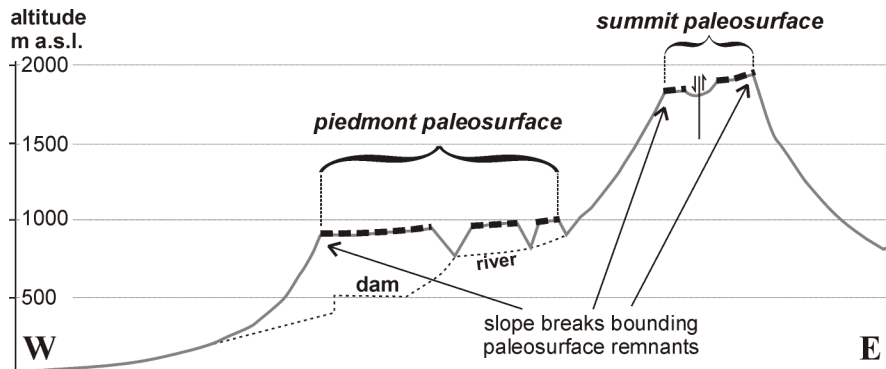


**Fig. 3-2:** Simplified topographic profile illustrating the geometric relation between summit and piedmont paleosurfaces (thick dashed lines) proposed by Kuhlemann et al. (2005a). For location of the profile see Fig. 3-1 (modified after Kuhlemann et al., 2005a).

Remnants of the **summit paleosurface** form plateaus and flat ridges, which are bound by cliffs or steep slopes (Fig. 3-4). They are located in the central parts of Variscan Corsica at the level of local summits (therefore "summit" paleosurfaces) at elevations from 300 up to 2300 m a.s.l. They are dissected by faults and tilted in variable direction around larger angles than the piedmont-type paleosurface. Slope angles of the summit paleosurface range between 8 and 40 degrees (Fig. 3-3). Steep slope angles are related to isolated durable knobs of cupola-type morphology (Glockenberge) and former knobs largely or completely decomposed to giant granite boulders (Felsburgen; Klaer, 1956), typically found in southern Corsica. Many summit surface fragments have been tectonically tilted by several degrees, which is largely transferred to an increase of the mean slope angle.

Remnants of the **piedmont-type planation paleosurface** (called piedmont paleosurface further on) are located along the eastern periphery of the Variscan basement at elevations from 250 to 900 m a.s.l., and bordered by cliffs and deep canyons. They are generally tilted to a lesser degree than the summit paleosurface - slope angle distributions reveal a median of about 8 degrees (Fig. 3-4). The direction of the tilt is uniformly towards the SW in the major part of Variscan Corsica. An exception is observed in the foothills along northern coast, where relics of the piedmont paleosurface are downthrown and tilted towards the inland (i.e., to the SE) due to NE-SW trending normal listric faults. The slightly tilted piedmont paleosurface areas never reach the sea-level,

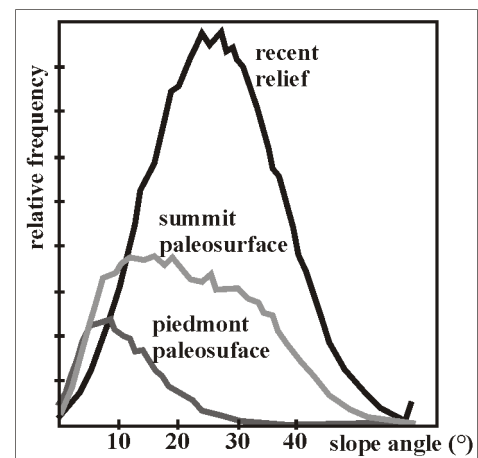


**Fig. 3-3:** Schematic diagram showing slope angle contrast between recent relief and two paleosurface generations (redrawn after Kuhlemann et al., 2005a).

but end at altitudes between 250 and 400 m, where they are substituted by recent relief continuing down to the coast.

According to Kuhlemann et al. (2005a), the relations between both generations of the paleosurfaces can be well examined in southern Corsica in the Incudine Massif. The Incudine massif represents the largest paleorelief area ( $\sim 30 \text{ km}^2$ ), with both generations preserved (Fig. 3-2). The summit surface at an elevation of  $\sim 2000 \text{ m}$  is cut by SW-NE trending faults, and dissected segments are vertically displaced and tilted to various directions. In contrast, the related piedmont paleosurface at elevations of  $\sim 900 \text{ m}$  displays a uniform tilt to the SW without relevant vertical displacement along the faults, which cut the summit surface. In other words, the piedmont paleosurface seal faults, which are cutting the summit paleosurface. This means that formation of the piedmont paleosurface postdates the dissection, vertical displacement and tilting of the summit paleosurface. Based on the available AFT data, sedimentological, structural and morphological observations, Kuhlemann et al. (2005a) proposed a scenario for relief evolution. According to this scenario, the summit paleosurface started to form after Late Eocene to mid-Oligocene uplift, during a phase of decline of relief until late Early Miocene time. At  $\sim 17 \text{ Ma}$ , a tectonic event caused uplift and tilting of the summit paleosurface. After this uplift pulse, during a subsequent stagnation period in the Middle Miocene the piedmont paleosurface formed. At  $\sim 11\text{-}10 \text{ Ma}$ , another event caused uplift and tilting of both piedmont and summit paleosurfaces.

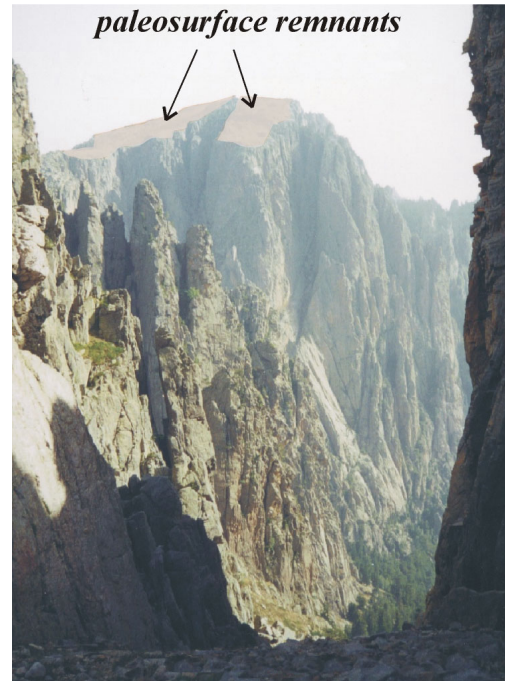


**Fig. 3-4:** Example of a summit paleosurface in southern Corsica. For location see Fig. 3-1 (courtesy of J. Kuhlemann).

## 4 FISSION TRACK AND (U-TH)/HE DATING TECHNIQUES

### 4.1 FISSION TRACK THERMOCHRONOLOGY

#### 4.1.1 Introduction

The following chapter contains an abridged description of the principles of the FT dating technique. For readers having solid theoretical background in the field of FT analysis it is recommended to skip this chapter. Readers interested in details of the method are referred to the book of Wagner and Van den haute (1992).

Fission track thermochronology as a geological dating tool was first introduced in the early 1960s (Price and Walker, 1963), and since then has been applied to a variety of geological problems, including the tectono-thermal evolution of mountain belts, passive and active margins, sedimentary provenance, and thermal history modeling of sedimentary basins.

#### 4.1.2 Fission track formation

Formation of a fission track is described by the ion spike explosion model (Fleischer et al., 1975). According to this model (Fig. 4-1), when a  $^{238}\text{U}$  atom decays by spontaneous fission, it splits into two highly charged particles, which travel through the crystal lattice of the host mineral in opposite direction, creating tiny linear zones of damage: fission tracks (Wagner, 1968; Fleischer et al., 1975). These natural tracks, or commonly referred to as spontaneous tracks, are produced almost exclusively by spontaneous fission of  $^{238}\text{U}$  in most natural materials, since other naturally occurring isotopes such as  $^{235}\text{U}$  and  $^{232}\text{Th}$  have much slower rates of decay by fission (Price and Walker, 1962). Fission tracks produced in the solids are very tiny (3-14 nm in width) and can be observed only under transmission electron microscope. However, Price and Walker (1962) showed that chemical etching enlarges the tracks so that they can be observed under an optical microscope (magnification > 500x; see Fig. 4-2).

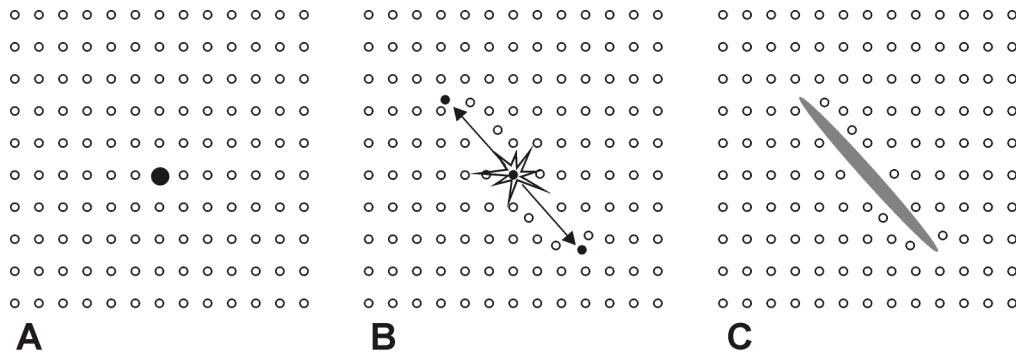


**Fig. 4-1:** Schematic illustration of the ion spike explosion model for the formation of a fission track (Fleischer et al., 1975). A: Trace amounts of  $^{238}\text{U}$  are present in the crystal lattice (black dot). B: Spontaneous fission of  $^{238}\text{U}$  produces two highly charged particles that recoil as a result of Coulomb repulsion. Passage of the charged particles causes damage to the crystal lattice through electron stripping and ionization. C: After the fission particles come to rest a damage trail, or fission track, is left. These cannot be observed optically unless chemically etched (redrawn after Gallagher et al., 1998).

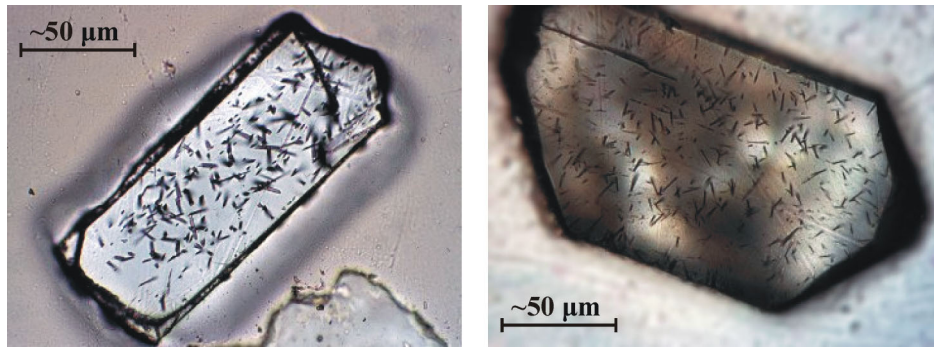


**Fig. 4-2:** Photographs of spontaneous fission tracks in apatite (left) and zircon (right) revealed by etching (modified from: Geotrack website, [www.geotrack.com.au](http://www.geotrack.com.au)).

### 4.1.3 Age calculation

The fact that the fission process occurs at a constant rate predestined the method as a tool for dating minerals. In principle, the method, similarly to other conventional isotopic dating methods, relies on the determination of the relative abundance of the parent and daughter product. In the case of fission track, the parent is  $^{238}\text{U}$  and daughter product is the physical damage to the crystal lattice, i.e. spontaneous fission tracks. The abundance of daughter product is determined by counting the number of spontaneous tracks on a given surface of a mineral grain. In order to determine the  $^{238}\text{U}$  abundance, the sample is irradiated with low-energy thermal neutrons, which induce fission in  $^{235}\text{U}$  and formation of induced fission tracks. Provided that the thermal neutron flux is monitored, the number of induced fission tracks is indicative of the abundance of  $^{235}\text{U}$ . Because the ratio  $^{235}\text{U}/^{238}\text{U}$  is constant in nature, it is possible to determine the abundance of  $^{238}\text{U}$ . In terms of the analytical procedure, there are several

techniques used for age determination (see Gleadow, 1981). In this study, the external detector method (EDM) has been used (Gleadow and Duddy, 1981; see Appendix B for detailed description), since this approach has several advantages (e.g., it allows to analyze individual grains) and was recommended by IUGS (Hurford, 1990a,b). Two problems arise: (i) uncertainty of the exact value of the decay constant of  $^{238}\text{U}$  and (ii) inaccurate determination of the neutron fluence. To overcome these problems, the  $\zeta$  ("zeta") calibration method has been introduced (Hurford and Green, 1983). In the  $\zeta$  method the age of a sample is calibrated against one or more age standards. The method consists of two steps. First, age standards are repeatedly irradiated and analyzed together with a uranium bearing glass monitor in order to establish a calibration factor  $\zeta$ .  $\zeta$  calibration factor (or zeta factor) is a personal value depending on the observer's ability of track recognition and is calculated as:

$$\zeta = \frac{(e^{\lambda_d T_{std}} - 1)}{\lambda_d \left( \frac{\rho_s}{\rho_i} \right)_{std} g \rho_d}$$

where  $\zeta$  is the zeta calibration factor ( $\text{year}/\text{cm}^2$ );  $\lambda_d$  is the decay constant of  $^{238}\text{U}$ ;  $T_{std}$  is age of the age standard used; for calibration  $t$  is the age;  $\rho_i$  is neutron-induced track density from  $^{235}\text{U}$  ( $\text{track}/\text{cm}^2$ );  $\rho_s$  is spontaneous track density from  $^{238}\text{U}$  ( $\text{track}/\text{cm}^2$ );  $g$  is the geometry factor (0.5 for EDM; Wagner and Van den haute 1992);  $\rho_d$  is track density in the external detector covering the glass dosimeter during irradiation ( $\text{track}/\text{cm}^2$ ). Author's zeta calculation and a list of age standards used in this study are presented in Appendix B.

The associated standard error for the  $\zeta$  factor is calculated according to Green (1981) as follows:

$$\sigma(\zeta) = \zeta \sqrt{\frac{1}{N_s} + \frac{1}{N_i} + \frac{1}{N_d} + \left[ \frac{\sigma(T_{std})}{T_{std}} \right]^2}$$

where  $N_s$ ,  $N_i$  and  $N_d$  are the numbers of spontaneous, induced and glass dosimeter tracks counted;  $\sigma$  ( $T_{std}$ ) and  $T_{std}$  are the standard error and age of the age standard used for calibration.

The final fission track age equation for a single grain is written as (Price and Walker, 1963; Naeser, 1967):

$$t = \frac{1}{\lambda_d} \ln \left( \lambda_d \frac{\rho_s}{\rho_i} \rho_d \zeta g + 1 \right)$$

where  $t$  is the age;  $\rho_s$  and  $\rho_i$  are the spontaneous and induced track densities.

The age calculation used in the EDM is based on Poissonian statistics, assuming that all grains are from a single population. To test whether all grains are indeed from a single population, a  $\chi^2$ -test is

performed on single grain data (Galbraith 1981). A value of  $P(\chi^2) < 5\%$  is accepted by a major fraction of the FT community as the evidence of a heterogeneous population. Typically the age of the sample is presented as some kind of average of the individual (usually  $> 20$ ) single grain ages. There are three age calculations in common use: the mean, pooled, and central ages. Throughout this study the fission track ages are reported as central ages with  $2\sigma$  errors, calculated according to Galbraith and Laslett (1993) as:

$$T_{central} = \left(\frac{1}{\lambda_d}\right) \ln \left[ 1 + (g\lambda_d \zeta \rho_d) \frac{\eta}{1-\eta} \right]$$

where  $T_{central}$  is the central FT age (Ma);  $\eta$  is the weighted mean average of  $N_s/N_i$  with weight  $w_j$ .

#### 4.1.4 Fission track annealing and modeling

Fission tracks are metastable features that fade, which lead to their shortening until they totally disappear. This process is called "annealing" and is mainly controlled by the temperature (Fleischer et al., 1964, 1965, 1975; Wagner, 1968). Nevertheless the chemical composition of the crystals, crystal structure and pressure also play roles (Green et al., 1986; Carlson, 1990; Wendt et al., 2002; Barbarand et al., 2003). Annealing occurs over a certain temperature range, generally referred to as the partial annealing zone, or PAZ (e.g., Wagner 1979). Above this temperature range the fission tracks are completely annealed for a residence time of less than  $10^6$  years, and this zone is referred to as the total annealing zone. As a consequence of the track shortening, the fundamental parameter in FT analysis is the track length distribution, which, vice versa, contains information on the thermal history of a sample.

For the fission track system of apatite, the PAZ ranges from  $\sim 60^\circ\text{C}$  to  $\sim 120^\circ\text{C}$  (see Fig. 4-4), with a mean effective closure temperature of  $110 \pm 10^\circ\text{C}$  (Laslett et al., 1987; Green and Duddy, 1989). Two additional factors control the annealing of apatites: chemical composition and the track orientation with respect to the crystallographic c-axes. The influence of the apatite chemical composition on annealing is still not comprehensively understood, despite the large number of studies. It is accepted that the relative proportions of Cl and F play important roles in the annealing process. Cl-apatite is more resistant to annealing than F-apatite (Gleadow and Duddy, 1981; Green et al., 1986; Green, 1988; Donelick, 1991; O'Sullivan and Parrish, 1995), which has direct impact on the limits of the PAZ (e.g., Carlson et al., 1999). However, relatively little is known about the role of other ions such as OH or Mn (Ravenhurst et al., 1992; Bergman and Corrigan, 1996). Regarding the track orientation with respect to the crystallographic c-axes, it was shown that tracks at higher angles to the

c-axis anneal faster than tracks at lower angles (Green et al., 1986; Donelick et al., 1990; Crowley et al., 1991).

Annealing behavior can be characterized in different manners, for instance by determination of the Cl content. In this study, the annealing kinetics was assessed by measurement of parameter called "Dpar" (Dpar - is the etch pit diameter of fission track parallel to the crystallographic c-axis at the polished, etched, and analyzed apatite surface; Crowley et al., 1991; Naeser, 1992; Burtner et al., 1994), as it is regarded as the best parameter to characterize the effect of chemical composition on annealing (Ketcham et al., 1999). A small Dpar value (1.50-2.00  $\mu\text{m}$ ) is typical of faster-annealing F-apatite and a larger Dpar value (2.00-5.00  $\mu\text{m}$ ) is typical of slower-annealing Cl- and OH-apatites.

Despite several recent studies in the recent times (e.g., Hasebe et al., 1994; Yamada et al., 1995a,b; Tagami et al., 1998), the knowledge of zircon partial annealing is not yet as advanced as that of apatite so far. The most recent results suggest a range of temperatures for the zircon PAZ between 200°C and ~350°C (Tagami et al., 1998), and an effective closure temperature of  $240 \pm 50^\circ\text{C}$  for cooling rates of  $\sim 10^\circ\text{C}/\text{My}$  (Hurford, 1986).

In case of apatite, a combination of the FT age and related track length distribution enables one to decipher the thermal history of a sample, since the apatite annealing characteristics obtained from laboratory experiments were described by several mathematical models (e.g., Laslett et al., 1987; Carlson, 1990; Crowley et al., 1991; Ketcham et al., 1999). To date, several sophisticated modeling programs exist, which enable to model the time-temperature (tT) path of a sample. For this study the HeFTy Beta Release 1a (later referred to as HeFTy) written by R. Ketcham with the multi-kinetic annealing model of Ketcham et al. (1999) and Dpar values as kinetic parameter was used for the thermal history modeling. The program defines time-temperature (tT) paths, passing statistical criteria and conforming to user-entered constraints, that best reproduces the measured data. A more detailed description of what the program does is given in Appendix B.

## 4.2 APATITE (U-TH)/HE THERMOCHRONOLOGY

This chapter presents a more detailed description of basic principles of the (U-Th)/He dating method (with focus on apatite) since this method is newly adopted at Tübingen University, and in this project the setup of the He measuring facility was a difficult challenge with which to cope.

### 4.2.1 Introduction

At the beginning of the 20th century, the decay of U and Th to He was already recognized by scientists and used as a potential tool to date minerals (Rutherford, 1905; Strutt, 1905, 1908, 1909). However, the technique was effectively abandoned, as it frequently yielded unreasonably low ages (Hurley, 1954), and relegated by other, better-developed dating methods such as U/Pb or K/Ar. During the late 1980's and early 1990's, renewed interest in the method and improvements in analytical technique led to better understanding of the behavior of helium, and resulted in the first successful dating of U and Th bearing minerals (e.g., Zeitler et al., 1987; Lippolt and Weigel, 1988; Wernicke and Lippolt, 1992, 1994a,b; Lippolt et al., 1994; Wolf et al., 1996a,b, 1998; Warnock et al., 1997). Modern experimental results show that the (U-Th)/He system of apatite is sensitive to temperatures between ~40-80°C (calculated closure temperature is ~75°C at a cooling rate of 10°C/km) that is the lowest temperature zone among all radiometric methods (Wolf et al., 1996a). Further, it was demonstrated that this technique could be successfully used to answer various geological questions concerning rock cooling in the uppermost crust (e.g., House et al., 1997, 2001; Stockli et al., 2000; Persano et al., 2002; Foeken et al., 2003; Balestrieri et al., 2005).

### 4.2.2 He ingrowth

(U-Th)/He dating is based on the ingrowth of  $^4\text{He}$  nuclei ( $\alpha$  particles) produced by the series decay of  $^{238}\text{U}$ ,  $^{235}\text{U}$ , and  $^{232}\text{Th}$ . In time  $t$  the amount of  $^4\text{He}$  produced in a mineral is given by the following equation:

$$^4\text{He} = 8^{238}\text{U}(\exp(\lambda_{238\text{U}}t)-1) + 7(^{238}\text{U}/137.88)(\exp(\lambda_{235\text{U}}t)-1) + 6^{232}\text{Th}(\exp(\lambda_{232\text{Th}}t)-1)$$

where  $^4\text{He}$ ,  $U$ , and  $Th$  refer to present-day amounts of parent and daughter nuclides;  $\lambda$ 's are the decay constants ( $\lambda_{238\text{U}} = 1.55125 \cdot 10^{-10} \text{ a}^{-1}$ ,  $\lambda_{235\text{U}} = 9.8485 \cdot 10^{-10} \text{ a}^{-1}$ ,  $\lambda_{232\text{Th}} = 4.9475 \cdot 10^{-11} \text{ a}^{-1}$ ); 137.88 $^{-1}$  is the present-day  $^{235}\text{U}/^{238}\text{U}$  ratio;  $t$  is the accumulation time, which can be calculated numerically (by applying Taylor expansion) since there is no analytical solution for  $t$ . This equation holds for secular

equilibrium among all daughters in the decay chain and assumes that initial  $^4\text{He}$  present in the crystal being dated is zero. However, the latter is not always true, because He is often trapped in the fluid inclusions hosted by the dated crystals. This He is inherited from some prior history but does not originate from U and Th of the apatite grain itself, and thus will result in older ages. Furthermore, apatite grains often contain solid inclusions of other U or Th rich minerals such as zircon or monazite (Ehlers and Farley, 2003), that would also result in erroneously high He ages and poor He age reproducibility of samples. In order to overcome problems with inclusions, the crystals are microscopically examined and only inclusion-free grains selected for further work. However, inclusions can be too small to be detected under a normal microscope. Moreover, in the majority of the samples it is very difficult to find completely inclusion free apatites. In order to check the accuracy of the analytical technique it is recommended to measure a sample in several replicates and test whether they reproduce well or scatter due to possible presence of inclusions.

### 4.2.3 Alpha recoil correction

Alpha particles (i.e. helium nuclei) emitted during U and Th series decay have high kinetic energy (4-8 MeV), which mean that they can travel several micrometers through the solid matter before coming to rest. The traveled distance, known as the stopping distance, varies between ~11 and 34  $\mu\text{m}$  for the various U and Th series decay (Ziegler, 1977), whereby the series averaged mean stopping distance for  $^{238}\text{U}$ ,  $^{235}\text{U}$ , and  $^{232}\text{Th}$  is 19.68  $\mu\text{m}$ , 22.83  $\mu\text{m}$ , and 22.46  $\mu\text{m}$ , respectively (Farley et al., 1996). Consequently,  $\alpha$  particles may be ejected from crystal rims or injected from surrounding grains, which may have an effect on the final age (see Fig. 4-3). Farley et al. (1996) developed a quantitative model for correcting He ages for the effects of  $\alpha$  stopping distances based on measured grain geometry and size. The model requires the following assumptions: (i) homogenous distribution of U and Th in dated crystal; (ii) implantation of  $\alpha$  particles from the surrounding matrix is insignificant; (iii) hexagonal prism or spherical geometry of dated crystals. If these assumptions are met, the total amount of  $\alpha$  particles retained in the apatite crystal is described by the  $F_t$  correction factor (Farley et al., 1996), and the measured age must be divided by the  $F_t$  factor to obtain the "corrected age". For a hexagonal prism, the  $F_t$  factor is calculated as follows:

$$F_t = 1 + a_1\beta + a_2\beta^2$$

where  $a_1$  and  $a_2$  are fit parameters incorporating the stopping distance and density of the stopping medium. For an apatite hexagonal prism,  $a_1 = -5.13$  and  $a_2 = 6.78$  for the  $^{238}\text{U}$  series;  $a_1 = -5.9$  and  $a_2 = 8.99$  for the  $^{235}\text{U}$  and  $^{232}\text{Th}$  series (Farley, 2002);

$$\beta = (2.31L + 2R) / RL$$

where  $R$  is the radius and  $L$  is the length of the prism. Given that stopping distances of parent nuclides are slightly different, the mean  $F_t$  is calculated as follows (Farley, 2002):

$$^{mean}F_t = a_{238}^{U238} F_t + (1 - a_{238})^{Th232} F_t$$

where  $F_t$ 's are correction factors of corresponding parent nuclides;  $a_{238}$  is the fraction derived from  $^{238}\text{U}$  that can be exactly calculated from the first equation, or approximated from the measured Th/U ratio for integration period of  $< \sim 200$  My as:

$$a_{238} = (1.04 + 0.245(Th/U))^{-1}$$

The  $\alpha$  corrected He age is then calculated as:

$$\text{Corrected Age} = \text{Measured Age} / ^{mean}F_t$$

From the calculation presented above it is clear that smaller grains require greater correction. Farley (2002) argued that  $F_t$  correction in the range of  $\sim 0.65$  to  $\sim 0.85$  can be reproduced by individual

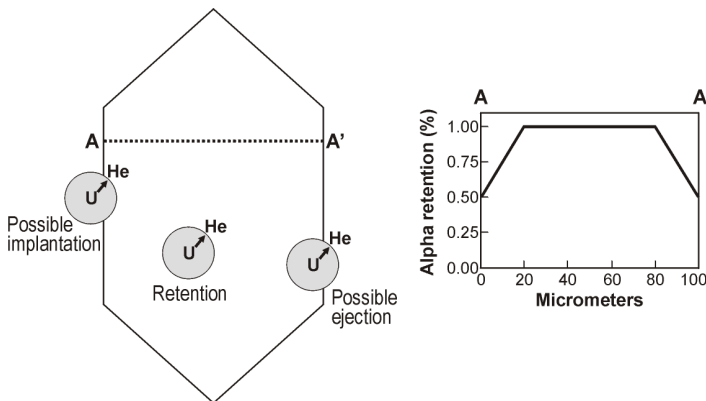


**Fig. 4-3:** The effects of long  $\alpha$  stopping distances on He retention. The left figure illustrates the three relevant possibilities within a schematic crystal:  $\alpha$  retention, possible  $\alpha$  ejection, and possible  $\alpha$  implantation. “U” denotes the site of the parent U or Th nuclide, and the edge of the shaded sphere labeled He indicates the locus of points where the  $\alpha$  particle may come to rest; the arrow indicates one possible trajectory. The right plot shows schematically how  $\alpha$  retention changes from rim to core to rim along the path A-A’ (modified after Farley, 2002).

observers to  $\sim 1\%$ . However at smaller grain size ( $F_t < 0.65$ ) the error is much higher, which would lead to erroneous "correction" of measured ages. Therefore for a proper  $\alpha$  ejection correction, the big crystals (prism width  $> \sim 70 \mu\text{m}$ ) with appropriate morphology (in best case euhedral prisms) are required. To calculate  $F_t$ , the grains are photographed and width and length of the prism are measured. A description of the grain selection procedure used in TU is given in the chapter 5.4.1.

One of the problems with  $\alpha$  recoil correction is the assumption of a

homogenous distribution of parent nuclides (Farley et al., 1996; Farley, 2000; Meesters and Dunai, 2002b). If this assumption is not met,  $\alpha$  recoil correction is an oversimplification. In this study, the distribution of U was investigated on FT mounts, and no zonality was observed. Thus, assuming that Th distribution follows U,  $\alpha$  recoil correction is used as a safe approach.

Although the  $F_t$  correction is widely accepted and routinely applied as a robust procedure, Meesters and Dunai (2002b) noted that this approach must not always be correct even if all assumptions are met. They showed that in the case when a sample with homogenous U and Th distribution spends substantial time close to the closure temperature for the system, the diffusion significantly affects the final He age, and applying the  $F_t$  correction will result in overcorrection of the He age. Conversely, in the case of quickly cooled rocks, which experience little diffusive loss, the  $F_t$  correction can be used as a safe approximation for correcting He ages.

#### 4.2.4 Sensitivity of the apatite (U-Th)/He thermochronometer

Pioneering studies demonstrated that helium retention in apatites occurs at very low temperatures  $< 100^\circ\text{C}$  (Lippolt et al., 1994). Based on the laboratory He diffusion characteristics, Wolf et al. (1998) showed that for a constant holding time, the He age decreases with increasing temperature over a fairly narrow temperature range. This range is named the Helium Partial Retention Zone - HePRZ, and is defined as a temperature range, in which between 5 and 95% of the He is retained in a crystal. The HePRZ is analogous to the apatite partial annealing zone (see chapter 4.1.4). Assuming an

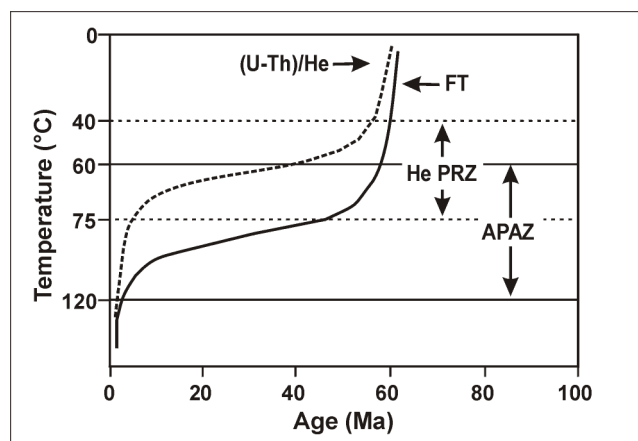


**Fig. 4-4:** Apatite helium partial retention zone (He PRZ) compared to apatite fission track partial annealing zone (APAZ), modified after Farley (2002).

isothermal holding time of 100 Ma and zero exhumation, it has a characteristic sigmoidal shape (Fig. 4-4), where the ages above the HePRZ are old, documenting complete retention of helium; ages within the HePRZ decrease rapidly with increasing temperature, where helium diffusion is neither fast enough to maintain a zero concentration, nor slow enough for complete retention of helium; ages are  $\sim 0$  Ma below HePRZ, because helium readily diffuses. Further laboratory experiments showed that helium diffusion is a function

of crystal size (Fig. 4-5) and shape, cooling rate, holding time and distribution of parent nuclides in the crystal (Lippolt et al., 1994; Wolf et al., 1998; Farley, 2000; Meesters and Dunai, 2002a,b). Variation

in any of these parameters results in a change of the amount of helium retained in a crystal, and consequently influences the temperature range of the HePRZ. For instance, for a holding time of 50 Ma and cooling rate of  $10^{\circ}\text{C}/\text{Ma}$ , the HePRZ is between  $\sim 40\text{-}75^{\circ}\text{C}$  (Wolf et al., 1998).

The apatite (U-Th)/He system records the temperature history experienced by rocks in the uppermost  $\sim 3$  km of the crust. He ages can be basically interpreted in two ways, as (i) "cooling" ages or (ii) "apparent" ages. Interpretation of cooling ages is based on the concept of "closure temperature" (Dodson, 1973) and can be used for samples, which experienced constant monotonic cooling. In this case, He age records a time since a sample passed through the closure temperature isotherm. However, for complex thermal histories the assumption of monotonic cooling is not met, thus the interpretation as "cooling age" is not relevant and modeling of time-temperature ( $tT$ ) history is required (Wolf et al., 1998). Since various  $tT$  paths modeled can yield the same He age (see Fig. 4-6, next page), and He ages do not necessarily refer to a distinct geological event, interpretation as "apparent" ages is rather used (as often in the case of FT ages). Thermal history and corresponding He age must be therefore tested by a model.

In this study, (U-Th)/He ages were modeled, like in the case of AFT data, by the computer program HeFTy. Description of the program is presented in Appendix B. An advantage of HeFTy is its capability to model both AFT and (U-Th)/He data. A combination of (U-Th)/He and AFT systems offers an opportunity to reconstruct detailed cooling histories through the temperature range of  $\sim 120$  to  $40^{\circ}\text{C}$ , since the sensitivity zones of both systems partly overlap (PAZ:  $\sim 60\text{-}120^{\circ}\text{C}$ , HePRZ:  $\sim 40\text{-}75^{\circ}\text{C}$ ) (see Fig. 4-4). The advantage of this approach is that it relies on two completely independent methods, providing important cross-validation of both systems, and therefore helps to reduce the number of acceptable thermal histories.

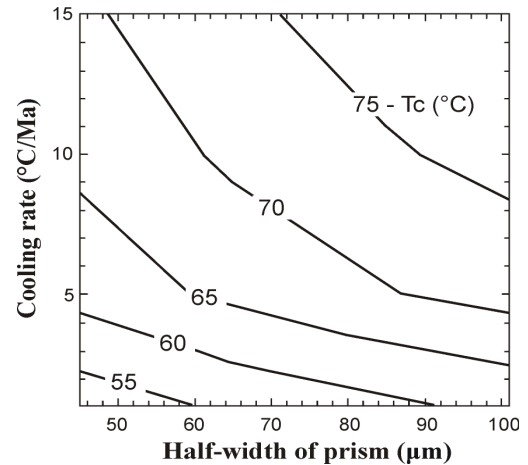


**Fig. 4-5:** Helium closure temperature ( $T_c$ ) as a function of grain size and cooling rate.  $T_c$  calculated assuming an activation energy of  $33 \text{ kcal/mol}$  and a diffusivity at infinite temperature of  $50 \text{ cm}^2/\text{sec}$  assuming spherical geometry and including the effects of  $\alpha$  ejection (redrawn after Farley, 2002).

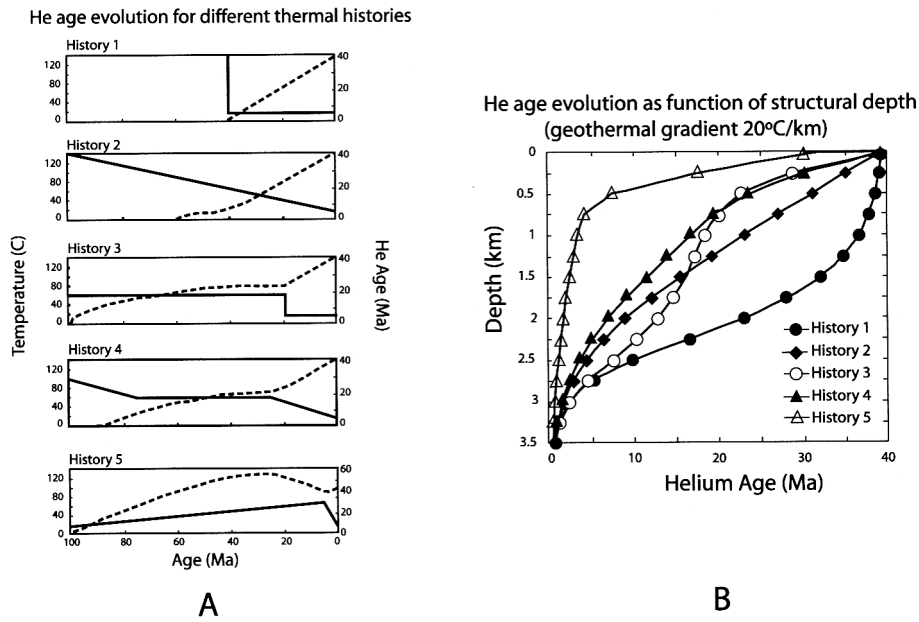


**Fig. 4-6:** A: Apatite He age evolution curves (dotted lines) for several representative time-temperature paths (solid lines). All paths yield a He age of 40 Ma. B: He age as a function of structural depth in a 20°C/km thermal gradient for the time-temperature histories shown in A. The histories can be resolved with measurements of apatite He ages spanning ~1.5 km of structural relief; similar resolution using apatite fission track ages would require more than 2 km (after Wolf et al., 1998, adopted from Foeken, 2004).

## 5 DATING PROCEDURE

### 5.1 SAMPLING

The sampling campaign used in this study focused on the crystalline basement of Variscan Corsica (Fig. 5-1), particularly on those regions, from which no AFT ages of previous studies have been reported. Series of samples were taken from the Eocene flysch along the Alpine deformation front to investigate possible reset of AFT ages in these sediments. Special interest was dedicated to sample the remnants of the summit and piedmont paleosurfaces in order to predate and bracket the time of their formation. Elevation profiles in steep relief regions from homogenous blocks possibly without faults were sampled in order to evaluate exhumation rates. The sampling points of this study are distributed over entire Variscan Corsica. In addition, some samples were taken from the Tenda Massif. A total of 157 samples of granitoids, gneisses and flysch was collected, however many lithologies were surprisingly poor in apatite, thus only 67 out of the set contained sufficient amounts of datable apatite crystals.

The amount of sample material was in the range of 5 to 10 kg. Samples dedicated for (U-Th)/He dating were taken from below the surface, and the uppermost 20 cm of the rock was removed prior to processing in order to minimize the effect of He loss by insolation (Wolf et al., 1996b) or, more importantly, wildfires (Mitchell and Reiners, 2003) that yearly affect large parts of Corsica.

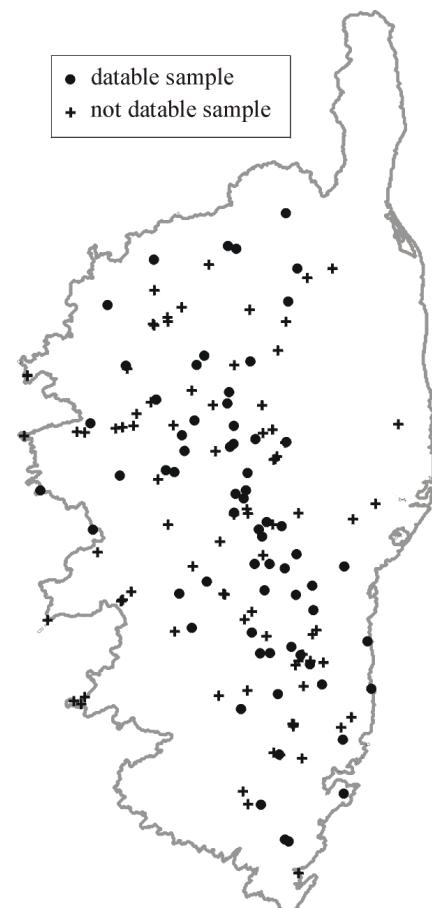


**Fig. 5-1:** Localities of samples collected during this study. Circles represent samples dated by FT method, crosses represent those samples, where dating was not possible.

## 5.2 MINERAL SEPARATION

Apatite and zircon concentrates for FT and (U-Th)/He analyses were obtained using standard magnetic and heavy liquid separation techniques (see Appendix A).

## 5.3 FISSION TRACK ANALYSIS

For FT analysis the external detector method (Gleadow and Duddy, 1981) was used. FT ages were calculated using the  $\zeta$  (zeta) age calibration method (Hurford and Green, 1983). Modeling of the low-temperature thermal history was carried out using the HeFTy modeling program (Ketcham et al., in press). A detailed description of the analytical procedure used (including mound preparation, etching protocol, packing, irradiation, fission track counting and length measurements technique,  $\zeta$ -factor calculation, age calculation, and thermal modeling procedure) are found in Appendix B.

## 5.4 (U-TH)/HE ANALYSIS

(U-Th)/He analysis was carried out in a frame of cooperation between Tübingen University (TU) and Scottish Universities Environmental Research Centre (SUERC) in East Kilbride (United Kingdom). At Tübingen University, the helium measurements were carried out on a new Helium Extraction Line constructed by Patterson Instruments Ltd.<sup>©</sup>. The instrumentation and techniques are based on those employed and successfully demonstrated in Prof. Farley's laboratory at California Institute of Technology (CalTech). A short description of the system can be found in Appendix C. It must be noted that during this study, the laboratory procedure for He measurements were still under development at TU, and may be modified in the future. U and Th measurements were carried out at SUERC.

### 5.4.1 Apatite grain selection

Most of the samples was not suitable for (U-Th)/He measurements due to poor apatite content and bad quality of apatite grains. Apatite crystals for He analysis were separated as follows:

Approximately 50-100 apatite grains were handpicked from non-magnetic heavy mineral fraction (used also for AFT analysis) under a stereomicroscope with respect to size and morphological

characteristics: only big (prism diameter > ~60  $\mu\text{m}$ ), euhedral prismatic grains were selected, while small, needle-like, fragmentary, rounded, subhedral grains were avoided. Afterwards the grains were inspected at 200x magnification under cross-polarized light for inclusions, fractures, and other "damages", and the best possible grains of similar size were selected. If no high-quality apatites could be selected for a sample of particular interest, the most acceptable imperfect grains were chosen. All grains that were finally selected were photographed under a stereomicroscope equipped with a Sony DXC-930P 3-CCD camera, and magnification used was recorded in a logbook. The dimensions of grains (prism diameter and length) were measured by using the Scion Image software, and  $F_t$  factors were calculated for each grain assuming hexagonal geometry (Farley et al., 1996; Farley, 2002). Then the grains with similar  $F_t$  factors were grouped in order that the standard deviation of the recoil correction in each population was  $\pm 0.5\%$ . From each sample analyzed, 2 to 6 aliquots were prepared in order to replicate the measurement and verify reproducibility of results. In this study, apatites from all samples yield homogenous U distribution as inferred from fission track distribution; Th distribution was assumed to be identical with U. This justifies the application of  $F_t$  correction.

### 5.4.2 The $^4\text{He}$ analysis

Selected apatite crystals were loaded into stainless steel capsules (composed of cup, lid, nut and bolt, see Fig. 5-2), which were degassed at 950°C for one hour prior to loading in order to avoid possible  $^4\text{He}$  contamination. A batch of capsules (throughout this study loading of six capsules is



**Fig. 5-2:** Photograph of stainless steel capsules (dismantled and closed) used during this study to load apatite crystals.

possible at TU) with crystals was loaded into a "feeding rod" and mounted on the top of the furnace. After pumping and furnace degassing (usually at 950°C for 30 minutes), a hot blank was performed. If the hot blank was unacceptably high, the furnace was degassed again. After an acceptable hot blank was obtained (at level of less than ~0.002 ncc of  $^4\text{He}$  STP => 0.002 nano-cubic centimeters of  $^4\text{He}$  at Standard Temperature and Pressure = 0°C and 101 kPa), the capsule was dropped into the furnace and outgassed at 950°C for 8 minutes. The evolved gasses were then purified on a charcoal trap cooled by liquid

nitrogen and hot (~350°C) and cold TiZr (titanium-zirconium) getters, spiked with 99.9% pure  $^3\text{He}$  and introduced into a quadrupole mass spectrometer (Pfeiffer Prisma QMS-200) equipped with a Channeltron detector. The  $^4\text{He}/^3\text{He}$  ratio was measured in static mode over a period of 160 seconds,

and then the entire system was pumped. The sample was outgassed at the same conditions again, and the measurement procedure was repeated. This “re-extract” step should yield He at levels comparable to the preceding hot blank. If not, the most common cause was thought to be undetected inclusions releasing helium at higher temperatures than apatite. Such analyses were rejected as erroneous and a new aliquot of the sample analyzed until the re-extract step yielded helium at blank levels. Helium abundances measured in counts per second were recalculated to ncc at STP and corrected for blank. Typical hot blank over this study was  $\sim 0.0015$   $^4\text{He}$  ncc STP, which corresponds to 0.02 Ma of He age of a typical apatite with a radius of  $\sim 40$   $\mu\text{m}$ . The reproducibility of the  $^3\text{He}$  spike was determined from the measurements against an accurately known standard  $^4\text{He}$  (or “Q-standards”). Three Q-standards were measured before and after analyzing a sample. The precision of Q-standards was better than  $\pm 0.03\%$  ( $1\sigma$ ). Once all loaded capsules were analyzed, they were retrieved from the furnace and sent for U and Th analysis to SUERC.

### 5.4.3 U and Th analysis

U and Th were analyzed in aqueous solution using an Inductively Coupled Plasma Mass Spectrometer (ICP-MS). The quantities of U and Th were determined as the ratio of their concentrations ( $^{238}\text{U}/^{232}\text{Th}$ ) using isotopic dilution. In the following section the analytical procedures and the equipment used to perform the analysis are described (after Persano, 2003).

#### 5.4.3.1 APATITE DISSOLUTION AND ISOTOPIC DILUTION

The apatite crystals were retrieved from the capsules and transferred into a teflon beaker with 2 ml of 5% nitric acid and approximately 1.3 ng of  $^{235}\text{U}$  and 3 ng of  $^{230}\text{Th}$  spikes. The spikes were prepared by dissolving certified standard (courtesy of Dr. Ellam)  $^{235}\text{U}$  and  $^{230}\text{Th}$  powder in nitric acid and diluting to obtain a concentration of 15 ppb. Fractionation in the mass spectrometer was corrected using the U500 standard with a certified value  $^{235}\text{U}/^{238}\text{U} = 0.9997$ . U and Th were purified using conventional cation exchange chemistry (Luo et al., 1997). After equilibration, the solution was brought to 5 ml using 5% nitric acid and transferred in plastic tubes for ICP-MS analysis.

#### 5.4.3.2 ICP-MS ANALYSIS

U and Th concentrations were determined by VG PlasmaQuad PQ2 plus ICP-MS (VG Elemental, Cheshire, England) fitted with a Meinhard nebulizer and a Scott, double pass, water-cooled glass spray chamber. Instrumental parameters are given in Table 5-1 (Olive et al., 2001). The limits of

detection in a quadrupole ICP-MS are best presented in terms of detector noise (cps) rather than concentrations (Olive et al., 2001). The instrumental background level reported in Table 5-1 represents the mean of fifty 90s aspirations of the 5% nitric acid solution used to “purge” the instrument between samples. In order to monitor instrumental mass fractionation, repeated analyses of U500 standard were performed. Each sample run began with two U500 aliquots and subsequent analyses interspersed to bracket every three samples. The reproducibility of measuring 5 ppb U500 solution was approximately 0.15%. U and Th concentrations in the samples were accurate to  $\pm 2.5\%$  (1 sigma).

Sample uptake rate	0.8 ml.min <sup>-1</sup>
Washout time	180 s
Uptake time	90 s
Acquisition time	90 s
Data acquisition mode	Peak jumping
Dwell time	10.24 ms
Points per peak	3
No. of replicates	3
Blank (cps) for U	<100
Blank (cps) for Th	<100

**Table 5-1** ICP-MS acquisition parameters (Olive et al., 2001).

#### 5.4.4 Results of mineral standard

In order to verify stability and precision of the system, mineral standards of known age are regularly measured in the laboratories. To date, the Durango apatite (Young et al., 1969; apatite FT age:  $31.6 \pm 1$  Ma, Jonckheere et al., 1993; K/Ar age:  $30.3 \pm 0.4$ ; Naeser and Fleischer, 1975) is the most common standard in use. Values for this age standard reported from others He laboratories varies between 27.5 and 32.6 Ma (Warnock et al., 1997; Farley, 2002). In the Tübingen He laboratory, one capsule with Durango apatite is measured per each series of samples. Repeated analysis of Durango apatite over the period of this research yields an age of  $28.95 \pm 1.88$  Ma ( $n = 30$ ), which is well within the recently published range. Furthermore the ages reproduce to  $\sim 7\%$ , giving the confidence in the quality of the data and the performance of the laboratory procedures (Fig. 5-3).

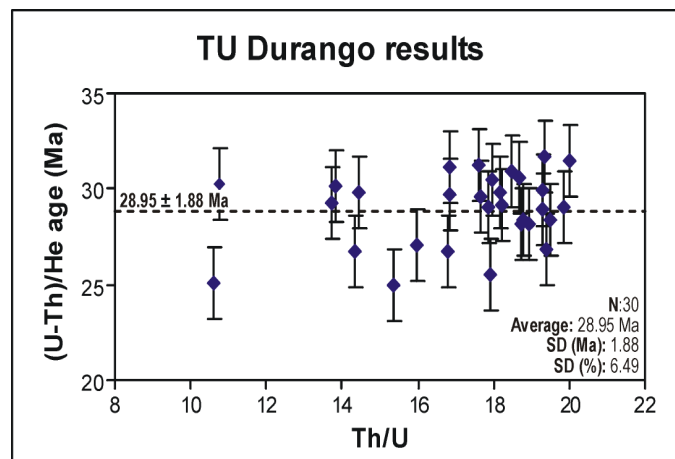


**Fig. 5-3:** Diagram showing He ages obtained on Durango apatites during this study as a function of Th/U ratio; an average age:  $28.95 \pm 1.88$  Ma ( $n = 30$ ).

### 5.4.5 Error calculation

To date, there is no "standard" consensus accepted of how to calculate an uncertainty (or error) of He ages. Reported uncertainties have been obtained in different ways (see e.g., House et al., 2001; Persano et al., 2002; Foeken et al., 2003; Hendriks, 2003; Foeken, 2004), sometimes the uncertainties are not reported at all (e.g., Wolf et al., 1996a). In this study, two principal types of uncertainties are distinguished: analytical uncertainty and mineralogical uncertainty.

The analytical uncertainty includes the uncertainties associated with the analysis (i.e., errors on He measurements, He calibration, U and Th measurements and calibrations,  $^3\text{He}$ , U and Th spikes, etc.). This uncertainty is typically less than ~5% at 1 sigma, and is calculated as follows:

$$A_E = \sqrt{He_E^2 + U_E^2 + Th_E^2}$$

where  $A_E$  refers to the total analytical error;  $He_E$ ,  $U_E$ ,  $Th_E$  are the errors of He, U and Th measurements, respectively.

The analytical error of helium measurements was calculated according to Patterson (pers. comm.) as:

$$He_E = \sqrt{\left(\frac{T_E}{T}\right)^2 + \left(\frac{Q_E}{Q}\right)^2 + \left(\frac{D_E}{D}\right)^2}$$

where  $He_E$  is the analytical error of He measurement;  $T$  is the "T-zero" intercept of  $^4\text{He}/^3\text{He}$  ratios measured on a sample;  $T_E$  is 1 sigma error of  $T$ ;  $Q$  is the average of Q-standards measured;  $Q_E$  is 1 sigma error of  $Q$ ;  $D$  is the depletion factor used;  $D_E$  is 1 sigma error of depletion factor.

The analytical error of uranium and thorium measurements was calculated after Persano (pers. comm.) as:

$$U_E = B \sqrt{\left(\frac{J_E}{J}\right)^2 + \left(\frac{K_E}{K}\right)^2}, \text{ and}$$

$$Th_E = C \sqrt{\left(\frac{G_E}{G}\right)^2 + \left(\frac{H_E}{H}\right)^2}, \text{ respectively,}$$

where  $U_E$  is the analytical error of U measurement;  $B$  is the amount of  $^{238}\text{U}$ ;  $J$  is the mass of the  $^{235}\text{U}$  spike added;  $J_E$  is 1 sigma error of  $J$ ;  $K$  is  $^{238}\text{U}/^{235}\text{U}$  ratio in sample;  $K_E$  is 1 sigma error of  $K$ ;  $Th_E$  is the analytical error of Th measurement;  $C$  is the amount of  $^{232}\text{Th}$ ;  $G$  is the mass of the  $^{230}\text{Th}$  spike added;  $G_E$  is 1 sigma error of  $G$ ;  $H$  is  $^{232}\text{Th}/^{230}\text{Th}$  ratio in sample;  $H_E$  is 1 sigma error of  $H$ .

The term "mineralogical uncertainty" is used here to denote the uncertainties associated with physical and chemical properties of dated crystals, such as crystal size, shape, presence of fissures, cracks, cleavages, and other damages in crystal lattice, heterogeneous distribution of parent isotopes, zoning, parent isotopes bearing inclusions, presence of parent isotopes in surrounding phases possibly inducing implantation of helium, and maybe some other yet unknown factors. Groups in East Kilbride or Amsterdam prefer to use the term "geological" instead of "mineralogical" uncertainty (Foeken, pers. comm.), but this study refers to the latter term, since the main controlling factors are more "mineralogical" rather than "geological" in origin. The integrated effect of all biasing factors are involved in "mineralogical uncertainty", which is unfortunately always present in (U-Th)/He analysis and is always much higher than the analytical one (up to ~30%). The mineralogical uncertainty is unique for each crystal and differs from sample to sample. Practically it cannot be measured, but it is possible to assess its magnitude.

The way in which to assess the magnitude of the mineralogical uncertainty is not strictly defined and several approaches have been used. For instance, the standard deviation of reproducibility observed on several replicates of an age standard is adopted as "error" for actual samples. In some laboratories the Durango age standard is used for this purpose. Nevertheless, the usage of Durango is not widely accepted due to some additional factors controlling the Durango age, such as zonation and inhomogeneous distribution of U and Th (Stuart, pers. comm.). Furthermore, there is no alpha recoil correction involved, and thus the usage of only Durango underestimates actual reproducibility.

The way to overcome this problem is to use an age standard, where the alpha recoil correction must be applied, for example the age standard 97MR22 was used in the study of House et al. (2000). However, throughout this study, this age standard was not in property of TU, therefore this approach was not applied.

Another way to assess the mineralogical uncertainty is by measuring several (5-6) replicates of the same sample and to calculate the error from them. This approach, although certainly the most expensive and time-consuming, is probably the best one, since, as discussed above, the mineralogical sources of error dominate and every sample is unique in a sense (Farley, pers. comm.).

In this study, total analytical error and mineralogical error are reported in the results table (Table 6-3). The total analytical error was computed as described above, and was in the range of 2-6%. The mineralogical error was computed based on the reproducibility of each sample as a standard deviation (expressed in %) of the entire dataset at 1 sigma translated to Ma.

## 6 RESULTS

### 6.1 ZIRCON FISSION TRACK RESULTS

ZFT ages were measured on 3 samples from the southern and central part of the Variscan granitic basement (Table 6-1, Fig. 6-1). All samples passed the  $\chi^2$ -test at a 95% confidence interval and are reported as central ages with  $\pm 1\sigma$  errors. The ZFT ages are  $144.6 \pm 10$  (XC-50),  $159.2 \pm 9.8$  (XC-46) and  $159.8 \pm 12.1$  Ma (KU-22) and are younger than intrusion age of the granites (~340-260 Ma; Cocherie et al., 1984).

### 6.2 APATITE FISSION TRACK RESULTS

AFT analyses were performed on 67 samples (Table 6-2, Fig. 6-1). All samples passed the  $\chi^2$ -test at the 95% confidence interval and are reported as central ages with  $\pm 1\sigma$  errors. The AFT ages from Variscan Corsica are younger than intrusion age of crystalline basement. All but two ages are Cenozoic, ranging from  $16.4 \pm 1.4$  Ma (XC-116) to  $46.4 \pm 4$  Ma (XC-81). Samples XC-2 and KU-22 from southernmost Corsica are Mesozoic ( $105.3 \pm 7.2$  and  $97.9 \pm 5.4$  Ma, respectively). AFT ages from Eocene flysch are all younger than the depositional ages (~60-40 Ma, Upper Paleocene to Middle Eocene; Durand-Delga, 1978; Rossi et al., 1980), ranging between  $16.4 \pm 1$  (XC-132) and  $30.6 \pm 1.6$  Ma (XC-85). Samples from the Tenda Massif yielded AFT ages in the range of  $16.4 \pm 1.4$  (XC-116) to  $24.9 \pm 2.7$  Ma (XC-42).

Track length distributions were measured on 29 samples (Table 6-2, Fig. 6-2). Mean confined track lengths (MTL) vary between  $12.2 \pm 0.2$   $\mu\text{m}$  (XC-2) and  $14.8 \pm 0.1$   $\mu\text{m}$  (XC-33) with standard deviations (SD) between 0.7 (XC-59) and 2.2  $\mu\text{m}$  (XC-2). All samples, with one exception (XC-2), yield narrow ( $\text{SD} \leq 1.6$   $\mu\text{m}$ ), unimodal track length distributions with relatively long MTL ( $\geq 13.2$   $\mu\text{m}$ ). Such distributions are characteristic for rapidly cooling rocks with fast passage through the apatite PAZ during exhumation. Sample XC-2 exhibits a broad ( $\text{SD} = 2.2$   $\mu\text{m}$ ), bimodal track length distribution with very short MTL ( $12.2 \pm 0.2$   $\mu\text{m}$ ), attesting to a complex thermal history (Gleadow et al., 1986a,b).

Dpar values range from 1.5 to 4.5  $\mu\text{m}$  (Table 6-2), pointing to a variable chemical composition of the samples. Nevertheless, in the majority of samples the Dpar values are small ( $\leq 1.7$   $\mu\text{m}$ ), thus in those samples a normal fluorine-apatite composition is supposed.

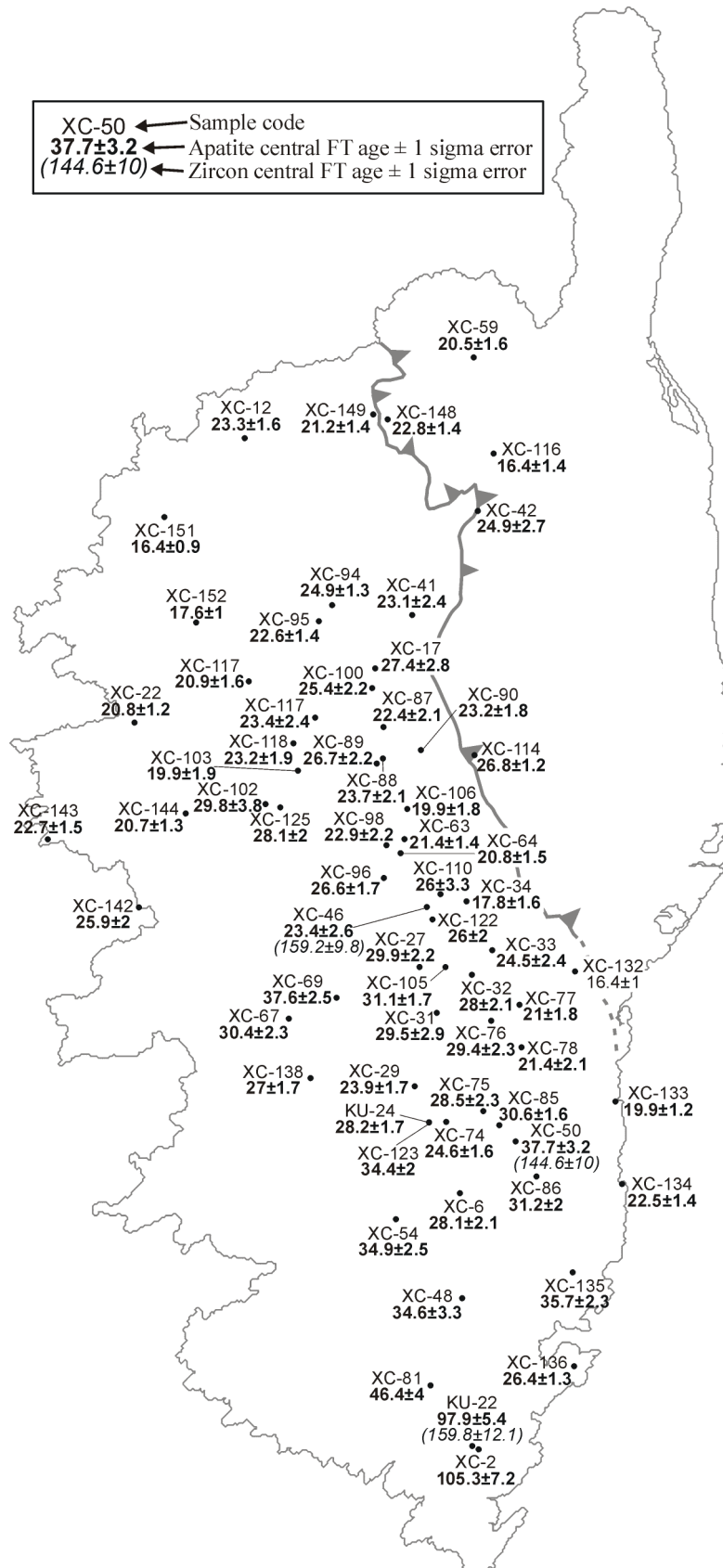


**Fig. 6-1:** Contour of Corsica with measured apatite (bold font) and zircon (numbers in brackets in italic font) fission track ages in Ma.

Table 6-1 ZFT data.

Sample code	UTM32/WGS84 X	UTM32/WGS84 Y	Altitude (m)	Tectonic unit	Petrography	N	$\rho_s$	$N_s$	$\rho_i$	$N_i$	$\rho_u$	$N_u$	$P(\chi^2)$ (%)	Age (Ma)	$\pm 1\sigma$ (Ma)
KU-22	515936	4593844	876	Variscan basement	granite	20	161.360	1163	34.825	251	5.637	2675	51.5	159.8	12.1
XC-46	510622	4656974	2247	Variscan basement	granite	25	193.548	1860	41.727	401	5.609	2675	100.0	159.2	9.8
XC-50	521008	4629515	500	Variscan basement	granite	25	59.364	1295	14.073	307	5.595	2675	100.0	144.6	10

N - number of dated apatite crystals;  $\rho_s$  ( $\rho_i$ ) - spontaneous (induced) track densities ( $\times 10^5$  tracks/cm<sup>2</sup>);  $N_s$  ( $N_i$ ) - number of counted spontaneous (induced) tracks;  $\rho_u$  - dosimeter track density ( $\times 10^5$  tracks/cm<sup>2</sup>);  $N_u$  - number of tracks counted on dosimeter;  $P(\chi^2)$  - probability obtaining Chi-square value ( $\chi^2$ ) for n degree of freedom (where n = No. of crystals - 1); Age  $\pm 1\sigma$  - central age  $\pm 1$  standard error (Galbraith and Laslett, 1993). Ages were calculated using zeta calibration method (Hurford and Green, 1983), glass dosimeter CN-2, and zeta value of  $123.92 \pm 2.53$  year/cm<sup>2</sup>.

Table 6-2(I) AFT data (continues to the next pages).

Sample code	UTM32/WGS84 X	UTM32/WGS84 Y	altitude (m)	Tectonic unit	Petrography	N	$\rho_s$	$N_s$	$\rho_i$	$N_i$	$\rho_u$	$N_u$	$P(\chi^2)$ (%)	Age (Ma)	$\pm 1\sigma$ (Ma)	MTL ( $\mu$ m)	SD ( $\mu$ m)	SE ( $\mu$ m)	N (L)	Dpar ( $\mu$ m)
XC-2	516683	4593456	280	Variscan basement	granite	25	12.842	564	11.453	503	5.575	4936	99.9	105.3	7.2	12.2	2.2	0.2	101	1.61
XC-6	514493	4623457	826	Variscan basement	granite	25	5.403	297	17.301	951	5.312	4936	100.0	28.1	2.1	13.2	1.1	0.1	95	1.79
XC-12	489324	4711884	550	Variscan basement	granite	25	4.268	338	16.783	1329	5.400	4936	100.0	23.3	1.6	14.3	1.0	0.1	100	1.52
XC-17	504586	4684921	1758	Variscan basement	granite	25	1.579	125	7.375	584	7.780	5426	99.9	27.4	2.8					3.24
XC-22	476440	4678574	60	Variscan basement	granite	25	5.761	413	28.302	2029	6.149	5647	99.5	20.8	1.2					3.48
XC-27	509772	4649947	1754	Variscan basement	granite	25	3.281	263	11.279	904	6.194	5647	100.0	29.9	2.2					3.86
XC-29	509206	4635978	940	Variscan basement	granite	26	3.422	272	15.011	1193	6.326	5647	100.0	23.9	1.7					2.27
XC-31	511783	4644575	800	Variscan basement	granite	25	2.497	155	7.877	489	5.487	4936	100.0	29.5	2.9	14.2	1.2	0.1	98	1.59
XC-32	515893	4649042	1065	Variscan basement	granite	25	2.992	243	12.906	1048	7.341	5426	86.7	28.0	2.1					3.78
XC-33	518273	4651914	1874	Variscan basement	granite	25	3.261	152	12.230	570	5.429	4936	100.0	24.5	2.4	14.8	0.9	0.1	85	1.68
XC-34	515262	4657639	800	Variscan basement	granite	27	3.026	164	16.328	885	5.796	5647	99.9	17.8	1.6	13.5	1.3	0.2	52	1.71
XC-39	483649	4690293	200	Variscan basement	granite	50	4.962	545	25.209	2769	5.283	4936	100.0	17.6	1.0	14.5	1.1	0.1	80	1.56
XC-41	508911	4691175	463	Variscan basement	granite	25	1.396	117	7.423	622	7.466	5426	85.1	23.1	2.4					1.60
XC-42	516582	4703360	230	Tenda Massif	orthogneiss	34	2.009	117	7.470	435	5.458	4936	100.0	24.9	2.7					1.50
XC-46	510622	4656974	2247	Variscan basement	granite	36	1.006	112	4.022	448	5.517	4936	100.0	23.4	2.6	14.2	1.2	0.1	65	1.63
XC-48	514759	4611153	1095	Variscan basement	granite	25	1.723	148	6.262	538	7.655	5426	98.6	34.6	3.3					3.29
XC-50	521008	4629515	500	Variscan basement	granite	25	3.896	234	9.091	546	5.195	4936	100.0	37.7	3.2	14.3	1.3	0.1	90	1.89

Table 6-2(2) AFT data.

Sample code	UTM32/WGS84 X	Y	altitude (m)	Tectonic unit	Petrography	N	$\rho_s$	$N_s$	$\rho_t$	$N_t$	$\rho_d$	$N_d$	P( $\chi^2$ ) (%)	Age (Ma)	$\pm 1\sigma$ (Ma)	MTL ( $\mu\text{m}$ )	SD ( $\mu\text{m}$ )	SE ( $\mu\text{m}$ )	N(L)	Dpar ( $\mu\text{m}$ )
XC-54	507010	4620408	321	Variscan basement	granite	25	7.804	291	22.072	823	5.953	5647	100.0	34.9	2.5	13.7	1.4	0.1	91	1.80
XC-59	516108	4721345	520	Tenda Massif	orthogneiss	30	4.590	251	21.488	1175	5.663	4936	100.0	20.5	1.6	14.7	0.7	0.1	81	1.59
XC-63	508011	4664924	2295	Variscan basement	granite	25	2.462	317	12.922	1664	6.839	5426	99.1	21.4	1.4					1.67
XC-64	507556	4663280	1410	Variscan basement	granite	25	1.732	248	9.826	1407	7.153	5426	99.7	20.8	1.5					1.63
XC-67	494484	4643898	200	Variscan basement	granite	25	3.357	241	12.175	874	6.643	5647	100.0	30.4	2.3	14.2	1.2	0.1	71	1.92
XC-69	500065	4646344	750	Variscan basement	granite	25	3.312	338	10.082	1029	6.964	5426	99.7	37.6	2.5					3.13
XC-74	512890	4631804	1627	Variscan basement	granite	25	3.007	352	13.276	1554	6.538	5647	97.8	24.6	1.6	14.3	1.1	0.2	43	1.66
XC-75	517225	4633070	2133	Variscan basement	granite	25	2.912	230	10.013	791	5.902	5647	100.0	28.5	2.3	14.3	1.0	0.1	46	1.79
XC-76	518153	4643651	1981	Variscan basement	granite	25	2.169	236	8.374	911	6.901	5426	100.0	29.4	2.3					1.73
XC-77	521458	4645523	530	Variscan basement	granite	25	1.463	177	6.620	801	5.781	5426	99.2	21.0	1.8					1.70
XC-78	521695	4640541	325	Variscan basement	granite	25	1.806	139	9.198	708	6.573	5647	100.0	21.4	2.1					2.25
XC-81	511052	4600940	300	Variscan basement	granite	25	2.630	206	7.010	549	7.529	5426	97.6	46.4	4.0					3.17
XC-85	519102	4631419	1880	Eocene flysch	arkose	35	5.379	581	19.404	2096	6.661	5647	99.9	30.6	1.6	13.9	1.5	0.2	81	1.66
XC-86	523445	4625414	1040	Variscan basement	granite	31	4.031	368	14.524	1326	6.785	5647	100.0	31.2	2.0					1.57
XC-87	505553	4678052	1033	Variscan basement	granite	25	1.338	148	7.097	785	7.215	5426	99.4	22.4	2.1					4.50
XC-88	505491	4674372	2404	Variscan basement	granite	30	1.686	169	7.173	719	6.080	5647	100.0	23.7	2.1					2.11
XC-89	504767	4673776	2620	Variscan basement	granite	25	2.975	205	12.641	871	6.838	5647	100.0	26.7	2.2					2.77
XC-90	509929	4675353	2453	Eocene flysch	arkose	25	4.446	232	20.716	1081	6.520	5647	100.0	23.2	1.8	14.2	1.1	0.1	86	1.74
XC-94	499551	4692333	2092	Variscan basement	granite	25	7.716	657	30.231	2574	5.917	5426	99.7	24.9	1.3					2.04
XC-95	498000	4690449	1588	Variscan basement	granite	25	3.429	404	16.958	1998	6.776	5426	90.1	22.6	1.4					1.56
XC-96	505599	4660375	876	Variscan basement	granite	25	2.469	336	10.832	1474	7.090	5426	99.6	26.6	1.7					3.26
XC-98	505899	4664212	2254	Variscan basement	granite	25	1.666	143	8.052	691	6.679	5647	100.0	22.9	2.2	14.3	1.2	0.1	68	1.74
xc-100	504231	4682617	1110	Variscan basement	granite	25	2.410	179	10.164	755	6.458	5647	100.0	25.4	2.2					2.02
xc-102	491762	4669028	443	Variscan basement	granite	21	2.371	85	8.230	295	6.238	5647	100.0	29.8	3.8					1.93
xc-103	495552	4672943	1375	Variscan basement	granite	25	1.713	150	8.601	753	6.029	5647	100.0	19.9	1.9	13.9	1.2	0.1	71	1.51
XC-105	512804	4649935	1950	Variscan basement	granite	25	3.530	518	14.413	2115	7.717	5426	97.3	31.1	1.7					2.22
XC-106	508337	4668458	942	Variscan basement	granite	25	1.306	150	8.185	940	7.592	5426	97.7	19.9	1.8					1.69
XC-110	512219	4658479	1667	Variscan basement	granite	26	1.091	83	4.126	314	5.927	5647	100.0	26.0	3.3					1.69
XC-114	516200	4674762	322	Eocene flysch	conglomerate	50	9.171	988	33.872	3649	5.978	5647	91.9	26.8	1.2	14.3	1.0	0.1	94	1.64
XC-116	518436	4710083	1448	Tenda Massif	orthogneiss	35	1.471	175	9.565	1138	6.414	5647	100.0	16.4	1.4					2.33
XC-117	497567	4679152	2319	Variscan basement	granite	25	1.234	120	5.501	535	6.282	5647	100.0	23.4	2.4					1.99
XC-118	495026	4676143	2098	Variscan basement	granite	25	2.012	197	10.396	1018	7.278	5426	93.6	23.2	1.9					1.50

Table 6-2(3) AFT data.

Sample code	UTM132/WGS84 X	UTM132/WGS84 Y	altitude (m)	Tectonic unit	Petrography	N	$\rho_s$	$N_s$	$\rho_t$	$N_t$	$\rho_d$	$N_d$	$P(\chi^2)$ (%)	Age (Ma)	$\pm 1\sigma$ (Ma)	MTL ( $\mu\text{m}$ )	SD ( $\mu\text{m}$ )	SE ( $\mu\text{m}$ )	N(L)	Dpar ( $\mu\text{m}$ )
XC-122	511286	4655519	2273	Variscan basement	granite	26	1.601	222	7.125	988	7.027	5426	89.1	26.0	2.0					2.55
XC-123x	510881	4631761	1702	Variscan basement	granite	25	3.648	455	11.672	1456	6.650	5426	100.0	34.2	2.0					2.21
XC-125	493486	4668642	500	Variscan basement	granite	30	2.156	283	8.463	1111	6.713	5426	98.8	28.1	2.0					3.04
XC-132	527956	4649430	140	Eocene flysch	arkose	25	3.894	366	23.025	2164	5.978	5193	99.8	16.4	1.0	13.6	1.5	0.2	67	1.56
XC-133	532680	4634195	30	Eocene flysch	arkose	30	5.074	432	25.627	2182	6.208	5193	95.1	19.9	1.2	13.7	1.4	0.2	75	1.50
XC-134	533453	4624534	20	Eocene flysch	arkose	25	5.791	399	23.061	1589	5.519	5193	95.2	22.5	1.4	13.9	1.0	0.1	67	1.52
XC-135	527680	4614182	160	Variscan basement	granite	31	3.314	392	9.527	1127	6.323	5193	67.7	35.7	2.3	13.8	1.5	0.2	90	1.71
XC-136a	527847	4603189	72	Eocene flysch	arkose	30	6.518	721	25.558	2827	6.381	5193	96.7	26.4	1.3	14.0	1.3	0.1	101	3.07
XC-138	497023	4636935	580	Variscan basement	granite	25	3.773	368	13.953	1361	6.151	5193	93.0	27.0	1.7	13.9	1.1	0.1	50	1.71
XC-142	476954	4656929	20	Variscan basement	granite	30	2.050	236	7.826	901	6.093	5193	100.0	25.9	2.0	13.9	1.1	0.1	54	1.54
XC-143	466297	4664907	120	Variscan basement	granite	25	2.826	311	12.178	1340	6.036	5193	100.0	22.7	1.5	13.6	1.6	0.2	100	1.55
XC-144	482427	4667932	480	Variscan basement	granite	25	2.699	380	11.940	1681	5.634	5193	99.5	20.7	1.3					1.52
XC-148	506041	4714089	787	Eocene flysch	arkose	25	7.673	393	31.100	1593	5.691	5193	98.6	22.8	1.4					3.73
XC-149	504357	4714672	770	Eocene flysch	arkose	25	4.584	315	21.932	1507	6.266	5193	98.1	21.2	1.4					1.65
XC-151	479928	4702645	443	Variscan basement	granite	25	10.087	569	57.400	3238	5.749	5193	62.6	16.4	0.9	13.5	1.5	0.2	90	1.54
XC-152	489803	4683398	960	Variscan basement	granite	25	1.846	221	9.671	1158	6.763	5193	99.4	20.9	1.6					1.50
KU-22	515936	4593844	876	Variscan basement	granite	32	5.150	785	5.603	854	6.603	5193	89.6	97.9	5.4					3.76
KU-24	510880	4631740	610	Variscan basement	granite	34	3.321	451	11.120	1510	5.864	5193	93.8	28.4	1.7	13.8	1.2	0.2	65	1.53

N - number of dated apatite crystals;  $\rho_s$  ( $\rho_t$ ) - spontaneous (induced) track densities ( $\times 10^5$  tracks/cm<sup>2</sup>);  $N_s$  ( $N_t$ ) - number of counted spontaneous (induced) tracks;  $\rho_d$  - dosimeter track density ( $\times 10^5$  tracks/cm<sup>2</sup>);  $N_d$  - number of tracks counted on dosimeter;  $P(\chi^2)$  - probability obtaining Chi-square value ( $\chi^2$ ) for n degree of freedom (where n = No. of crystals - 1); Age  $\pm 1\sigma$  - central age  $\pm 1$  standard error (Galbraith and Laslett, 1993); MTL - mean track length; SE - standard error of mean track length; SD - standard deviation of track length distribution; N(L) - number of horizontal confined tracks measured; Dpar - average etch pit diameter of fission tracks. Ages were calculated using zeta calibration method (Hurford and Green, 1983), glass dosimeter CN-5, and zeta value of  $324.93 \pm 6.46$  year/cm<sup>2</sup>.

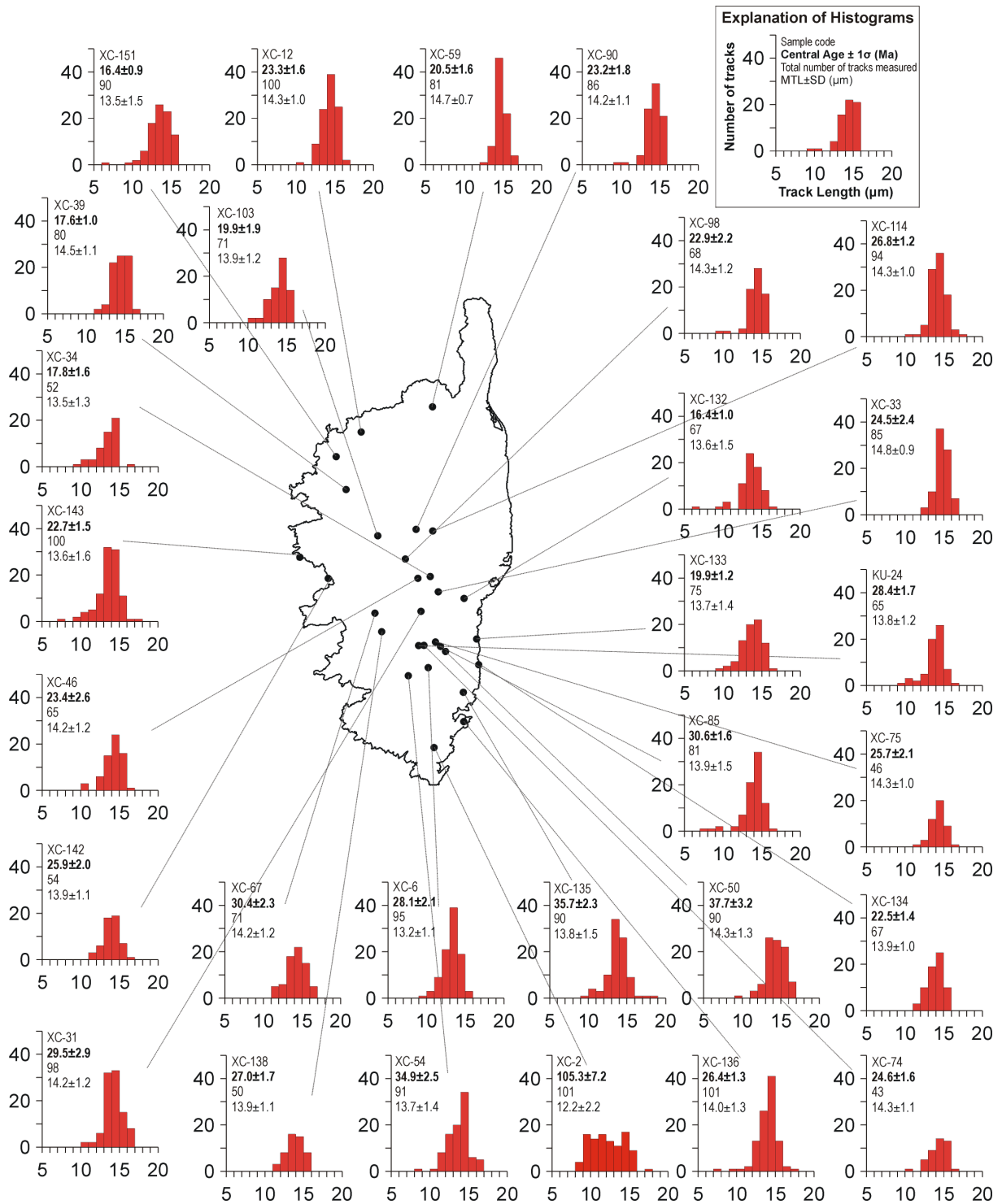


Fig. 6-2: Track length distribution of apatites.

### 6.3 APATITE (U-Th)/He RESULTS

The selection of the samples dedicated for (U-Th)/He analysis was made primarily on the following criteria: (i) preference was given to samples taken from both types of paleosurfaces ("summit" and "piedmont" paleosurfaces) in order to bracket the time of their formation and test a succession of their formation proposed by Kuhlemann et al. (2005a); (ii) the second important criterion was the quality of the apatite crystals (see chapter 5.4.1); (iii) and the third criterion was the geographic distribution of the selected samples: it was intended to attribute the He ages to as many paleosurface remnants as possible.

Mainly because of poor quality and low amounts of apatite crystals in most of the samples, a total of 40 (U-Th)/He ages (later referred to as He ages) were successfully determined on 12 samples (Table 6-3, Fig. 6-3): most of the ages are reported from the central southern Corsica, two ages are from central part (Rotondo and Niolo Massifs), one age is from the NNE part of the island (Balagne region). The results are presented in Table 6-3, where three types of ages are reported: raw ages, ages corrected for alpha recoil, and average ages calculated from the replicates of samples. The error was calculated following the procedure described (see chapter 5.4.5). In the following, He ages are reported as average ages with 1 sigma error.

Replicates of the samples reproduce well, giving the confidence of good quality of the data. Several samples contained only small apatite grains, yielding a low  $F_t$  factor. In order to overcome erroneous  $\alpha$  recoil correction, samples with  $F_t < 0.63$  were excluded from the dataset.

Average He ages corrected for  $\alpha$  ejection (assuming a hexagonal geometry, after Farley et al., 1996 and Farley, 2002) vary between  $16.0 \pm 2.3$  (XC-75) and  $22.1 \pm 0.9$  Ma (XC-76), they are consistently younger than the according AFT ages and indicate Early to Middle Miocene cooling. There is no obvious trend in the data with regard to elevation and geographical position (Fig. 6-3). Three samples from remnants of piedmont paleosurfaces (XC-6, XC-12, XC-138) yield He ages between  $17.6 \pm 2$  (XC-12) and  $19.7 \pm 4$  Ma (XC-138), which is well within the range of  $16.0 \pm 2.3$  (XC-75) to  $22.1 \pm 0.9$  Ma (XC-76) yielded by samples representing the summit paleosurface (KU-24, XC-46, XC-67, XC-74, XC-75, XC-76, XC-89, XC-105, XC-123).

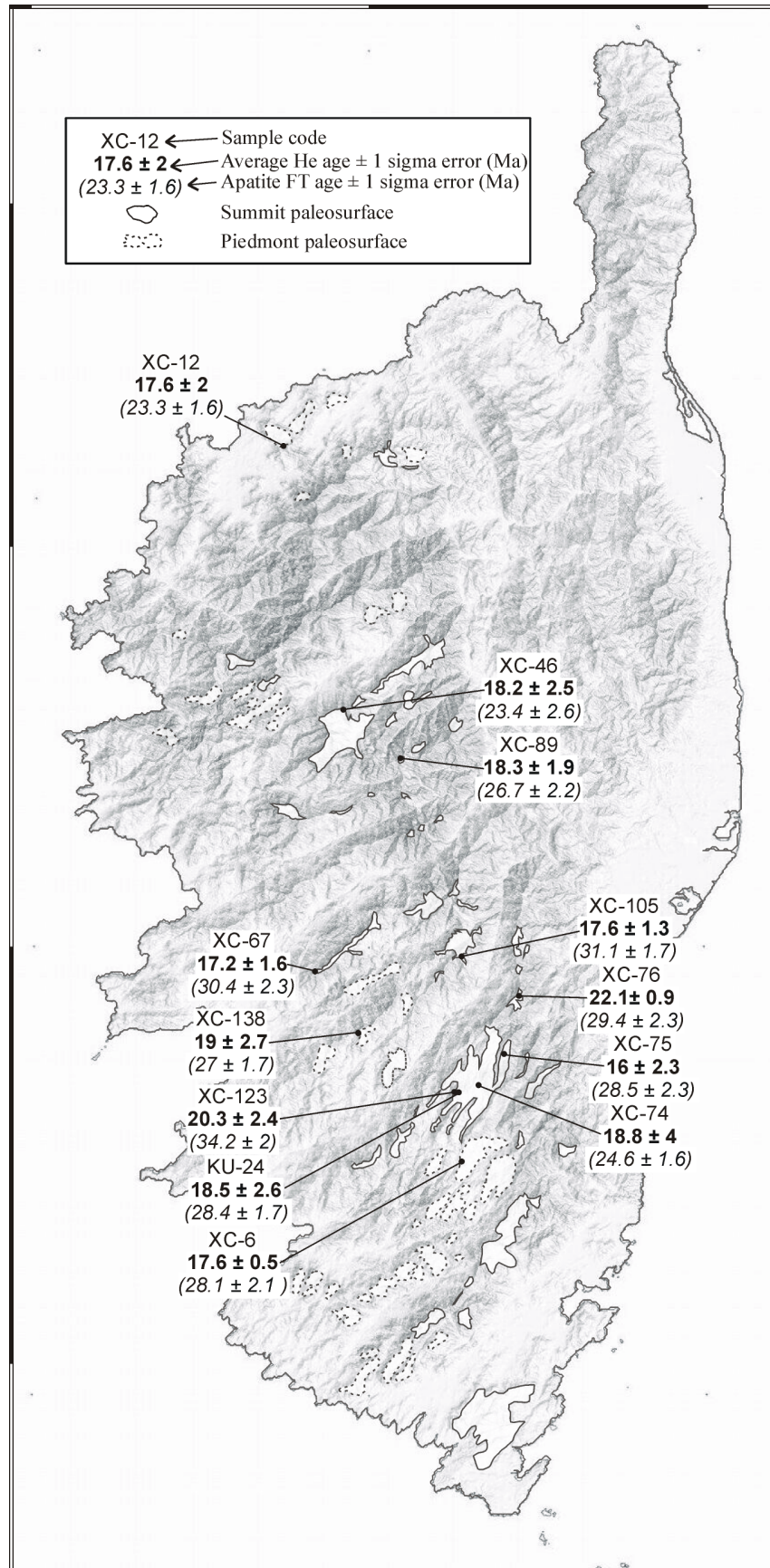


**Fig. 6-3:** Shaded DEM showing (U-Th)/He ages measured (in Ma) samples from both generations of paleosurface; related AFT ages are in brackets written in italic font.

**Table 6-3** (U-Th)/He data.

Sample code	Altitude (m)	PG	Nc	U (ng)	Th (ng)	<sup>4</sup> He ncc	TAE (%)	Unc. age (Ma)	F <sub>t</sub>	Cor. age (Ma)	Average age (Ma)	± 1σ (Ma)
XC-6	826	P	2	0.316	0.219	0.604	2.1	13.6	0.76	18.0	17.6	0.5
XC-6			1	0.200	0.187	0.414	1.9	14.0	0.81	17.3		
XC-12	550	P	1	0.076	0.149	0.178	3.4	13.2	0.69	19.0	17.6	2.0
XC-12			1	0.125	0.206	0.253	3.2	12.1	0.75	16.2		
XC-46	2247	S	1	0.037	0.061	0.078	2.9	12.7	0.69	18.3	18.2	2.5
XC-46			3	0.083	0.187	0.176	2.2	11.4	0.73	15.6		
XC-46			3	0.178	0.332	0.501	2.8	16.1	0.78	20.6		
XC-67	200	S	1	0.053	0.098	0.095	3.3	10.3	0.60	17.1	17.2	1.7
XC-67			1	0.058	0.113	0.117	3.3	11.4	0.73	15.5		
XC-67			1	0.035	0.082	0.082	2.8	12.3	0.65	18.9		
XC-74	1627	S	2	0.128	0.225	0.411	2.2	18.7	0.78	23.9	18.8	4.0
XC-74			2	0.272	0.408	0.719	1.8	16.1	0.81	19.9		
XC-74			2	0.124	0.210	0.260	2.0	12.4	0.76	16.3		
XC-74			1	0.077	0.102	0.146	2.4	12.0	0.79	15.2		
XC-75	2133	S	1	0.057	0.086	0.100	4.0	10.7	0.63	17.0	16.0	2.3
XC-75			1	0.082	0.163	0.145	2.6	9.9	0.75	13.2		
XC-75			1	0.112	0.187	0.238	2.3	12.6	0.76	16.5		
XC-75			1	0.095	0.152	0.165	3.0	10.4	0.73	14.2		
XC-75			1	0.076	0.154	0.198	2.5	14.5	0.76	19.1		
XC-76	1981	S	3	0.141	0.179	0.358	2.5	16.1	0.71	22.7	22.1	0.9
XC-76			1	0.040	0.040	0.080	2.7	13.4	0.63	21.4		
XC-89	2620	S	1	0.108	0.197	0.229	2.6	12.3	0.75	16.4	18.2	1.9
XC-89			2	0.118	0.186	0.277	2.2	14.1	0.78	18.1		
XC-89			2	0.148	0.299	0.395	2.4	15.0	0.74	20.3		
XC-105	1950	S	1	0.127	0.165	0.322	3.0	16.1	0.83	19.5	17.6	1.3
XC-105			1	0.045	0.070	0.100	3.6	13.5	0.79	17.0		
XC-105			1	0.090	0.132	0.187	2.2	12.8	0.74	17.3		
XC-105			1	0.050	0.060	0.089	3.5	11.5	0.70	16.5		
XC-123	1702	S	1	0.060	0.082	0.132	6.6	13.7	0.73	18.9	20.3	2.4
XC-123			1	0.095	0.147	0.216	2.2	13.7	0.73	18.9		
XC-123			1	0.099	0.103	0.245	2.8	16.4	0.71	23.1		
XC-138	580	P	1	0.077	0.170	0.186	2.1	13.1	0.73	17.9	19.7	4.0
XC-138			1	0.070	0.084	0.139	2.6	12.7	0.74	17.2		
XC-138			2	0.071	0.102	0.200	2.7	17.3	0.67	25.7		
XC-138			1	0.069	0.134	0.171	2.5	14.0	0.78	17.9		
KU-24	610	S	1	0.151	0.212	0.326	3.7	13.3	0.74	18.0	18.5	2.6
KU-24			1	0.175	0.306	0.469	2.1	15.7	0.77	20.4		
KU-24			1	0.068	0.138	0.134	2.5	10.9	0.71	15.4		
KU-24			1	0.060	0.081	0.148	2.1	15.4	0.71	21.7		
KU-24			1	0.073	0.103	0.142	2.8	12.1	0.71	17.0		

PG - paleosurface generation according to Kuhlemann et al.(2005a): P - piedmont paleosurface, S - summit paleosurface; Nc - number of dated apatite crystals; U - amount of <sup>238</sup>U + <sup>235</sup>U; <sup>4</sup>He - amount of in nano-cubic centimeters at Standard Pressure and Temperature (STP); TAE - total analytical error; Unc. age - uncorrected age; F<sub>t</sub> - correction factor calculated after Farley et al. (1996) and Farley (2002); Cor. age - corrected age.

## 7 INTERPRETATION AND DISCUSSION

### 7.1 ZIRCON FISSION TRACK DATA

#### 7.1.1 Introduction

Samples analyzed by zircon FT analysis were collected in the central and southern part of Variscan Corsica and ages are in the range ~140-160 Ma. These values are similar to those presented by Mailhé et al. (1986) and Zattin et al. (2001), but a full integration of their datasets is not possible, since the publications of these authors provide neither the analytical procedure nor the sample coordinates and the counting statistics. Nevertheless, there are some conspicuous features that can be extracted for further interpretation: the ages from the Variscan basement are in the range 244-110 Ma, the ages along the Alpine deformation front are in the range ~75-60 Ma, rocks from Alpine Corsica have zircon FT ages in the range ~40-19 Ma (Fig. 7-1-1).

Mailhé et al. (1986) interpreted the ZFT age pattern as a west-to-east younging trend, resulting from westward-decreasing thickness of Alpine thrust sheets that caused partial reset of Variscan zircon FT ages during the thrusting. Practically, these authors considered the zircon FT ages from Variscan Corsica as "mixed ages", which means Variscan ages partially reset during Alpine metamorphism.

In contrast, Vance (1999) recognized that zircon FT ages in the range 220-100 Ma are widely preserved within and adjacent to the Western Alpine orogenic system and interpreted them to be the result of high heat flow related to mantle upwelling during Late Triassic and Early Jurassic rifting and subsequent opening of the Ligurian-Penninic Ocean. This thermal event was long-lasting and was characterized by extremely high heat flow on both continental margins (Vance, 1999).

#### 7.1.2 ZFT domains

In order to interpret the ZFT data, Corsica is subdivided into three ZFT domains, according to similarities in the age pattern (Fig. 7-1-1):

**Domain I** - encompassing the major part of Variscan Corsica with zircon ages in the range ~244-130 Ma, the ages evidently lack a Tertiary thermal overprint and are interpreted as relating to the thermal event associated with the opening of the Ligurian-Piedmont Ocean, which evolved between the Laurasian (including Corsica-Sardinia block) and the African plate in the Jurassic between ~200

and 140 Ma (e.g., Frisch, 1981). There are several evidences favoring a "Piedmont" origin of the ZFT ages:

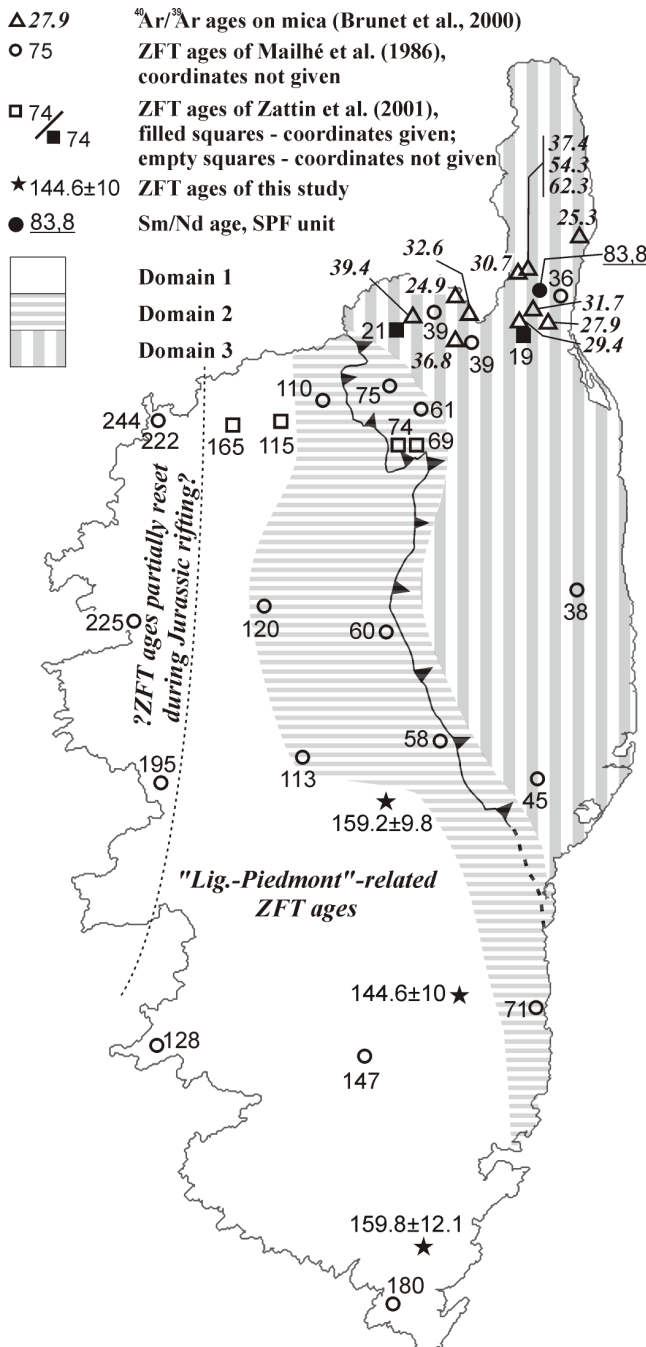


**Fig. 7-1-1:** Distribution of ZFT, <sup>40</sup>Ar/<sup>39</sup>Ar and Sm/Nd data and subdivision of Corsica into zircon fission track domains (see text for explanation).

- all samples (where counting statistic is given) pass the  $\chi^2$ -test indicating that these ages are not "mixed" as supposed by Mailhé et al. (1986);

- ZFT ages are juxtaposed to the rifted European continental margin (with respect to the Ligurian-Piedmont Ocean), and the data range perfectly fits to the time interval of rifting and opening of the Ligurian-Piedmont Ocean;

- the ages are getting older in roughly NW direction, away from the rifted continental margin (in the NW part of Domain I the ages are therefore only partially reset). This pattern is consistent with the existence of the heat source, which remained "fixed" while the adjacent continental margins slowly moved apart during continental rifting and subsequent seafloor spreading;

- the ages are similar to "Piedmont"-related ZFT ages reported from the adjacent Southern and Western Alps;

- it is improbable that Tertiary Alpine metamorphism would have uniformly and systematically partially reset pre-Alpine (or Variscan) ZFT ages exactly to Jurassic ages over wide areas, extending from Variscan Corsica to the South Alpine realm, the latter of which shows no evidence of Alpine metamorphism.

Except the group described above, there is also a group of samples with older ZFT ages within *Domain I*. This group of older ages (225-244 Ma) in NW Corsica can be interpreted in two ways: (i) Firstly, the ages record a thermal event related to Permian-Triassic magmatic activity accompanying

breakup of Pangea. Thus, the ages can be understood as cooling ages and should form one population. (ii) Secondly, the ages can be interpreted as Variscan ages related to intrusion age of the granitic basement, which were partially reset by thermal event related to Jurassic rifting. In this case, the ages should be understood as "mixed" ages. However, since all these ages were reported without counting statistics, it is not possible to decide whether the ages are "mixed" or make single population. Anyway, the author prefers the second option since the pattern of ages increasing with increasing distance away from the rift margin fits to the interpretation of "Piedmont"-related ZFT ages. So, this part of Variscan basement was too far from the heat source during the Jurassic rifting. Therefore the temperature was too low to cause total resetting of the ZFT system.

**Domain II** (see Fig. 7-1-1) - occupies a strip along the Alpine deformation front with Late Cretaceous - Paleocene ZFT ages (~120 and 58 Ma). Ages in this range were first presented by Mailhé et al. (1986), but were considered to be erroneous by other authors (e.g., Brunet et al., 2000; Cavazza et al., 2001; Zarki-Jakni et al., 2004), because they thought that these ages contradict the data obtained by other thermochronometers. However, a more recent study of Zattin et al. (2001) reported very similar ages probably from the identical region (neither the exact sample locations nor the relation to tectonic units is given in the publications of Mailhé et al., 1986 and Zattin et al., 2001), thus it seems that this age group is geologically meaningful and can give an important constraint to decipher the age of metamorphism in Alpine Corsica that has been a matter of debate for a long time (e.g., Mattauer et al., 1981; Jolivet et al., 1990, 1991, 1998; Egal, 1992; Caron, 1994; Lahondère and Guerrot, 1997; Brunet et al., 2000).

At first glance, these ages could be explained as to be related to some thermal event that influencing *Domain II* during Middle Cretaceous - Paleocene times. Such explanation would be acceptable since it is known that in the Late Cretaceous some tectonic units of Alpine Corsica were involved in the subduction process and experienced HP/LT metamorphism (e.g., Sm/Nd age of  $83.8 \pm 4.9$  Ma measured on SPF unit, see Fig. 7-1-1, chapter 2.6; Lahondère and Guerrot, 1997). This would however mean that the eastern margin of the Variscan basement (*Domain II*) was at that time likewise subducted. On the other hand, it is widely accepted that the Variscan basement collided with Alpine Corsica only during the Eocene, as indicated by Eocene flysch sediments and the Eocene age of metamorphism of some of its parts (e.g., Tenda Massif; Jolivet et al., 1998; Brunet et al., 2000). Thus the ZFT ages of *Domain II* are interpreted as apparent ages. Prior to collision, these ages were probably Jurassic and belonged to *Domain I* (as defined above). In the Eocene, this part of the basement was buried by eastward subduction to a depth with temperatures sufficient for partial reset of ZFT system. A conversion of temperature to depth, by assuming a thermal gradient of 15°C/km acceptable for subduction zones, revealed that *Domain II* must have been buried to a depth of at least 15 km and therefore it can be presumed that large part of *Domain I* was also buried during subduction.

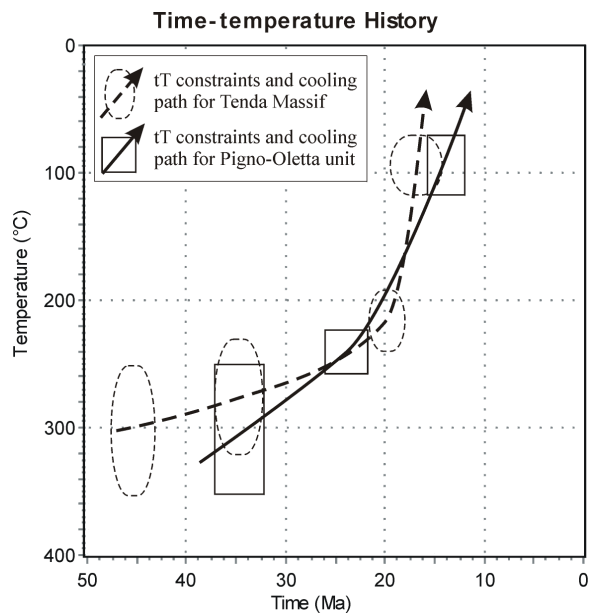


**Fig. 7-1-2:** Time-temperature evolution of Domain III demonstrated on the example of two Alpine tectonic units (Tenda Massif - rectangles and solid lines, and Pigno-Oletta unit - ellipses and dashed lines). Cooling paths are reconstructed from P-T and thermochronological data (Lahondère, 1991; Egal, 1992; Jolivet et al., 1998; Brunet et al., 2000; Zattin et al., 2001).

**Domain III** (see Fig. 7-1-1) - covers most of Alpine Corsica where ZFT ages are in the range ~45-19 Ma. These young ages are in accord with  $^{40}\text{Ar}/^{39}\text{Ar}$  ages on micas, ranging between ~45 and 22 Ma (Brunet et al., 2000), and indicate fast cooling following the stage in the MP/LT metamorphic conditions as it is shown on tT diagram (Fig. 7-1-2). Following the interpretation of Jolivet et al. (1998) and Brunet et al. (2000), the cooling path can be explained as follows: in the Eocene, the Alpine units were dragged down into the subduction zone and metamorphosed at MP/LT conditions. In the Early Oligocene, at ~33 Ma, the compressional regime changed to an extensional one (Jolivet et al., 1990; Fournier et al., 1991; Brunet et al., 2000), the accretionary complex started to collapse, thrust planes were reactivated as normal faults, and

the units were tectonically exhumed as core complexes (Rosenbaum et al., 2005). Time of tectonic denudation can be bracketed according to  $^{40}\text{Ar}/^{39}\text{Ar}$  and ZFT data between ~33 and 19 Ma.

### 7.1.3 Conclusions

Based on the ZFT data, Corsica can be subdivided into three domains: *Domain I*, encompassing a major part of Variscan basement, records a thermal event related to the Jurassic opening of the Ligurian-Piedmont Ocean. Since then it was spared of any thermal activity relevant to the ZFT system. *Domain II*, occupying a strip along Alpine - Variscan boundary, incorporates the units that were partially reset during Eocene metamorphism. This domain, although including Cretaceous ages, was not affected by a Cretaceous thermal event. *Domain III*, including most of Alpine Corsica, records a tectonic denudation of Alpine units between ~33 and 19 Ma, related to the collapse of the accretionary wedge.

## 7.2 APATITE FISSION TRACK DATA

### 7.2.1 Elevation profiles and exhumation rates derived from AFT data

#### 7.2.1.1 TERMINOLOGY

There has been considerable confusion concerning the terminology describing vertical movement and cooling of rocks in the literature. In this study, the terminology after England and Molnar (1990), Ring et al. (1999) and Stüwe (2002) is used:

*Uplift* and *subsidence*, describe vertical motion [uplift - motion upwards; subsidence - motion downwards] relative to a reference level (e.g., relative to the geoid). Both can be determined for instance from paleobotany, paleoclimatology, and sediments in surrounding basins, but can not be inferred from thermochronology. England and Molnar (1990) further distinguished *surface uplift*, meaning the vertical motion of the Earth's surface relative to a reference level, and *rock uplift*, meaning the vertical motion of rock relative to a reference frame. Both terms should be used together with a specification of the reference frame. In this study, the term *uplift* is used as equivalent of *surface uplift* with the sea level as the reference frame, while the term *rock uplift* is not used, because of lack of quantifying data.

*Exhumation* and *burial* describe vertical displacement of rocks relative to the surface [exhumation - motion towards the surface; burial - movement away from the surface]. They can be determined from geochronology, geobarometry, and geothermometry.

In recent years, the terms exhumation and denudation are used as synonyms in the literature, although a subtle distinction is sometimes made about the frame of reference. Some authors consider the usage of the term *denudation* instead of exhumation to be more appropriate (e.g., Summerfield, 1991; Brown et al., 1994; Fitzgerald et al., 1995), as the term *exhumation* in geomorphological use means the re-exposure of a formerly inhumed (or buried) rock or topographic surface rather than the general movement of rock with respect to the Earth's surface. According to Ring et al. (1999), the term *denudation* means the removal of rock by tectonic (e.g., by normal faulting - *tectonic denudation*) and/or surficial processes (e.g., by erosion - *erosional denudation*) at a specified point at or under the Earth's surface.

*Erosion* is the surficial removal of mass at a point in the landscape by both mechanical and chemical processes.

### 7.2.1.2 THEORY

One of the prominent features of FT system is that it can yield quantitative information on cooling and exhumation of the rocks. In this study, exhumation rates were calculated by the altitude-dependence method, which relies on analysis of two (or more) samples collected in different heights using the same dating method (most commonly FT on apatite; Wagner and Reimer, 1972; Wagner et al., 1977; Fitzgerald and Gleadow, 1988). In this approach it is assumed that samples taken from greater altitudes crossed the closure temperature isotherm earlier than the lower samples, resulting in increased FT ages with elevation, and that the slope of the age-elevation trend is proportional to the exhumation rate. The exhumation rate is calculated as:

$$\text{exhumation rate} = \Delta \text{ elevation} / \Delta \text{ age}$$

The main advantage of this approach is that it is nearly independent of any assumptions about geothermal gradients provided the critical isotherms were at the same depth for each sample (Mancktelow and Grasemann, 1997). Nevertheless, reasonable exhumation rates can be calculated by this method only if several crucial assumptions are valid. Some typical problems of this approach include: the assumption that cooling is solely the result of erosion; the neglecting of the PAZ; the implicit assumption that a rock sample is transported perpendicularly to the isotherms; changes in the spatial relationship between samples (e.g., owing to faulting) no longer reflect the original sample depth in the crust; the neglecting of the influence of topography and heat advection (see Stüwe et al., 1994; Mancktelow and Grasemann, 1997; Gallagher et al., 1998; Stüwe and Hintermüller, 2000). In the following, relevant factors are discussed with regard to Corsica, and the procedure to calculate the exhumation rates is explained.

**The neglecting of the PAZ:** The neglecting of the PAZ and relating of FT age to closure temperature is only plausible when no significant annealing occurred in post-closure time and the rocks experienced rapid cooling. The validity of this assumption in the case of Corsica can be demonstrated by the track length distribution: all samples used for exhumation rate calculation revealed narrow track length distributions with long MTL, characteristic of rapidly cooling rocks, which spent only short time within the PAZ (see Figs. 6-2 and 7-2-11).

**Assumption of rock transport perpendicular to the isotherms:** This assumption is definitely not met in Corsica, since it is known that during the Miocene the Variscan basement was segmented by faults to numerous rigid blocks, which experienced tilting (8 to 40°) and rotation, which is difficult to quantify. Due to tilting, the present-day arrangement of the samples no longer represents the original distance that can result in underestimation of true exhumation rates.

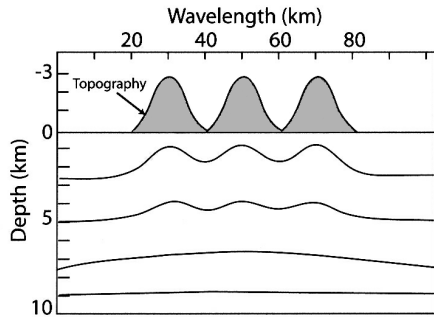


**Fig. 7-2-1:** Illustration showing the influence of topography on perturbation of isotherms. Shallow isotherms follow topography closely, while deeper isotherms are less influenced by topography (after Stüwe et al., 1994; adopted from Foeken, 2004).

***Influence of topography (ridge and valley effect):***

Several studies demonstrated that topography may significantly influence the shape of isotherms (Stüwe et al., 1994; Mancktelow and Grasemann, 1997; Stüwe and Hintermüller, 2000; Braun, 2002). The critical parameters that perturb the shape of isotherms are the exhumation rate and the topographic wavelength and amplitude. Assuming a steady-state situation, Stüwe et al. (1994) noted that at high exhumation rates (~1000 m/Ma), a topographic relief of 3 km and a wavelength of ~20 km, the ~100°C isotherm is perturbed by at least 1 vertical kilometer (Fig. 7-2-1). The effect increases for larger amplitudes and wavelengths and higher exhumation rates. The effect decreases to negligible values for denudation rates below ~500 m/Ma. Mancktelow

and Grasemann (1997) further refined the model of perturbing isotherms by incorporating a time-dependent heat advection equation. They noted that for topographic wavelengths < 6000 m, a relief of ~3 km and the exhumation rates on the order of 1000 m/Ma will not warp the ~100°C isotherm, and the error resulting from using the standard one-dimensional altitude dependence technique to calculate exhumation rates is geologically insignificant.

The regions sampled in this study for elevation profiles exhibit a maximum relief of less than ~2000 m, wavelengths in the range of ~15-20 km (Fig. 7-2-2), and estimated exhumation rates of less than 500 m/Ma. These values are clearly too low to have some impact on the bending of the 110°C isotherm. Therefore a possible effect of the topography on the shape of the 110°C isotherm in Corsica is ruled out, and the exhumation rates are calculated by the using one-dimensional model and

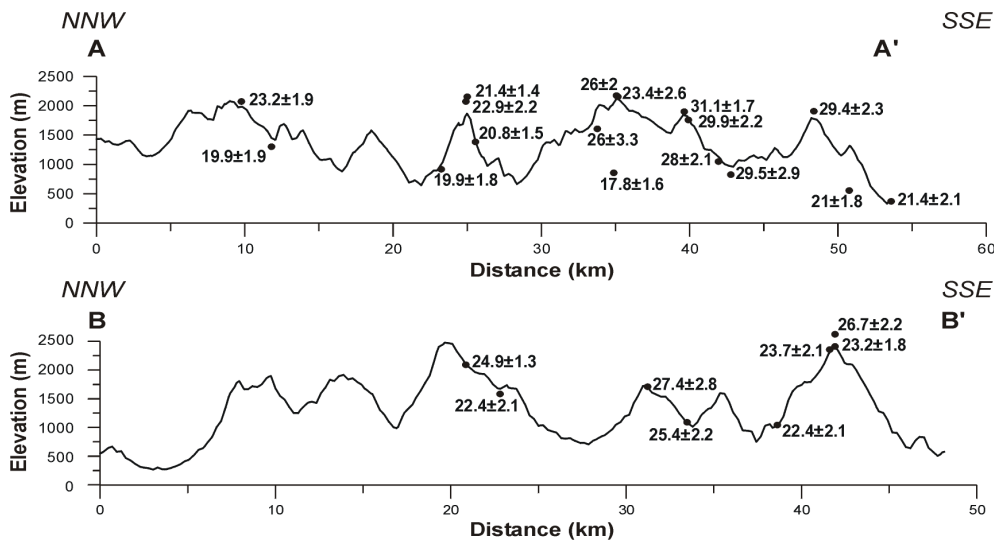


**Fig. 7-2-2:** Elevation profiles across steep relief regions of Variscan Corsica with plotted AFT ages dedicated to determination of exhumation rates. Traces of the profiles can be found in Fig. 7-2-3.

assuming the isotherm parallel to the mean surface.

**Changes in the spatial relationship between samples:** The spatial relationship between the samples should not be disturbed by an active fault, so as the samples represent original depth in the crust. This is a serious problem since in all orogens rather complex fault patterns are present. The problems with faults can be overcome by applying proper sampling strategies. Usually, the samples are taken in a vertical elevation profile from boreholes or over a significant range of vertical relief. Except in the case of boreholes or mines, an elevation profile will never be truly vertical. Regardless, it is important to minimize the horizontal distance between samples. Moreover, one should always be certain that samples are collected from a single tectonic block not disturbed by faults.

### 7.2.1.3 RESULTS

In this study, altogether eight elevation profiles were sampled in the main ridges with the steepest relief in central and northern Variscan Corsica (Fig. 7-2-2). Unfortunately, many of the samples yielded un-datable amounts of apatites, thus some profiles are calculated from two samples

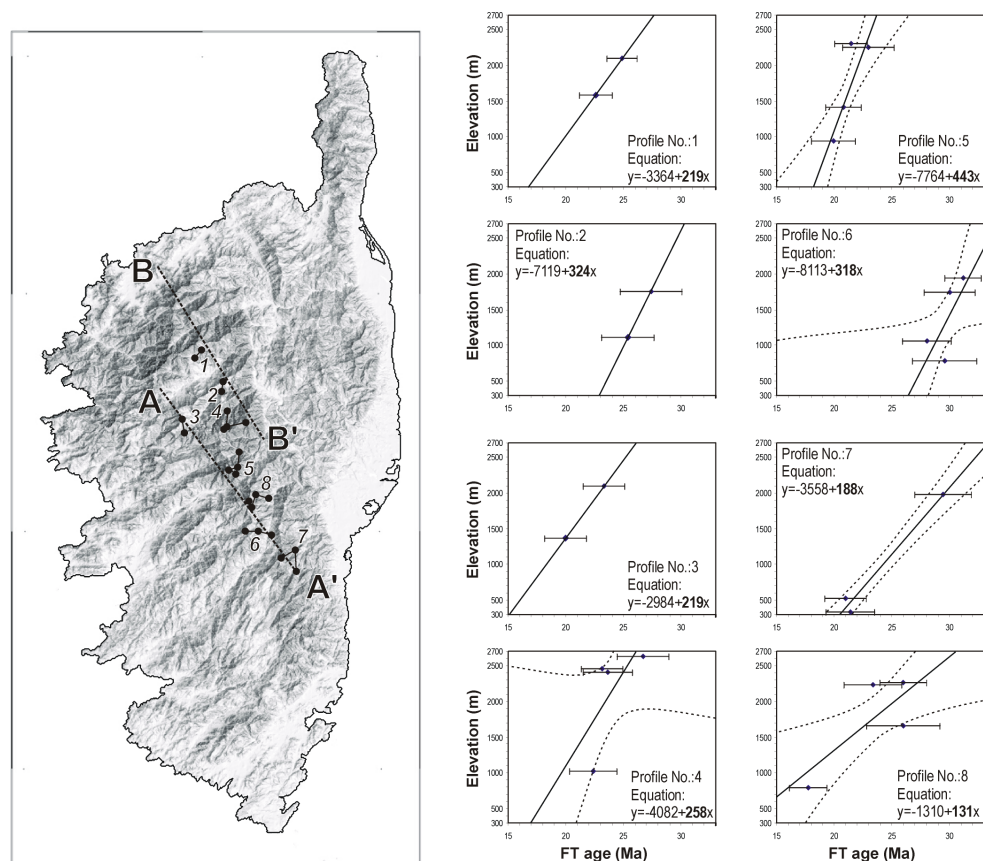


**Fig. 7-2-3:** Left panel: shaded DEM depicting traces of elevation profiles from Fig. 7-2-2 and location of elevation profiles representing individual blocks (labeled with numbers). Right panel: age-elevation plots of individual blocks (numbers refer to those in left panel) with calculated exhumation rates. Exhumation rates (in m/Ma) equal to the slope of linear regression (bold font) and are calculated as error-weighted linear best fit (solid line) with 95% confidence level (dashed line).

only. The samples yielded positive age-elevation relationships. Exhumation rates were computed as error-weighted linear best fit. Then the obtained values were corrected for tilting that was assessed from the tilt grade of corresponding paleosurfaces. Results are presented in Fig. 7-2-3 and range between ~100 and 450 m/Ma, indicating moderate cooling of the basement during Late Oligocene to Early Miocene times, and no significant difference in exhumation rate among the sampled tectonic blocks. It has to be kept in mind that these values are only approximate, since there are numerous factors that may under- or overestimate the true values.

#### 7.2.1.4 AGE-ELEVATION PATTERN IN REGIONAL SCALE

When looking at the age-elevation relationship in the entire dataset, there is no obvious correlation between elevation of the samples and their ages: The data form one cluster with two outliers (Fig. 7-2-4). This is not surprising, since it is known that Corsica does not form a single tectonic block, but is fragmented by a complex network of faults. In order to clarify age-elevation relationships, Variscan Corsica was subdivided into divisions defined according to similar age patterns

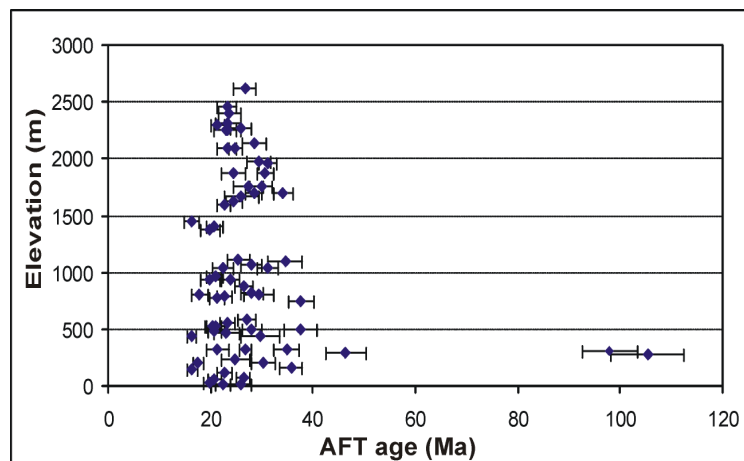


**Fig. 7-2-4:** Age-elevation plot of all measured samples, where no clear trend in age-elevation relationship is evident.

and obeying the distribution of major faults separating main ridges (Fig. 7-2-5). Even so, there is, with one exception (Domain I. in Fig. 7-2-5), no evident correlation between the AFT ages and sample elevation - the trends are not clearly positive or negative, but rather vertical. This is interpreted as a consequence of intensive tectonic activity that must have occurred after the cooling of the basement - probably after the Early Miocene. During faulting the island was segmented into numerous blocks, which experienced tilting and differential vertical and lateral displacement, and therefore the FT ages from foothills can be older than those from the mountain tops.

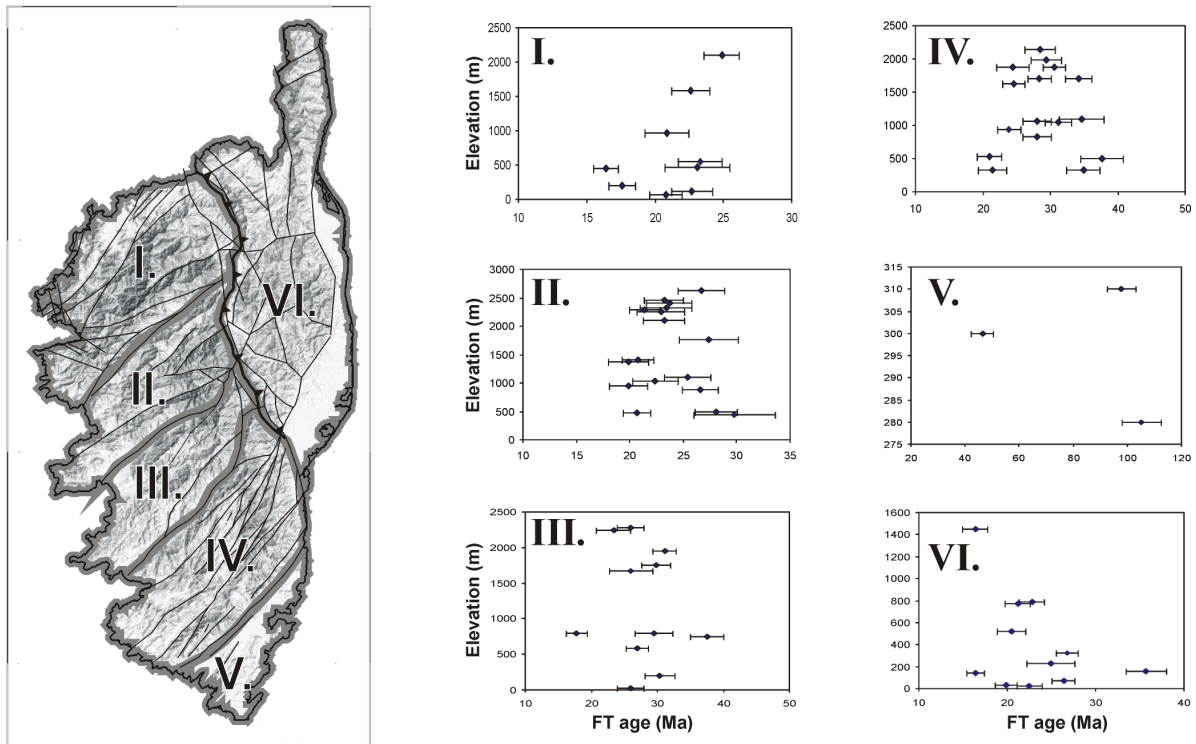


**Fig. 7-2-5:** Shaded DEM showing subdivision of Corsica into six domains, defined according to the orientation of major faults (left panel), and related age-elevation plots (right panels) where no clear relationship between AFT age and sample elevation can be observed.

### 7.2.1.5 CONCLUSIONS

Exhumation rates, calculated from the elevation profiles in steep relief regions by the altitude-dependence method that is not biased by the thermal gradient adopted, are in the range of ~100 and 450 m/Ma. These values indicate moderate cooling of the basement during Late Oligocene to Early Miocene times.

Due to the intensive post-Early Miocene tectonic activity, at present the island displays a complex mosaic of numerous small blocks that are no longer arranged in their original position, and that is why in regional scale no obvious age-elevation dependence can be observed.

## 7.2.2 Trends and patterns in apatite fission track data

### 7.2.2.1 TREATMENT PROCEDURE ON AFT DATASETS OF PREVIOUS STUDIES

As mentioned in chapter 2.6, there have been several studies reporting apatite FT data from Corsica, but not all of them seem to be entirely correct. The older studies were found to present erroneous FT ages, but there is still a large dataset of modern studies (Jakni et al., 2000; Cavazza et al., 2001; Fellin, 2003; Zarki-Jakni et al., 2004; Fellin et al., 2005), which have to be considered. However, even these modern studies do not always provide critical information such as sample localization and laboratory procedures used, or they provide statistically inadequate results. All these attributes make an incorporation of different datasets difficult. Thus, the data definitely require some treatment. In this study, the datasets of other studies were filtered out according to the following criteria:

- FT dating procedure must be reported
- localization of the samples must be given in any kind of coordinate system
- 15 or more apatite crystals must have been counted per sample in order to provide statistically robust results
- samples where the FT age was not reproduced within  $1\sigma$  errors by the own results from the very same locality were expelled
- ages with dubious meaning were expelled (e.g., if a FT age was reported in a Ph.D. thesis, but was omitted in a related publication based on that thesis)
- when presenting track length distributions, at least 35 horizontal confined tracks must have been measured per sample, and standard deviation and standard error must be reported

The data fulfilling these conditions were rectified to a UTM32/WGS84 coordinate system and used for further work.

### 7.2.2.2 SPATIAL DISTRIBUTION OF AFT AGES

As already discussed in chapter 7.2.1.4, due to extensive faulting there is no clear correlation between apatite FT age and sample elevation on the regional scale. Therefore, negligible impact of the elevation on the age pattern can be assumed, and, in the first approach, the apatite FT ages (combined with the treated data of other studies) are presented in a spatial distribution not corrected for altitude (Fig. 7-2-6). In order to provide better visualization of the final version of the dataset used for further work, the FT ages are presented in three ways: 1) FT ages are plotted as numbers on the DEM of Corsica with the Alpine deformation front, errors are not included; 2) FT ages are displayed in a form of circles of 8 km radius (bigger circles), where the age values are indicated by the color of circles, the

error ranges are displayed as smaller circles in the center of the bigger circles, values are indicated by colors; 3) FT ages are interpolated and smoothed, errors are not included.

When looking at the spatial distribution of all AFT ages in Corsica, several patterns and trends can be immediately recognized. Most of the ages are reported from a W-E trending profile across the Tenda Massif and adjacent Alpine units. Variscan Corsica is satisfactorily covered by the data in the central band running from south to north through the whole island, meanwhile the western peninsulas and NW part would require more data. So far, no FT data are available from a major part of Alpine Corsica.

It is obvious that FT ages form a more complicated picture than proposed by Zarki-Jakni et al. (2004). Instead of clearly visible crescent-shaped bands of similar ages (see Fig. 2-7 in chapter 2.6), there are instead several smaller and larger age clusters that form a fairly complex mosaic.

Prevailing ages are in the range ~20-27 Ma (mostly green and green-yellow circles in the Fig. 7-2-6B), encountered mainly in the central and western parts of the island, covering the major part of the Variscan basement and also the western margin of Alpine Corsica in its central part. As an exception in this cluster, there are two slightly higher ages of  $29.3 \pm 3.6$  and  $30.5 \pm 3.2$  Ma reported by Fellin et al. (2005) from the Corte region close to the Alpine front (blue circles).

Further to the south, in the Bavella and Incudine regions of Variscan Corsica, a cluster of slightly higher ages in the range ~25-35 Ma can be identified (mainly blue and blue-green circles in the Fig. 7-2-6B). The southernmost extremity of Corsica is characterized by the by far oldest AFT ages around 50 Ma (dark blue and purple colors), with two exceptionally high ages of  $97.9 \pm 5.4$  and  $105.3 \pm 7.2$  Ma from the Chera region (black circles). Another old sample of  $53.8 \pm 4.1$  Ma was reported by Zarki-Jakni et al. (2004) from the westernmost extremity of a peninsula west of Ajaccio. This sample does not conform to the regional pattern, since all samples from the vicinity are younger than ~20 Ma. However, there was no reason to exclude this sample from the dataset since it fulfilled all prescribed criteria. So as to verify the accuracy of this age, this locality was re-sampled three times, nonetheless the sampled rocks never contained enough apatite crystals. Thus the verification of this age remains for future research, and this sample is not included in further discussion.

The youngest ages in the range ~10-23 Ma (yellow, but mainly red circles) form two well-defined and one ill-defined clusters. The first well-defined cluster is located in the northern part of Corsica, and covers the Tenda Massif and Alpine nappes around St. Florent region. The second cluster covers the area along the southern part of the Alpine front, south-west of the Oriental Plain. The remaining ill-defined cluster (~15-23 Ma) can be identified in the northwestern part of Variscan Corsica, south of Calvi. This cluster may in fact belong to the young age group of the Tenda region, but there is a gap in data between these two clusters.

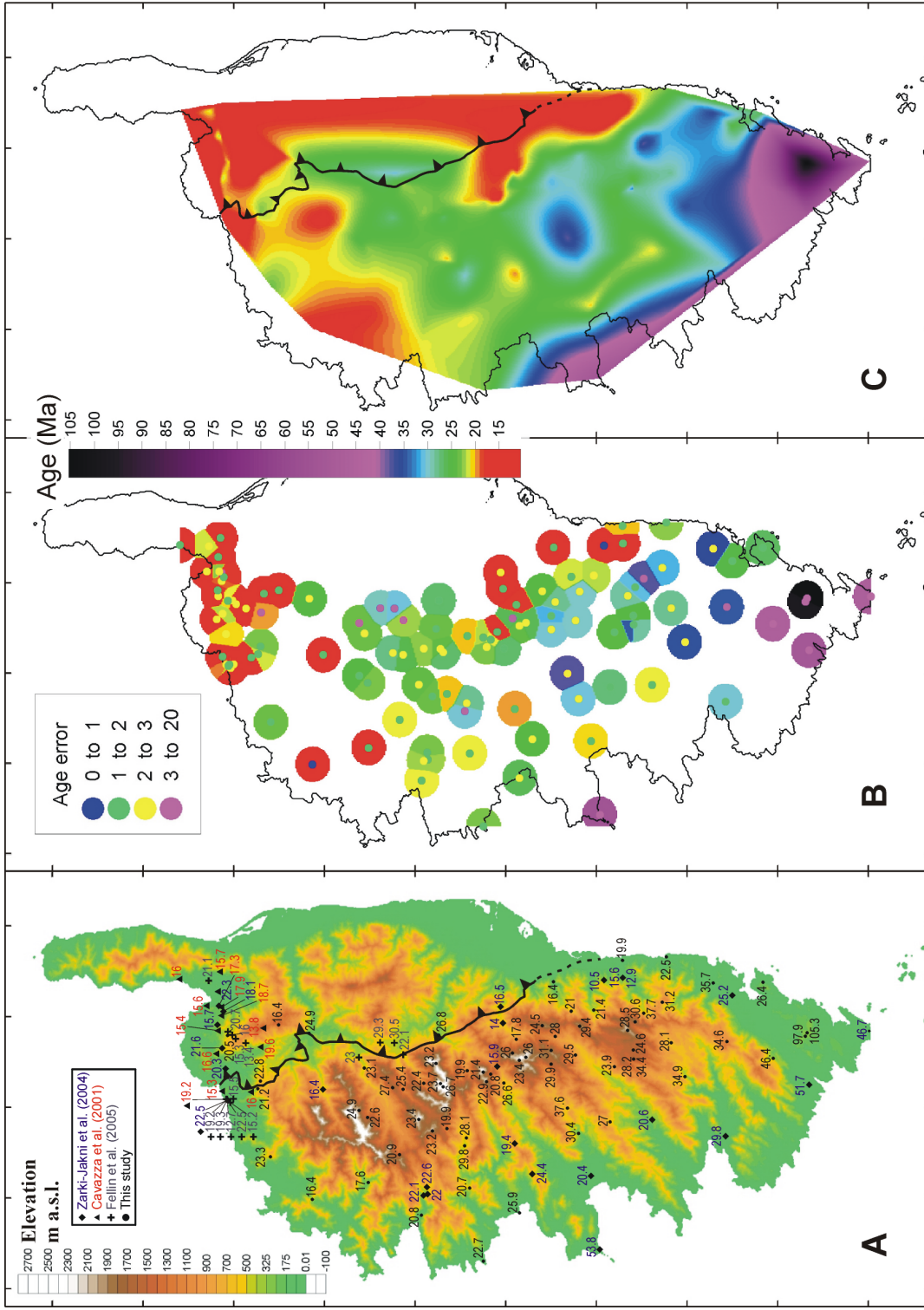


**Fig. 7-2-6:** FT database containing all available AFT data, which passed prescribed criteria. A: DEM with contour of Alpine front and AFT ages expressed as numbers (in Ma), errors not included; B: FT ages expressed in a form of circles of 8 km radius (bigger circles), where age values are indicated by the color of circles, error ranges as smaller circles in the center of bigger circles, values are indicated by colors; C: pattern of FT ages obtained by interpolation and smoothing of existing dataset, errors not included. Note that N-S trending red strip running across Alpine Corsica is not based on the existing data but is an effect of interpolation.

## 7.2.2.3 TRENDS AND PATTERN IN TRACK LENGTH DATA

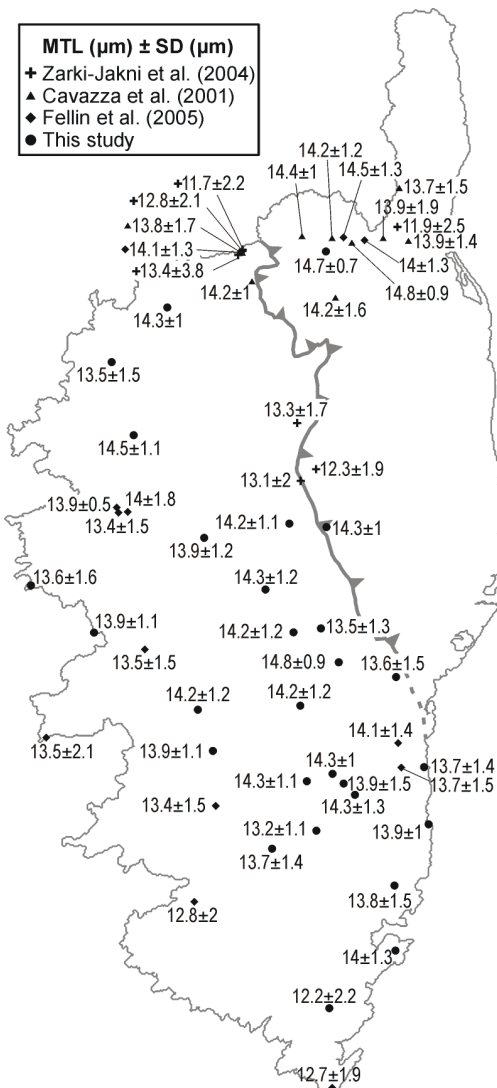


**Fig. 7-2-7:** Illustration of Corsica depicting all available track length data.

and a surprisingly broad distribution ( $SD = 3.83 \mu\text{m}$ ) from the Variscan basement in the Balagne region. Fellin et al. (2005) argued that this kind of "strange" track length distribution was produced by monotonous cooling of the sample through the PAZ.

The relationships between FT age and MTL (Fig. 7-2-8 second diagram), and FT age versus SD (Fig. 7-2-8 third diagram), show that most of the samples belong to a distinct cluster with FT ages of  $\sim 10$  to  $40$  Ma, relatively long MTLs of  $> \sim 13.4 \mu\text{m}$ , and relatively narrow track length distributions expressed by low values of  $SD (< \sim 2 \mu\text{m})$ . Such data indicate that these samples experienced cooling through the apatite PAZ in a simple, rapid fashion but not necessarily at the same time. Besides, there are some few scattered samples not belonging to this cluster, having ages in the range  $\sim 12$  to  $105$  Ma,

In the spatial distribution of the mean track lengths a certain similarity to the pattern of the FT ages can be recognized (Fig. 7-2-7). A vast majority of the samples is characterized by relatively narrow ( $SD < 2 \mu\text{m}$ ), unimodal track length distributions with relatively long mean track lengths ( $> 13.5 \mu\text{m}$ ). These samples cover almost the entire island with FT ages  $< 40$  Ma, excluding its southernmost part and some local exceptions. Samples with relatively wide ( $SD > 2 \mu\text{m}$ ), bimodal track length distribution and short MTL ( $< 13.5 \mu\text{m}$ ) are encountered principally in the southern- and southwesternmost parts of the island, where the samples with the oldest ages ( $> 50$  Ma) are concentrated.

In order to detect some trends in the FT data, FT ages, MTLs, and SDs were plotted against each other. These interrelationships are displayed in Fig. 7-2-8.

The relationship between mean track length and its standard deviation is, with one exception, as it is expected (Fig. 7-2-8 first diagram): higher SD values with relatively short MTLs and lower SD values with relatively long MTLs. The exception, which obviously does not obey the trend of decreasing SD with increasing MTL, is a sample presented by Fellin et al. (2005) with the age of  $15.2 \pm 2.2$  Ma, MTL of  $13.43 \mu\text{m}$

clearly shorter MTLs ( $< \sim 13.4 \mu\text{m}$ ), and wider track length distributions ( $\text{SD} > \sim 2 \mu\text{m}$ ). Such values indicate that these samples did not experience a single stage cooling history, but instead have resided within the apatite PAZ for a relatively long time, or have been reheated to the temperatures of the PAZ at some stage.

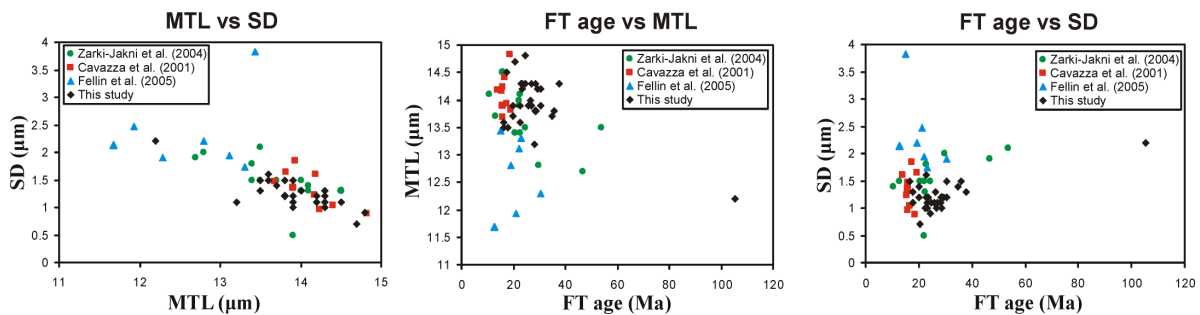


**Fig. 7-2-8:** Interrelationships of AFT age, mean track length (MTL) and standard deviation (SD) of mean track length for Corsican samples.

On this point, it may be worthwhile to discuss the track length data reported by Fellin et al. (2005). The authors presented seven track length distributions (passing the criterion of minimum 35 lengths measured) of the samples coming from regions with young FT ages, usually less than  $\sim 30$  Ma. Their data reported from the Balagne region in first glance seem not to be in accord with those published by Cavazza et al. (2001) and Zarki-Jakni et al. (2004) from the very same localities, who presented the MTL values up to  $\sim 1 \mu\text{m}$  longer than Fellin et al. (2005) (see Fig. 7-2-8). However, clearly bimodal shape of some distributions in the Corte, Balagne and St. Florent regions presented by these authors provide evidence that the cooling history of some areas is complex and can vary over distances of a few tens of meters, and is probably controlled by the activity of faults (Fellin et al., 2005).

#### 7.2.2.4 CHEMICAL COMPOSITION OF THE APATITES

According to Dpar values, most of the samples contain normal fluorine-apatites. However, there are also several samples with larger Dpar values, pointing to higher proportion of Cl or OH in the apatites (Fig. 7-2-9). These samples should be more resistant to annealing, have higher closure temperature and yield older FT ages than those with fluorine-composition (e.g., Green et al., 1986; Carlson, 1990; see also chapter 4.1.4). When plotting the FT ages of the present dataset against Dpar values, the distribution does not obey an expected positive correlation between these two parameters. In contrast, it is rather difficult to recognize some pattern or trend in the dataset (Fig. 7-2-9). Thus it is assumed that variation in apatite chemical composition of the samples did not have an impact on the final FT ages. This phenomenon can be explained in two ways:

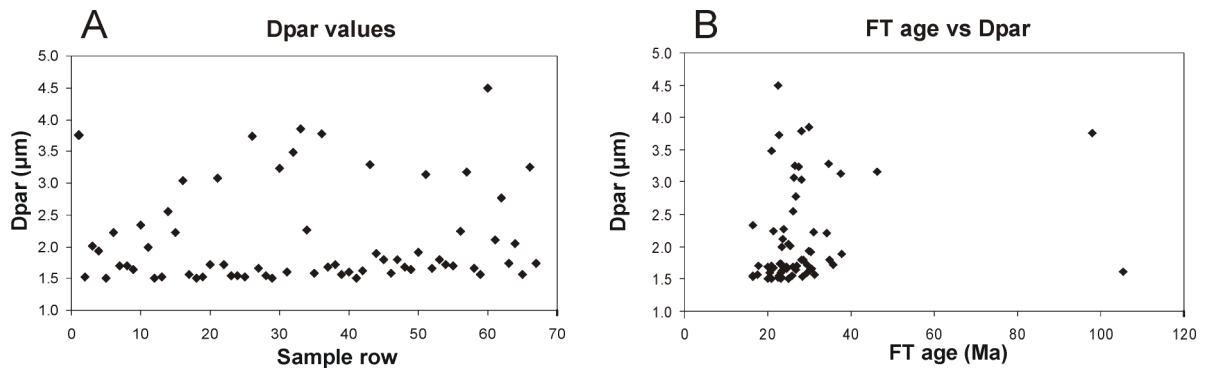


**Fig. 7-2-9:** A: plot showing measured range of Dpar values; B: FT age plotted as a function of Dpar (right); see text for explanation.

First, the samples were cooling very fast through the PAZ. Rapid cooling produced only minimal differences in the FT ages of samples with different apatite composition, and the resolution of the FT dating method is not sufficient to detect them.

Second, during cooling through the PAZ, the width of the PAZ was low, for instance, due to an increased thermal gradient inducing compression of isotherms. In this case, the cooling need not have been so extreme as in the first case, but nonetheless the samples could pass through the narrow PAZ virtually faster, again producing undetectable differences in FT ages among samples with various apatite composition.

The first option can be favored by the track length distributions, which are generally unimodal with long MTLs (often  $> 14 \mu\text{m}$ ) pointing to very rapid cooling through the PAZ. However, since the exhumation rates, calculated independently from the thermal gradient (see chapter 7.2.1.3), infer only moderate exhumation rates ( $\sim 100\text{-}450 \text{ m/Ma}$ ), the validity of the second option is more likely: during Oligocene to Miocene cooling, Corsica was surrounded by two active rift systems (Ligurian-Provençal and Tyrrhenian rifting). During these periods the thermal gradient increased and isotherms were compressed towards the surface that led to the establishment of a fairly narrow PAZ. Therefore, although the cooling rate was only moderate, the samples could cross the PAZ relatively fast.

### 7.2.2.5 CONCLUSIONS

Large differences in the FT ages and variation in parameters describing fission track data indicate that all of Corsica cannot be considered as one simple tectonic block with a uniform thermal history, but represents a complex mosaic of several domains, which experienced cooling at different times and in different fashion. Therefore, Corsica needs to be subdivided into smaller domains for which the thermal history must be individually reconstructed, and the observed pattern must be explored through thermal history modeling.

Increased heat flow during opening of the Ligurian-Provençal and the Tyrrhenian oceanic domains in Oligocene to Middle Miocene times induced compression of the isotherms to the surface, producing a narrow PAZ. In such a setting, moderate cooling through the PAZ could produce a narrow unimodal track length distribution with long MTLs.

### 7.2.3 Subdivision into AFT domains

According to similarities in FT data and considering the major structural boundaries, the following AFT domains were defined: (I) Variscan Corsica excluding its southernmost part, (II) southernmost Variscan Corsica, (III) Eocene flysch sediments, (IV) NE Corsica (including Tenda region, St. Florent and Francardo Basins). For the central and southern parts of Alpine Corsica together with the Oriental Plain no AFT data exist.

#### 7.2.3.1 DOMAIN I

*Domain I* encompasses the vast majority of the Variscan basement except its southernmost part (Fig. 7-2-10). The AFT ages within this domain exhibit a fairly wide range between  $16.4 \pm 0.9$  and  $34.6 \pm 3.3$  Ma, suggesting cooling during Oligocene and Miocene times. A common characteristic of the samples is a narrow ( $SD \leq 1 \mu\text{m}$ ), unimodal track length distribution with long MTL ( $\geq 13.8 \mu\text{m}$ ), pointing to fast cooling through the PAZ.

Thermal history modeling reveals similar  $tT$  paths for all modeled samples, characterized by fast cooling through the PAZ followed by a period of modest decrease in temperature until present (Fig. 7-2-11). As can be predicted from the apparent AFT ages, fast cooling occurred in different periods: samples from the south cooled through the PAZ in the Oligocene, whereas samples more towards the NNW experienced cooling only in the Miocene.

The time interval delimited by FT data was very eventful, when several events occurred

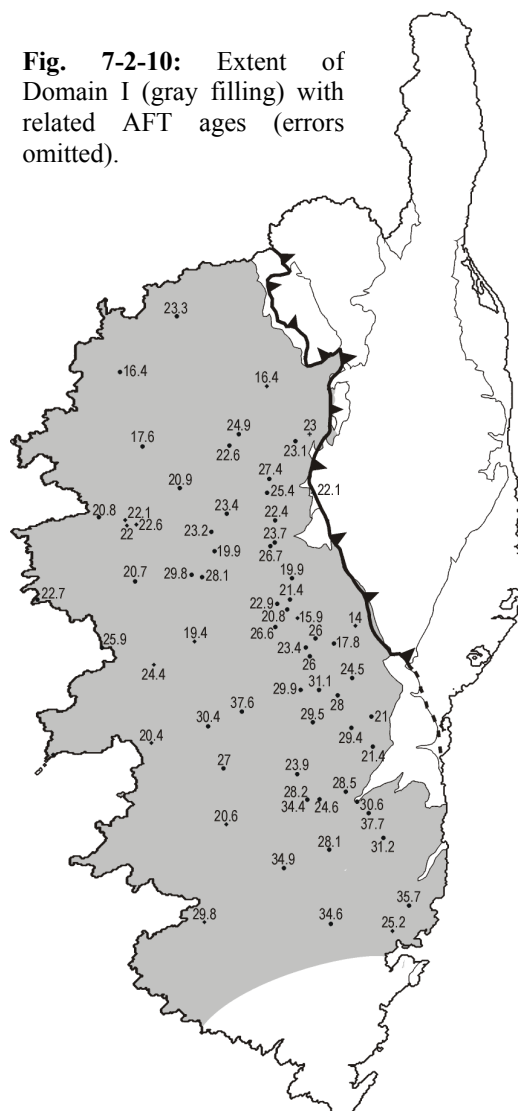


**Fig. 7-2-10:** Extent of Domain I (gray filling) with related AFT ages (errors omitted).

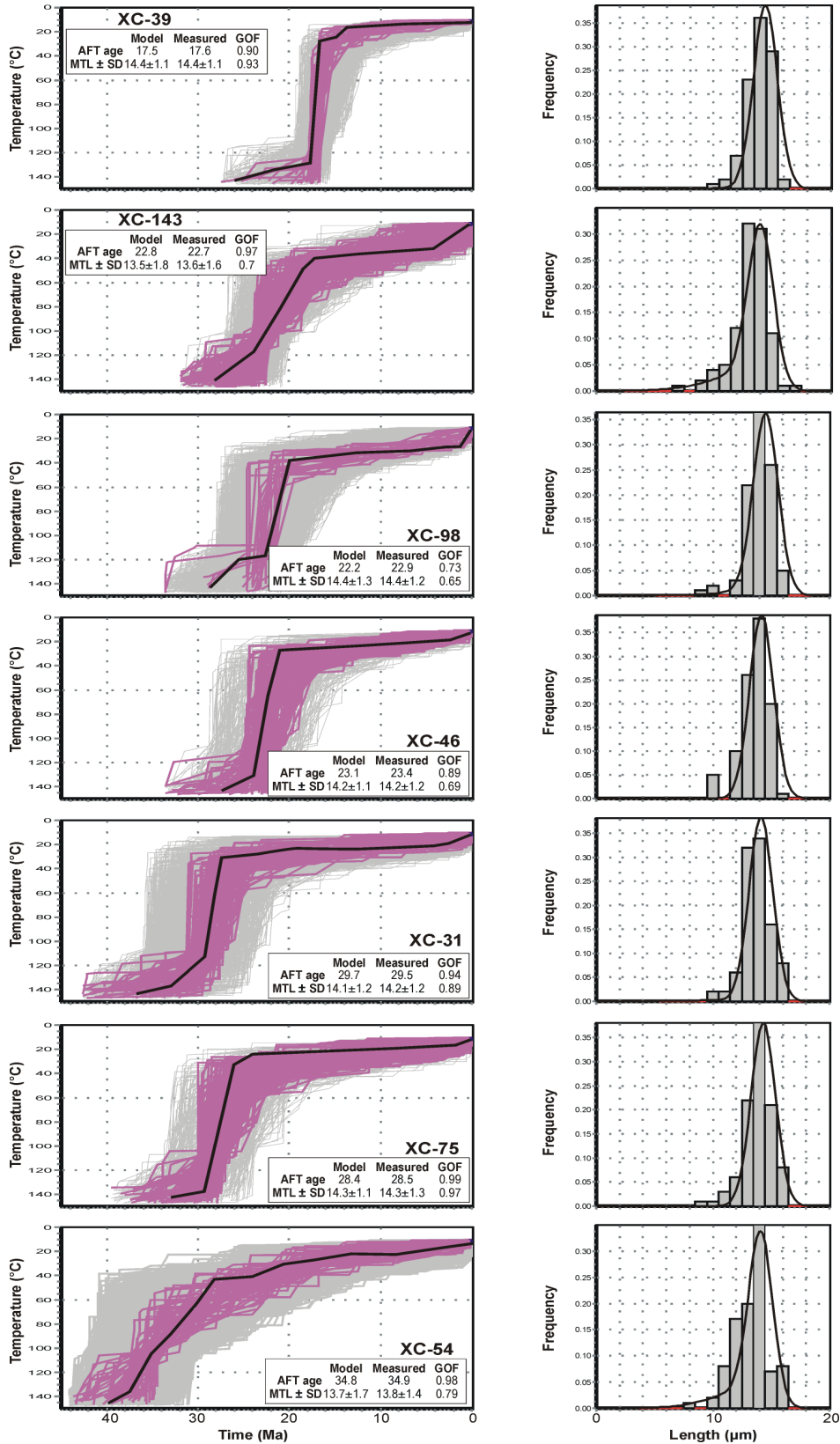


Fig. 7-2-11: Thermal modeling results of AFT data of some representative samples from Domain I obtained with HeFTy (Ketcham et al., in press). Results are displayed in time-temperature diagrams, frequency distribution of measured confined track length data (right diagram) is overlain by a calculated probability density function (best fit) of a sample. Light gray paths: acceptable fit; dark gray paths: good fit; thick black line: best fit; MTL: mean track length in  $\mu\text{m}$ ; SD: standard deviation in  $\mu\text{m}$ ; GOF: goodness of fit (see Appendix B for explanation).

data, all known events need to be revised:

According to Brunet et al. (2000), Alpine collision lasted until ~33 Ma, creating an accretionary wedge that was partly covering Corsica. The period of collision was terminated by a period of "tectonic reorganization", which later completely changed the picture of the Western Mediterranean region: at ~33 Ma, the boundary conditions changed from compression to extension and the overthickened crust started to collapse, which led to exhumation of buried units (Jolivet et al., 1990; Jolivet et al., 1998; Brunet et al., 2000). There are several opinions on the initiation of this stage of post-orogenic extension. For instance, the extension was induced by the eastward rollback of the newly evolved Apennine subduction (Fournier et al., 1991; Jolivet et al., 1991; Daniel et al., 1996), or it was a consequence of isostatic rebound responding to the slab break off in the east-dipping Alpine subduction zone, which had to precede the formation of the new west-dipping Apennine subduction zone (Malavieille et al., 1998).

From ~33 to 25 Ma, the Alpine thrust front with top-to-west sense of shear was reactivated as ductile to brittle-ductile shear zones with top-to-east sense of shear, as recorded by  $^{40}\text{Ar}/^{39}\text{Ar}$  data (Jolivet et al., 1990; Fournier et al., 1991; Brunet et al., 2000).

At ~30 Ma, rifting of the Ligurain-Provençal Basin started. This age is recorded by synrift sediments in the Gulf of Lion (29 Ma; for review see Gorini et al., 1994; Chamot-Rooke et al., 1999; Séranne, 1999), on the Sardinia margin (30 Ma; Cherchi and Montadert, 1982), and in Corsica (25 Ma; Ferrandini et al., 1999). The drifting event is constrained by the counterclockwise rotation of the Corsica-Sardinia block between 21 and 16 Ma (Van der Voo, 1993; Vigliotti and Kent, 1996; Chamot-Rooke et al., 1999).

Inferring from the events listed above and with respect to FT data, one can assume that cooling and denudation evolution of Domain I can be linked to two principal processes: (i) either to the rifting of the Ligurian-Provençal Basin or (ii) to the collapse of the wedge, or to both of them. This relationship can be examined by plotting the AFT ages as function of distance to some representative markers. In such plots, when the ages are related only to the Ligurain-Provençal rift system, they should be younging in eastward direction towards the rift margin and the ages closest to the margin should be of the same age, or younger than ocean spreading (Gallagher and Brown, 1997; Gallagher et al., 1998). In contrast, when the ages are related to collapse of the wedge, they should be younging in westward direction towards the wedge front. In case that ages are related to both, rifting and wedge collapse, a kind of "antagonistic" trends can be expected: the ages should increase from west to east and concurrently from east to west. To test this hypothesis, the AFT ages of Domain I were plotted as a function of (i) distance between sampling points and a boundary of the transitional domain of Ligurian-Provençal rift and continental margin defined after Rollet et al. (2002; Fig. 7-2-12), and (ii) as a function of distance between sampling points and present-day Alpine front. The results are presented in the Fig. 7-2-12. One can see that in both cases the observed somewhat ill-defined trends

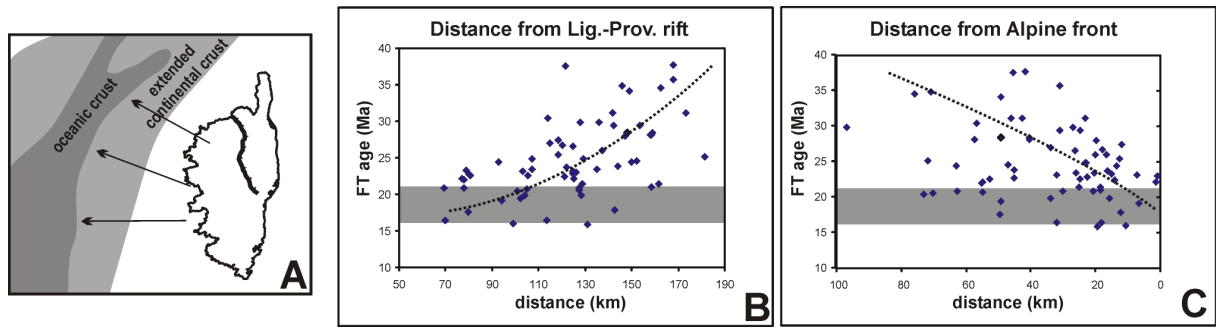


**Fig. 7-2-12:** A: Schematic figure showing the way of measuring distance to the Ligurian-Provençal rift. B: AFT age as a function of distance from the Ligurian-Provençal rift, where a trend showing increase of ages inland can be visible. C: AFT ages as a function of distance from the Alpine front, where an ill-defined trend of ages decreasing towards the front is visible. C: The same plots from other passive margins, showing similar trends to that of Corsica (after Gallagher and Brown, 1997). The gray bands in B and C represent the time of full ocean spreading.

show decrease in age towards the defined boundaries. This indicates, that cooling and denudation of the basement is indeed related to the Ligurain-Provençal rift system and also to the collapse of the Alpine wedge. Both these principal processes, resulting from the Oligocene tectonic reorganization, were contemporaneous in time and space, and their coupled interplay governed the exhumation of the Variscan basement.

A remaining task to be solved is to attribute specific ages of *Domain I* to one of these two processes. This can be realized when sketching a maximum extent of the wedge with the foreland basin, and an external boundary of the zone thermally affected by rifting. The first one is reconstructed in chapter 7.2.3.3.1. The latter one can be reconstructed from the present-day position of the rift, and from the

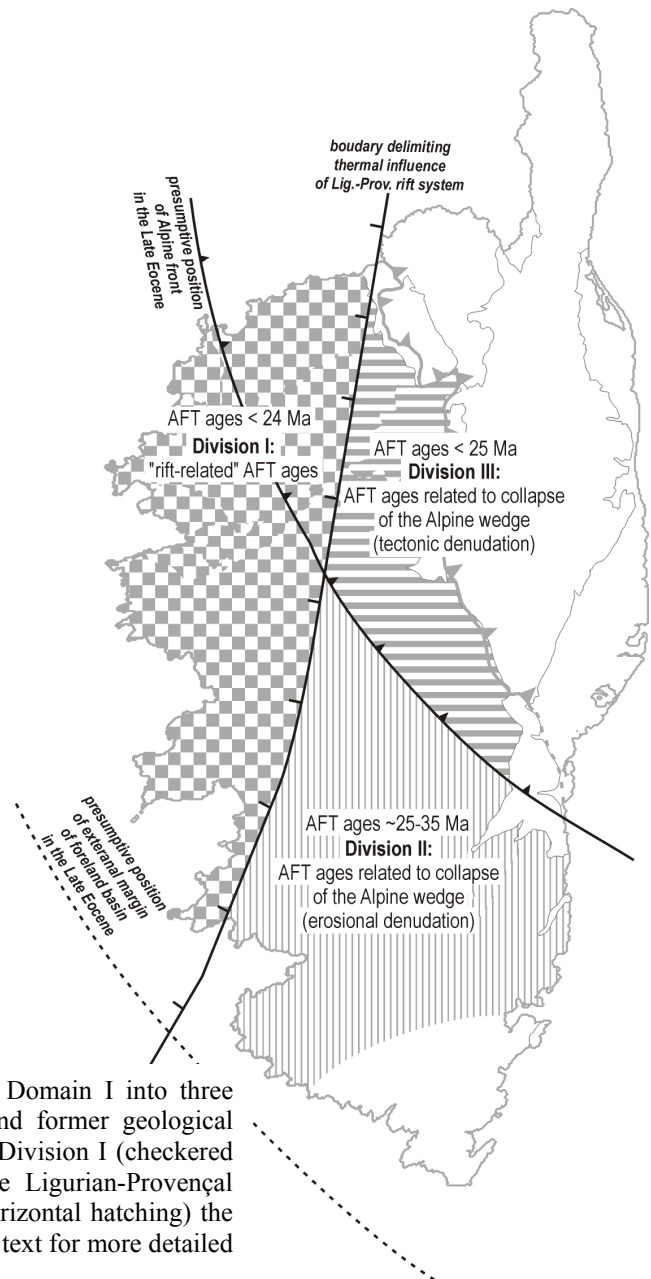


**Fig. 7-2-13:** Illustration showing a subdivision of Domain I into three divisions according to similarities in AFT ages and former geological boundaries (as reconstructed in chapter 7.2.3.1). In Division I (checkered fill pattern), the ages record the spreading of the Ligurian-Provençal Ocean; in Division II (vertical hatching) and III (horizontal hatching) the ages are related to collapse of the Alpine wedge (see text for more detailed explanation).

assumption that AFT ages are younger or of the same age like onset of ocean spreading (Gallagher et al., 1998). In this way the *Domain I* can be subdivided into three divisions (Fig. 7-2-13):

The first division encompasses the NW part of Variscan basement with the ages younger than ~24 Ma. Ages within this division are interpreted as to be reset due to increased heat flow related to mantle upwelling during rifting and spreading of the Ligurian-Provençal Ocean.

The second division covers the southern part, which was covered by undeformed foreland sediments representing the external periphery of the wedge. As mentioned above, there are several options to explain the AFT ages, such as exhumation due to isostatic rebound or to shoulder uplift of the evolving Ligurian-Provençal rift. No matter which process prevailed, the flysch cover was removed from top of the basement solely by erosion, thus the denudation can be understood as erosional in origin.

The third division encompasses the parts formerly involved in the subduction. The AFT ages are younger than those from the previous division, ranging between ~25 and 15 Ma and are younging towards the present-day Alpine front. These younger ages can be explained as a consequence of the burial to great depths in the subduction zone. In the Oligocene, when the basement started to exhume and the wedge to collapse, the samples were exhuming from greater depth than those covered only by the flysch (previous division). Therefore they reached the PAZ with a delay - in the Early Miocene. However, since it is well known that the Alpine thrust front was reactivated during exhumation as an extensional shear zone (see above), it is likely that denudation of this part of basement from below the Alpine nappes was tectonic in origin.

Thus in brief, the exhumation of *Domain I* can be summarized as the removal of the Alpine nappes, realized partly by the erosional denudation, partly by the tectonic denudation, and was also thermally influenced by the opening of Ligurian-Provençal Ocean.

#### **7.2.3.1.1 CLASSIFICATION ACCORDING TO PASSIVE MARGIN MODELS**

At present-day tectonic setting, the *Domain I* can serve as an example of a high elevated passive margin related to the Ligurian-Provençal rift system. However, it is not a classical example of passive margin (like, for instance, SE Australia or SE Brazil, see Fig. 7-2-14), since it was demonstrated in previous chapter that its formation was not related only to the uplift of the rift-flanks, but also to the tectonic or erosional removal of Alpine cover. Nevertheless, at present there is a relief evolved in Corsica that can be tested by FT thermochronology, and possibly classified according to the passive margin models.

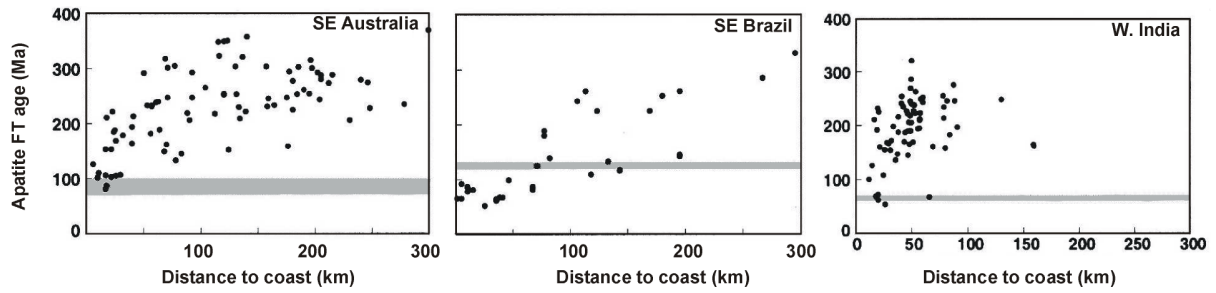


**Fig. 7-2-14:** AFT age as a function of distance from the present-day coast - examples from some "classical" passive margins (after Gallagher et al., 1998), showing a pattern similar to those observed in Corsica (see Fig. 7-2-12B); the gray bands in B and C represent the time of full ocean spreading.

A comprehensive overview of the AFT age patterns associated with three different types of passive margin development was presented by Gallagher et al. (1998) (Fig. 7-2-15). In the **downwarp model** the margin is initially formed by a long-wavelength flexure of the lithosphere. The margin topography is characterized by a broad monocline with a very low gradient, and faulting is minimal. Between the coast and the escarpment only moderate amounts of denudation occur, resulting in moderately reduced AFT ages. Inland of the escarpment denudation is negligible. The isostatic response to denudational unloading is not taken into account in this model. In the **scarp retreat model** the margin is characterized by a steep escarpment formed by differential vertical displacement along normal faults. Denudation progressively moves inland and the maximum amount of denudation occurs near the coast. In the interior only moderate to low amounts of denudation will occur. This will result in a strong gradient in AFT ages: the oldest ages occur in the continental interior and ages decrease towards the coastline. The youngest AFT ages may be similar to, or younger than, the timing of rifting and continental break-up. In addition, the time of peak denudation rate occurs later inland

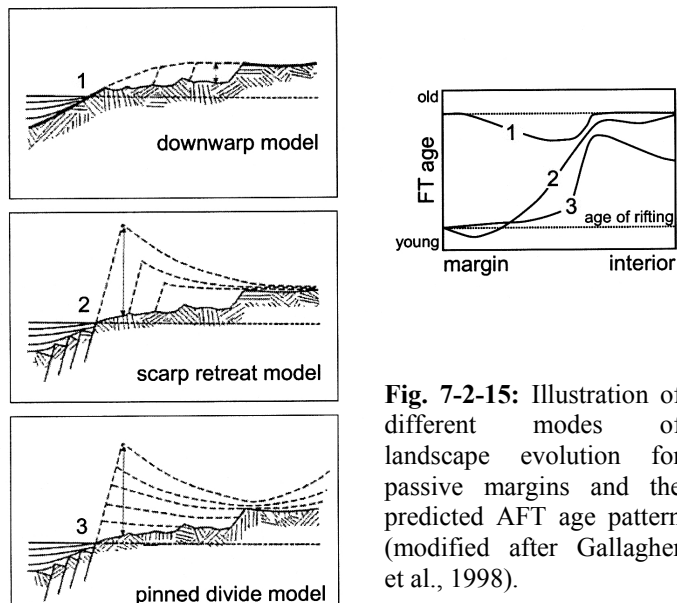


**Fig. 7-2-15:** Illustration of different modes of landscape evolution for passive margins and the predicted AFT age pattern (modified after Gallagher et al., 1998).

from the coast toward the final position of the escarpment. Similar to the scarp retreat model is the **pinned divide model**. The most important difference between these two models is the incorporation of a preexisting drainage divide inland of the initial escarpment in the pinned divide model. Seaward of the initial divide rapid river incision will take place, with more or less uniform denudation rates.

The pattern of denudation is more like 'down wearing' than scarp retreat. The predicted pattern of AFT ages has an even stronger gradient near the escarpment than in the scarp retreat model, and inland of the escarpment the AFT ages will be reduced with respect to the ages near the escarpment.

All of these models are 2D conceptual models of passive margin development and represent end-member configurations. Because the final configuration of any passive margin is the product of the complex interaction of many parameters (e.g. pre-rift configuration, climate, sediment distribution, lithology, lithospheric structure, etc.), it is unlikely that a particular passive margin will fit perfectly with any of the models presented by Gallagher and Brown (1997) and Gallagher et al. (1998). Even so, classification of passive margins into one of these models can help to understand the evolution of a given margin.

From Fig. 7-2-12B it is clear that the downwarp model cannot explain the observed AFT age pattern (see also Fig. 7-2-15). Instead, the observed pattern is much more similar to that predicted by the scarp retreat and pinned divide models. When the morphological characteristics of Variscan Corsica are taken into account, the pinned divide model can be ruled out because the drainage divide was not "pinned", but was rather migrating landward in time as documented by its asymmetrical shape (Fig. 3-1A). Thus, it can be concluded that, according to the AFT pattern and morphological characteristics, the Variscan basement of Corsica best fits a type of scarp retreat model.

### 7.2.3.2 DOMAIN II

*Domain II* encompasses the southernmost part of Variscan Corsica in the region of the settlements Chera, Figari and Bonifacio (Fig. 7-2-16). Samples from this domain yielded by far the oldest AFT ages (in the range  $46.4 \pm 4$  to  $105.3 \pm 7.2$  Ma), and the bimodal track length distributions ( $SD = 2.2 \mu\text{m}$  (XC-2)) with by far the shortest MTL ( $12.2 \pm 0.2 \mu\text{m}$  (XC-2)), pointing to a complex thermal history, are markedly different from those of rest of the island. It must be emphasized that the middle Cretaceous apparent AFT ages ( $105.3 \pm 7.2$  and  $97.9 \pm 5.4$  Ma) were recognized for the first time in Corsica and that this is the only place on the entire island, where a Mesozoic "AFT memory" of the crystalline basement was not reset and can be possibly revealed by thermal modeling.

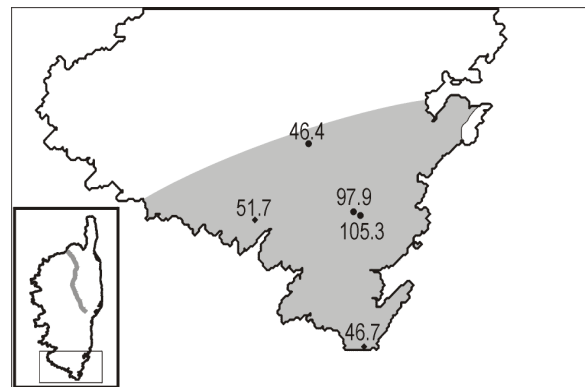


**Fig. 7-2-16:** Domain II (gray filling) covers the southernmost part of Variscan Corsica and contains by far the oldest AFT ages (errors omitted).

Thermal history modeling, constrained by a ZFT age of  $159.8 \pm 12.1$  Ma (KU-22), reveals a tT path with cooling through the PAZ from the Middle Jurassic to the Early Cretaceous, stagnation above the PAZ until the Paleocene, then a temperature increase into the PAZ in the Eocene, and fast cooling to surface temperature in the Oligocene (Fig. 7-2-17). The modeled cooling path is interpreted as follows:

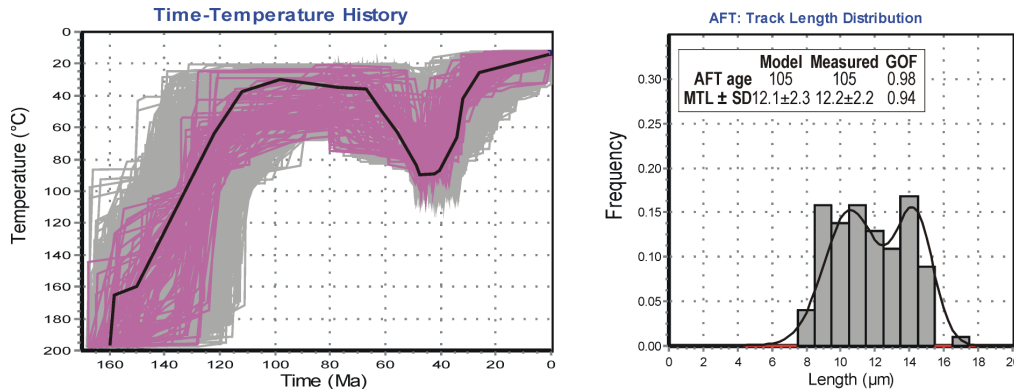


**Fig. 7-2-17:** Thermal modeling results of AFT data of some representative samples from Domain II obtained with HeFTy (Ketcham et al., in press). Results are displayed in time-temperature diagrams; frequency distribution of measured confined track length data (right diagram) is overlain by a calculated probability density function (best fit) of a sample. Light gray paths: acceptable fit; dark gray paths: good fit; thick black line: best fit; MTL: mean track length in  $\mu\text{m}$ ; SD: standard deviation in  $\mu\text{m}$ ; GOF: goodness of fit.

After the Jurassic thermal event related to the opening of the Ligurian-Piedmont Ocean that is recorded by ZFT data (see chapter 7.1.2), the basement was cooling through the PAZ at moderate rates. This cooling phase lasted until the middle Early Cretaceous, and can be related to two processes: (i) As the rifting stage transformed to the spreading stage, the basement drifted away from the spreading center, which was accompanied by a decrease in temperature. (ii) The second process, which might have governed cooling, is the exhumation of the basement owing to a rift shoulder uplift. Since it is well known that during rifting, rift flanks are rapidly exhumed and uplifted to significant elevations creating a relief (e.g., Summerfield, 1991; van der Beek, 1995; Summerfield and Brown, 1998), it is likely that the Variscan basement behaved in the same way as other typical passive margins. Thus, it was probably exhumed and uplifted after the break-up, which was accompanied by cooling.

During mid-Cretaceous to Paleocene times, the actual exposed level of the basement was residing in levels above the apatite PAZ according to the modeling results. For the morphological evolution, this indicates that either the basement was at a depth of up to  $\sim 1.8$  km (assuming thermal gradient of  $25^\circ\text{C}/\text{km}$ ) possibly being covered by sediments, or it was close to the to erosion surface, and already evolved topography might have been beveled off by erosion creating a peneplain. Unfortunately, AFT data do not allow us to decide which option is correct, since the AFT thermochronometer is not sensitive enough for such a low temperature zone. From the sedimentary

records preserved in Corsica this question can also not be satisfactorily answered, since due to severe Tertiary erosion there are only scarce remnants of Cretaceous to Paleocene sediments preserved in Corsica. However, there are some lines of evidence indicating that the basement might have been eroding in the Cretaceous: Prone and Rousset (1981) argued that in Cenomanian deposits of the Provence Basin (southern France) there are occurrences of characteristic detrital quartz grains derived from Permian rhyolites of Corsica. According to Rossi et al. (1980), in Cretaceous sequences of some of the Alpine nappes (e.g., Santa Lucia di Mercurio, Balagne) there are abundant occurrences of coarse grained detrital material derived from the Variscan basement of Corsica (gneisses, rhyolites, granites; Rossi et al., 1980). These evidences justify the idea of peneplain formation prior to the Eocene collision, but this will be elaborated upon in more detail in the chapter 7.3.

Until the Early Eocene, the cooling history of the Variscan basement is supposed to be identical for the whole Variscan basement of Corsica (including *Domain I* described above). From the Early Eocene onward, the cooling history of the Variscan basement shows some diachronic evolution in cooling that is discussed above.

In the Eocene, inverse modeling results for the *Domain II* revealed reheating to the levels of the PAZ. This period of heating perfectly fits perfectly to the time of collision between Variscan and Alpine Corsica, when a nappe stack and a flysch trough developed between Variscan basement of southern Europe and Alpine Corsica, and indicates that this part of the basement was also buried beneath a rock pile with significant thickness. The thickness of the cover can be roughly estimated from the modeling results: assuming a thermal gradient of 20°C/km (a characteristic value for foreland basin; Turcotte and Schubert, 2002), surface temperature 10°C, and the fact that the sample reached the temperature range of ~70-90°C at ~40 Ma, simple calculation gives a final thickness of ~4 km. If this value holds, and if given that *Domain II* was buried to the shallowest level within Variscan Corsica (since this the only domain with pre-Tertiary AFT memory), then it means that the entire basement of Variscan Corsica was buried beneath a rock pile of at least ~4 km thickness during the Alpine collision, although at present there is almost no evidence of the presence of flysch or Alpine nappes on top of the Variscan basement.

In the Oligocene, the inverse modeling results indicate fast cooling to the surface conditions followed by stagnation lasting to the present. This cooling phase is similar to that of *Domain I* (see chapter 7.2.3.1) and is interpreted as reflecting the erosional denudation of the basement from below the foreland flysch..

### 7.2.3.3 DOMAIN III

Domain III comprises all occurrences of the Eocene flysch sediments (Fig. 7-2-18), because AFT ages measured on flysch samples revealed certain similarities. As described in chapter 2.4.1, the remnants of Eocene flysch are present along the contact zone between Alpine and Variscan Corsica.

AFT ages are in the range  $16.4 \pm 1$  Ma (XC-132) to  $30.6 \pm 1.6$  Ma (XC-85). An identical feature of all flysch samples is that AFT ages are always younger than the depositional age, indicating a thermal reset after deposition. In addition, all track length distributions are always unimodal, narrow ( $SD \leq 1.5 \mu\text{m}$  (XC-132)), with long MTLs ( $\geq 13.6 \pm 0.2 \mu\text{m}$  (XC-132)), characteristic of rapidly cooling rocks with fast passage through the apatite PAZ. Thermal history modeling was constrained by the depositional age of the Eocene sediments ( $\sim 56$ -40 Ma, Early to Middle Eocene; Durand-Delga, 1978; Rossi et al., 1980) and revealed fairly similar cooling paths for all samples (Fig. 7-2-19): after deposition in the Eocene, the samples were heated to temperatures of at least  $\sim 110^\circ\text{C}$ , and consequently completely annealed. The reset was followed by fast cooling to near-surface conditions, where the samples stayed until present. The *tT* path is interpreted as follows:

During the Eocene collision, the flysch was deposited in the trough in front of the approaching Alpine nappes. As the collision continued, the flysch samples were continuously buried below an increasing rock column until they reached temperatures of more than  $\sim 110^\circ\text{C}$  where the AFT memory was reset. Two questions arise in this point: 1) of what type was this cover?; and 2) what was the thickness of the cover?

The first question to be addressed involves the composition of the lid. Relation of Eocene flysch with Variscan and Alpine units is complex and changes from the north towards the south (for details see chapter 2.4.1; Egal, 1992). In the northern and central areas of Corsica, in the Balagne and Corte regions, Eocene flysch formations are essentially autochthonous with regard to the Variscan basement, but are largely overlain by Alpine nappes including the Corte slices. Bézert and Caby

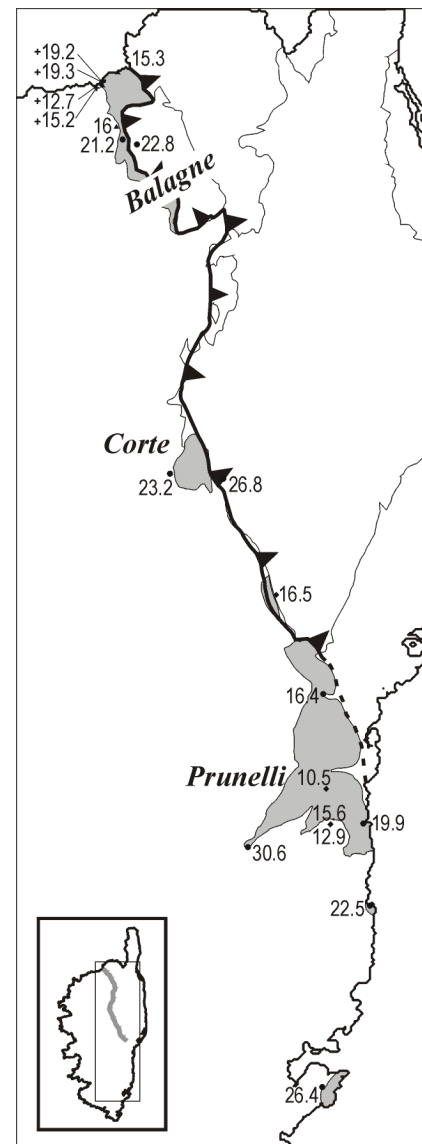


**Fig. 7-2-18:** Domain III (gray filling) encompasses the areas with preserved flysch sediments; the most conspicuous feature is overall reset of Eocene sediments.

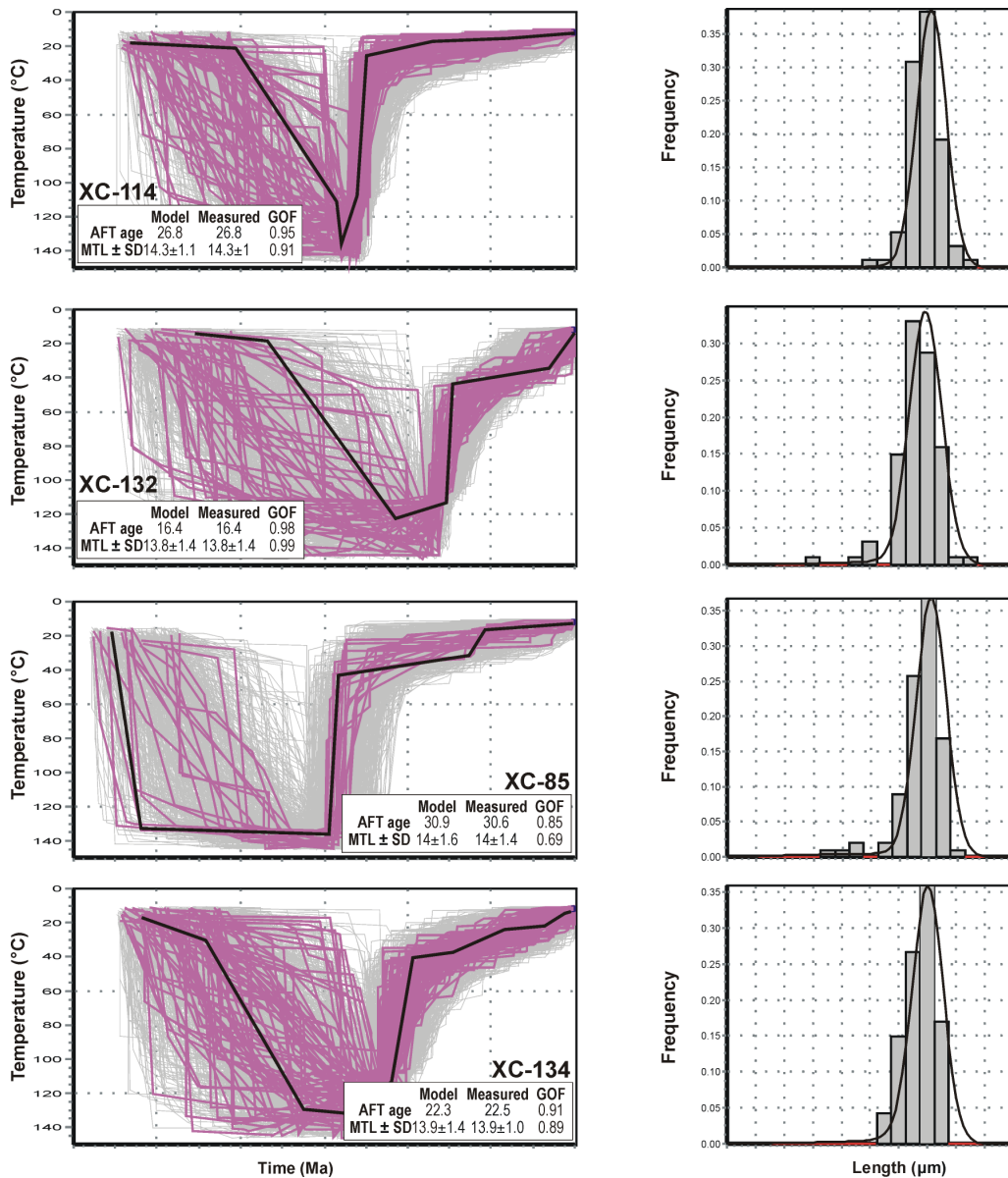


**Fig. 7-2-19:** Thermal modeling results of AFT data of some representative samples from Domain III obtained with HeFTy (Ketcham et al., in press). Results are displayed in time-temperature diagrams, frequency distribution of measured confined track length data (right diagram) is overlain by a calculated probability density function (best fit) of a sample. Light gray paths: acceptable fit; dark gray paths: good fit; thick black line: best fit; MTL: mean track length in  $\mu\text{m}$ ; SD: standard deviation in  $\mu\text{m}$ ; GOF: goodness of fit. All flysch samples are characterized by the complete reset of AFT ages, related to burial in the subduction zone.

(1988, 1989) described blue amphibole present in the Bartonian flysch near Corte, pointing to Late Eocene metamorphism of the flysch at MP/LT conditions (i.e.,  $P = 0.5 \text{ GPa}$ ,  $T = 300 \pm 50^\circ\text{C}$ ). Thus the Eocene flysch from northern and central Corsica was involved in the subduction process and buried below the Alpine nappes in the accretionary wedge. Therefore the rock column responsible for reset of AFT ages in the Eocene samples was made up of a folded flysch wedge but mainly of Mesozoic Alpine tectonic units. Estimates on depth of burial, based on thermobarometry, and the

assumption of low thermal gradient (15°C/km - a typical value for subduction zones; Turcotte and Schubert, 2002), gives a burial depth of ~15 km.

Further to the south, in the Prunelli region, the situation is different: the Eocene "Prunelli" flysch is devoid of any metamorphic assemblages and lies unconformably on the Variscan basement as well as on the Alpine nappes. Egal (1992) stated that the Eocene sediments in Prunelli are not deformed, and the contact to the underlying Variscan and Alpine units is an undisturbed onlap. This suggests that the Prunelli flysch was not involved in the subduction process, but represents the most distal part, outside the accretionary wedge. Nevertheless, AFT ages show reset (AFT ages between  $16.4 \pm 1$  and  $30.6 \pm 1.6$  Ma) requiring burial below a thick rock column. And if the statement of Egal (1992) is true, then the reset of the AFT ages in the Eocene samples from the Prunelli region was induced by a thick rock column made up merely by the flysch sequence without nappes (in contrast to the previous case where the cover was composed of flysch and Alpine nappes).

To estimate the thickness of the covering rock column from thermal modeling results, it is necessary to assess the thermal gradient. AFT ages as well as modeled  $tT$  paths suggest that the samples were passing the PAZ during Late Oligocene to Middle Miocene times. This period is characterized by the beginning and full evolution of the rifting activity in the surroundings of Corsica (i.e., rifting in the Ligurian-Provençal and Tyrrhenian Basins) that was likely accompanied by increased thermal gradient of up to ~35-40°C/km (Turcotte and Schubert, 2002). When assuming such a high thermal gradient, a surface temperature of 17-20°C, and the fact that the sample reached the temperature range of ~110°C, the resulting thickness of the cover that loaded the actual exposed flysch samples, is ~2.5 km. However, this result seems to be in conflict with the result obtained from thermobarometric data, suggesting a burial to the depth of ~15 km (see above). This apparent discrepancy can be explained as follows: samples entered and passed the PAZ during Oligocene to Miocene times as indicated by the AFT data, when the thermal gradient was probably quite high (35-40°C/km). An important point is that all memory prior to entering PAZ was lost (except the depositional age recorded by foraminifers) and there is no AFT record from the "collision" times, when the samples were more or less involved in the subduction zone with fairly low thermal gradient (10-15°C/km). Practically it means that samples might have been reset right after their deposition in the foreland basin with cold thermal gradient. Consequently, when converting temperature to depth, the lesser values of the thermal gradient will result in much greater values for cover thickness, similar to those demonstrated by results obtained from thermobarometry. Therefore it must be kept in mind that the values for the cover thickness estimated from AFT data provides the minimal values, and in the reality the thickness of Alpine cover might have reached a thickness of up to 15-20 km. This once again supports the idea inferred from *Domain II*, claiming that during Eocene collision entire Corsica was covered by a huge pile of flysch and Alpine nappes, which was later significantly eroded, and present-day Alpine Corsica is only its small remnant.

The Oligocene to Miocene reset of the samples was followed by fast cooling to near-surface conditions as suggested by the modeling results. This cooling phase is, as in the case of *Domain I*, interpreted as an exhumation related to the collapse of the Alpine wedge, when the samples were tectonically denuded from below the Alpine nappes in central and northern Corsica and erosionally denuded from below the foreland sediments in southern Corsica.

### 7.2.3.3.1 TENTATIVE RECONSTRUCTION OF THE ALPINE ACCRETIONARY WEDGE AND FORELAND BASIN

To reconstruct the extent of the former accretionary wedge and the foreland basin, it is necessary to identify all relevant facts: the first important characteristic is the present-day extent of Alpine Corsica, representing a reminder of the former wedge. It encroaches the NE third of the island, and the Alpine front runs in a NNW-SSE direction. The second important attribute is the character of the flysch sediments. They are encountered along the contact between Alpine and Variscan Corsica, always contain coarse granitic material, and AFT ages are everywhere reset. From the Prunelli region southward, the sediments are undeformed, in a normal stratigraphic position, and devoid of any metamorphic assemblages. This area represents a foreland basin undisturbed by the subduction process. In contrast, north of Prunelli the flysch is deformed, including in the imbrications and underthrust below the Alpine nappes. It contains metamorphic assemblages indicating involvement in the subduction process. Thirdly, although there are no geologic evidences of an existing Alpine cover, the southernmost part of the Variscan basement was buried at the shallowest level among all other parts during Eocene collision, as indicated by the AFT data. Furthermore, AFT data suggest a burial beneath an at least ~4 km thick rock pile (see chapter 7.2.3.2).

All of these fact enable us to restore the possible extent of the wedge, which probably covered the whole Variscan Corsica. Its front was running in a NNW-SSE direction (in present coordinates) similar to the present-day

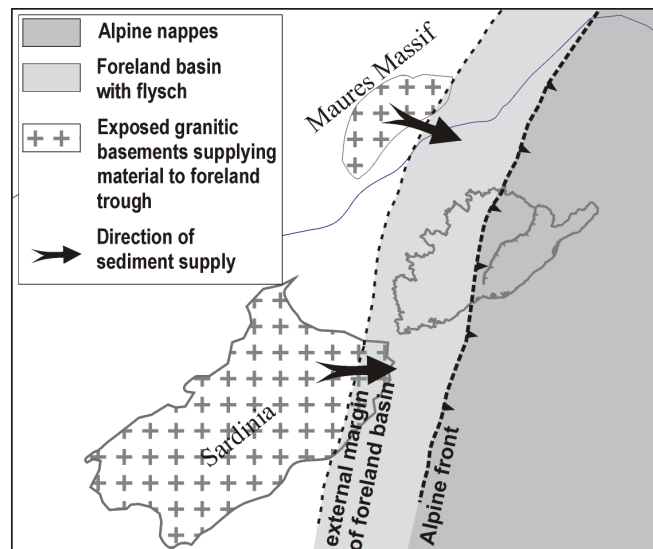


**Fig. 7-2-20:** Illustration showing reconstruction of the possible extent of Alpine wedge and foreland basin during Eocene collision ca. at 40 Ma: Corsica-Sardinia block formed SE margin of European plate; all of Variscan Corsica was covered by Alpine nappes or foreland flysches; granitic material was shed from emerged Sardinian and Maures Massifs to foreland trough. Wedge boundaries are only approximate.

situation, and its thickness diminished in roughly SSW direction. In such a setting, the source area of granitic detritus for the flysch trough was not the basement of Corsica, but rather some other adjacent granitic basement (probably Sardinia or the Maures Massif), covered neither by the Alpine wedge nor by the foreland sediments at that time (Fig. 7-2-20).

#### 7.2.3.4 DOMAIN IV

The NE part of Corsica, including the Tenda Massif, the St. Florent Basin and adjacent regions make up the *Domain IV* (Fig. 7-2-21). The vast majority of the AFT data from this domain was reported by previous studies (Jakni et al., 2000; Cavazza et al., 2001; Fellin, 2003; Zarki-Jakni et al., 2004; Fellin et al., 2005). In this study only three additional AFT ages and one track length distribution were measured on the samples from the Tenda Massif. Measured ages are in the range  $16.4 \pm 1.4$  to  $24.9 \pm 2.7$  Ma indicating Miocene cooling that is in accord with previously reported data ( $15.3 \pm 1.5$  -  $22.3 \pm 2.2$  Ma). Observed track length distribution (sample XC-59) is unimodal, narrow ( $SD = 0.7 \mu\text{m}$ ), with very long MTL ( $14.7 \pm 0.1 \mu\text{m}$ ), indicating fast cooling through the PAZ, again in line with previous data.

Modeled cooling paths revealed fast cooling for the Tenda Massif (Fig. 7-2-22). An extremely high cooling rate (up to  $60^\circ\text{C}/\text{Ma}$  that is equivalent to an exhumation rate of  $\sim 2 \text{ km}/\text{Ma}$ , assuming a thermal gradient of  $35^\circ\text{C}/\text{km}$ ) is interpreted to reflect the tectonic denudation of the Tenda Massif as a metamorphic core complex from below the Alpine nappes (Jolivet et al., 1990; Fournier et al., 1991; Rosenbaum et al., 2005). As already discussed in chapter 7.1.2, the Tenda Massif represents a part of the Variscan basement that was underthrust below the Schistes Lustrés nappes and metamorphosed at MP/LT conditions during the Eocene ( $\sim 46$  Ma). In the Oligocene, when the tectonic regime changed ( $\sim 33$  Ma), the massif started to be tectonically exhumed as a metamorphic core complex, which is recorded by  $^{40}\text{Ar}/^{39}\text{Ar}$  ages on micas from the thrust plane that was reworked as an extensional shear zone with top-to-the-east sense of displacement (Jolivet et al., 1998; Brunet et al., 2000; Rosenbaum et al., 2005). Fast exhuming

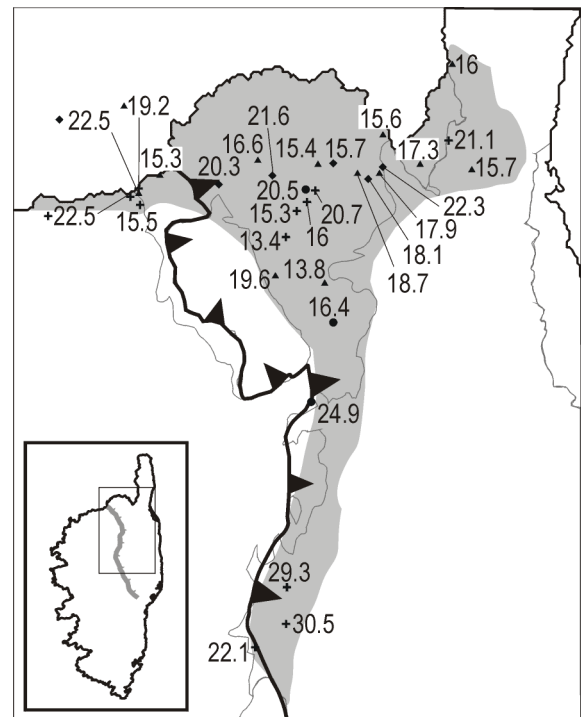


**Fig. 7-2-21:** Domain IV (gray filling) covers the NE part of Corsica and is characterized by Oligocene to Miocene AFT ages, provided mainly by other studies errors omitted.

crystalline rocks reached the erosional level during the Late Burdigalian when their debris was first shed to the neighboring St. Florent basin.

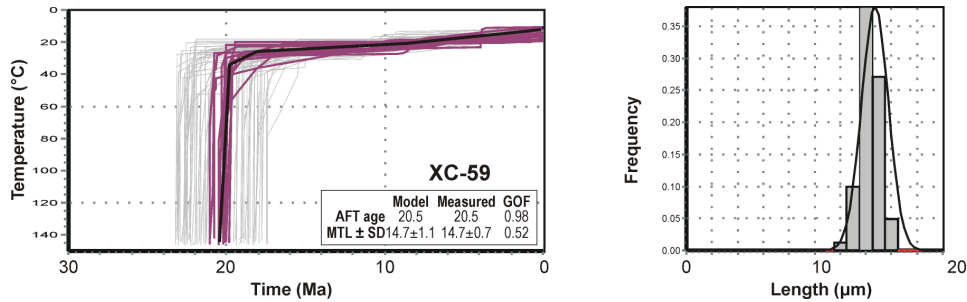


**Fig. 7-2-22:** Thermal modeling results of AFT data of some representative samples from Domain III obtained with HeFTy (Ketcham et al., in press). Results are displayed in time-temperature diagrams, frequency distribution of measured confined track length data (right diagram) is overlain by a calculated probability density function (best fit) of a sample. Light gray paths: acceptable fit; dark gray paths: good fit; thick black line: best fit; MTL: mean track length in  $\mu\text{m}$ ; SD: standard deviation in  $\mu\text{m}$ ; GOF: goodness of fit.

A different thermal history was determined by Fellin et al. (2005) in the St. Florent, Balagne, and Francardo regions, which surround the Tenda Massif and at present form morphological depressions (Balagne) or host Miocene basins (Francardo and St. Florent). These authors measured AFT ages between  $19.2 \pm 2.2$  and  $30.5 \pm 3.2$  Ma in samples from the hanging walls of Neogene grabens, similar to of footwalls (Tenda, Cap Corse or Variscan Corsica). However, the observed track length distributions are different. In case of footwalls, track length distributions are unimodal with long MTLs, whereas the samples from hanging-walls are broad, sometimes bimodal, with MTL shorter than in the case of footwalls. The authors argued that the thermal history of the depressions (basins) is complex and controlled by the activity of minor faults. Inverse modeling results revealed cooling paths perturbed by a heating event from ~19 to 14 Ma (Fig. 7-2-23).

This heating event is interpreted by the authors as relating to burial in the depressions during the

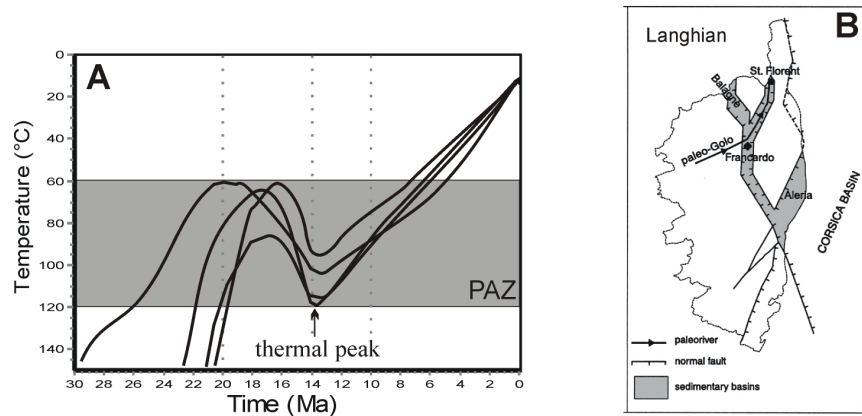


**Fig. 7-2-23:** A: Cooling path of the samples from Neogene grabens (hanging-walls in Francardo, Balagne, and St. Florent region) showing a distinct thermal event at ~14 Ma (redrawn after Fellin et al., 2005). The event is interpreted as reflecting maximum burial in the depressions, implying connection of the Balagne, St. Florent, and Francardo Basins during Langhian to Serravallian times (Fellin et al., 2005). B: Paleogeographic interpretation of the data after Fellin et al. (2005).

deposition of up to ~2 km thick Miocene successions, implying connection and a similar tectonothermal evolution of Balagne, St. Florent, and Francardo Basins during Langhian to Serravallian times (Fig. 7-2-23).

### **7.2.3.5 CONCLUSIONS**

AFT data revealed cooling of the Variscan basement, which followed the Jurassic thermal event related to the opening of the Ligurian-Piedmont Ocean. The basement cooled above PAZ already in the late Early Cretaceous and remained there until the Early Paleocene. Since the latest Paleocene, the basement was progressively buried below a pile of foreland flysch and later below Alpine nappes. In the Eocene, all of Corsica was covered by a thick pile of rocks, leading to total reset of the AFT system in the major part of the basement. In the Oligocene, after the tectonic reorganization, the basement started to exhume, which led to the removal of the thick cover from the top of the basement. The removal of the cover was realized by erosional denudation in the major part of Variscan Corsica, as well as by tectonic denudation in NE part of the island. NW part of the basement was in the Early Miocene thermally affected by a heating related to opening of the Ligurian-Provençal Ocean.

## 7.3 (U-TH)/HE DATA

### 7.3.1 Introduction

It has long been recognized that during long intervals of tectonic quiescence, topography can be beveled off by erosional processes, producing a low-relief landscape (or "peneplain"). When such a peneplain, characterized by slightly undulating and generally featureless topography, is uplifted tectonically, it can form prominent markers in the landscape.

There is a long-lasting debate about the evolution and the meaning of peneplains (or paleosurfaces) and there are several theories proposed by geomorphologists explaining that. To mention a few of them without going into detail, the theory dominating modern geomorphology was formulated nearly a century ago by Davis (1905), who supposed that landscapes did not develop haphazardly, but instead evolved through a series of stages as the stream drainage slowly eroded channels upslope and as valleys were progressively widened and deepened. According to Davis, the "youthful" stage of landscape evolution immediately follows uplift and is characterized by poor drainage and narrow, V-shaped valleys between flat and wide instream divides. After a few million years of erosion, the maximum relief "mature" stage would be achieved with well-integrated stream drainage, and deep, wide valleys, between narrow and rounded interstream divides. Finally, if erosion continued unchecked, the landscape could enter the "old age" stage where the surface becomes a poorly drained peneplain with streams of low gradient meandering over extensive flood plains at elevations just above sea level. In short, Davis' view is that landscapes are transient features having no permanence: they evolved. All features of the earth's surface are viewed by the Davisian system as being at various stages along a continuum of change.

An alternative idea is the *non-evolutionary* or what might be called the *catastrophic* theory for the origin of landscapes. Instead of being the products of a continuous process operating at an essentially modern rate, scale and intensity, landscapes could be remnants formed by catastrophic processes, which acted at a significantly increased rate, scale and intensity from what is observed today. The ancient processes forming the landscape would be discordant with modern processes acting on that landscape; no continuum of change and no stages of evolution would exist. Modern erosional processes would be viewed as entirely destroying an ancient landscape, not transforming it from one equilibrium stage to another. Such a landscape would contain relict landforms, surface features that were created by erosional or depositional processes no longer acting. Relict features on the earth's surface would make the landscape appear as a "museum", and such features, in contrast to the Davisian system, would have a great degree of permanence.

Regardless of which theory is correct, there are many elevated paleosurfaces preserved all around the world and it is accepted that their formation requires a long interval of tectonic quiescence; and due to extremely slow erosion on the top of them, they have survived until present.

### 7.3.2 Paleosurfaces in Corsica and available constraints

Remnants of paleosurfaces have since long been recognized in Corsica (Rondeau, 1961). These remnants are found exclusively in the Variscan part of the island in the form of flat ridges or plateaus at elevations of 250 to 2300 m. Kuhlemann et al. (2005a) distinguished two generations of paleosurfaces - summit and piedmont paleosurfaces (for details see chapter 3.2). According to these authors, the older summit paleosurface should form between mid-Oligocene to ~17 Ma, and the younger piedmont paleosurface should form between ~17 and ~11-10 Ma. The formation of both paleosurfaces was terminated by uplift pulses at ~17 Ma and ~11-10 Ma (see chapter 3.2).

If the scenario is correct, and when assuming that the present-day vertical difference between the two types of paleosurfaces is in some cases more than 1500 m, then it should be possible to get some record of thermal signal, related to rock exhumation in different time, in an appropriate low-temperature thermochronometer. Such a thermochronometer exists, for instance the (U-Th)/He system, since it is sensitive to record rock cooling at depths of ~1.5 km, and thus the evolution of the relief can be traced.

Before the integration of the He data to the proposed scenario can be accomplished, it is first necessary to evaluate all issues important relevant for further interpretation:

The first important issue is a proper evaluation of the actual meaning of the paleosurfaces: they are preserved exclusively in Variscan Corsica, and since there is almost no sedimentary record preserved on the top of the Variscan basement, they represent the only "stratigraphic" markers available in the basement that can serve to constrain rock uplift.

Paleosurfaces in Corsica form remarkably flat plateaus that presumably represent the relics of an ancient peneplain. It is accepted that peneplains, according to the Davisian theory representing the "old stage" of landscape evolution (see above), are formed by erosion during the long period of tectonic quiescence ("peneplainization") when the relief is smooth to form a flat peneplain with elevations of only few meters above sea level. The time span necessary to create a peneplain from a hilly landscape is still a matter of debate and depends on several factors, the most important being erodibility and climate. In the case of Corsica, where the peneplain was formed on the granite that is very resistant to erosion, it is likely that peneplainization must have taken at least several - perhaps several tens of - millions of years.

Erosion on the paleosurfaces should be very slow, otherwise no remnants would be preserved until present. This assumption was proven by Kuhlemann et al., (2005b), who reported extremely slow erosion rates (8-25 m/Ma) on the summit paleosurfaces in Corsica, calculated on the basis of concentrations of cosmogenic radionuclides ( $^{10}\text{Be}$ ) produced in situ.

The following stratigraphic constraints are available:

There is a 300 m thick conglomerate unit in Francardo Basin deposited at ~17 Ma, consisting of well rounded pebbles mostly derived from the Variscan basement. The unit is interpreted as deltaic sediments (Orszag-Sperber and Pilot, 1976; Ferrandini and Loÿe-Pilot, 1992; Kuhlemann et al., 2005a), indicating an uplift pulse that affected Variscan Corsica.

Another uplift event at ~11-10 Ma is recorded by first occurrences of material derived from Alpine Corsica in the sediments of the Oriental Plain and St. Florent Basin (Orszag-Sperber and Pilot, 1976; Ferrandini et al. 1998). Cessation of sedimentation in the intramontane basin of Ponte Leccia at ~10 Ma is also related to this uplift phase.

Early Pliocene marine sandy marls are found in several places on the SW coast. Although the global sea-level during the Early Pliocene was tens of meters higher than at present (Abreu and Anderson, 1998), Pliocene deposition in offshore neritic environment suggests that the basement has been uplifted by less than ~200 m since early Pliocene time. This also implies that the relief of Corsica acquired much of its present shape before the Pliocene and later was only slightly modified (Kuhlemann et al., 2005a).

### 7.3.3 Interpretation and discussion of (U-Th)/He data

When comparing data from the summit and piedmont paleosurfaces, there is no difference in the He ages (see Fig. 6-3 and chapter 6.3), although maximum vertical distance between piedmont and summit samples is more than 1600 m (summit sample XC-46: elevation 2247 m a.s.l., He age  $18.2 \pm 2.5$  Ma; piedmont sample XC-12: elevation 550 m a.s.l., He age  $17.6 \pm 2$  Ma). The data form a cluster of Early to early Middle Miocene ages. This means that all paleosurface samples were cooling through the He closure temperature at the same time and the differential uplift of individual blocks must have occurred after that time. Furthermore, there is no difference in cooling age between the two paleosurface generations, as would be expected from the scenario proposed by Kuhlemann et al. (2005a). Therefore it can be stated that all paleosurface remnants in Corsica have their origin in one single paleosurface.

One question to be answered involves the time of paleosurface formation. In order to answer this question, thermal modeling based on AFT and (U-Th)/He data was performed on those paleosurface samples, where He age, AFT age and track length distribution are available. In all cases

the revealed cooling paths show a similar pattern of fast cooling through the PAZ and HePRZ lasting from the Oligocene to the early Middle Miocene, followed by thermal stagnation in the near-surface conditions from the Middle Miocene until present (Fig. 7-3-1). According to such cooling paths, a bracketing of peneplain formation can be inferred as follows: fast cooling during Oligocene to Early Miocene times indicates tectonic activity, when the paleosurface samples were exhumed in the course of rift shoulder uplift. This process means a morphotectonic activity that was creating a topographic relief in Variscan Corsica, therefore no peneplain could have been formed at that time. In the Middle Miocene (~16 Ma), when the samples reached near-surface conditions and the cooling curves plateau off, it can be assumed that the denudational system had reached a state of sufficiently low energy to infer that base level stabilized and planation occurred at the surface (interval denoted as "*period of 'apparent' peneplainization*" in Fig. 7-3-1). During this period of tectonic quiescence and absolute morphotectonic standstill a peneplain could have formed in the Variscan basement. A "terminal age" of the peneplainization can not be deduced from the modeled cooling paths since the modeling results suggest that the phase of stagnancy lasts until present. Since it is known from stratigraphic record that Corsica acquired much of its present shape at ~5 Ma (see above), the phase of peneplainization thus can be bracketed between Middle and Late Miocene (~16-6 Ma).

However, there are some serious discrepancies that contradict this model. Firstly, sediments in Francardo Basin show that at ~17 Ma the first conglomerate fans appeared within the eastern

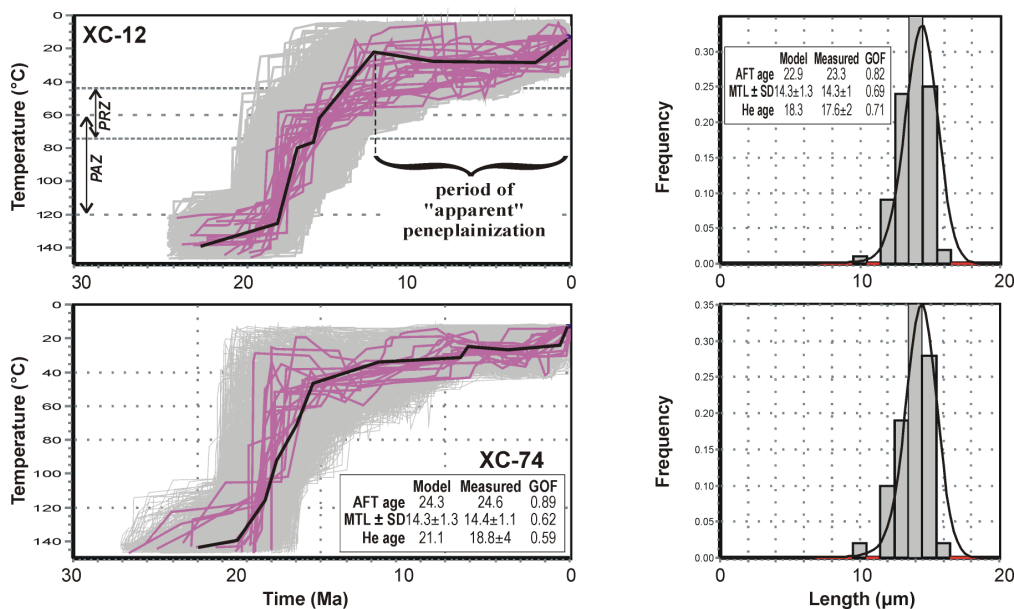


**Fig. 7-3-1:** Thermal modeling results of AFT and (U-Th)/He data of the samples XC-12 and XC-74 obtained with HeFTy (Ketcham et al., in press). Results are displayed in time-temperature diagrams (left) and frequency distribution diagram of measured confined track length data is overlain by a calculated probability density function (best fit) of a sample. Light gray paths: acceptable fit; dark gray paths: good fit; thick black line: best fit; PAZ: apatite partial annealing zone; PRZ: helium partial retention zone; GOF: goodness of fit between modeled and calculated values. According to modeled cooling path, a stagnation period starting at ~16 Ma can mark the onset of "peneplainization", which is however not in line with stratigraphic constraints (see text for explanation).

periphery of the Variscan basement, pointing to a growing relief of at least few hundred meters in Variscan Corsica, the source area for the conglomerates. This uplift pulse correlates with the cooling recorded by the He ages. According to the model proposed above, this relief should be later on beveled off by erosion to the peneplain. If this were true then all of Corsica (including the Alpine part) would form a peneplain in the Late Miocene, and today it should be possible to find the rest of this peneplain also in the Alpine part. But this is clearly not the case, since there are no paleosurface remnants in Alpine Corsica.

Secondly, there are clear evidences of tectonic activity at ~11-10 Ma recorded in sediments that mirror an uplift of Corsica (see above). This tectonic activity clearly conflicts with the period of quiescence between ~16 and 6 Ma proposed by the model.

Thirdly, according to the modeling, the period of peneplainization should last less than ~10 Ma, which is in author's opinion too short to transform a mountainous landscape, consisting largely of granitic bodies very resistant to erosion, to a peneplain located close to the sea level.

Because of the facts described above it can be concluded that the model proposed on the basis of thermal history modeling that bracketed the time of peneplainization between ~16 and 6 Ma cannot be and as a result, another solution for the age of the peneplain must be found. It is also evident that the peneplain must be older than ~17 Ma, as constrained by the stratigraphic record in the Francardo Basin.

Kuhlemann et al. (2005a) proposed that the peneplain could have formed after Late Eocene to mid-Oligocene exhumation. This is however not justified by the AFT and (U-Th)/He data of this study, because during the Oligocene the paleosurface samples were cooling through the PAZ, which contradicts tectonic quiescence. A possibility of peneplain formation in the Eocene is ruled out by the fact that the Variscan basement was at that time covered by a thick pile of flysch and partly Alpine nappes, as stated in chapter 7.2.3.3.1.

An elegant answer solving the enigma of the peneplain age might be a Cretaceous peneplainization age, with the key to understanding the whole story can be found in southernmost Corsica, defined as *Domain II* in chapter 7.2.3.2. As shown in that chapter, this area is the only part of Corsica where a Mesozoic AFT memory remained preserved. Since the associated cooling path indicates stagnation above PAZ, lasting from mid-Cretaceous to Paleocene time, it is proposed here that the peneplain formed during this period. Obviously, this can be the correct solution and the whole story can be explained as follows (Fig. 7-3-2): after the Jurassic thermal event related to opening of the Ligurian-Piedmont Ocean, the Variscan basement of Corsica was cooling through the PAZ. As indicated by thermal modeling results, the samples presently exposed on the surface, could have reached near-surface conditions already in the late Early Cretaceous. It is likely that after this cooling event a topographic relief (hilly to mountainous), as inferred from the abundant occurrences of coarse grained detrital material derived from the Variscan basement in Cretaceous sequences of some of the

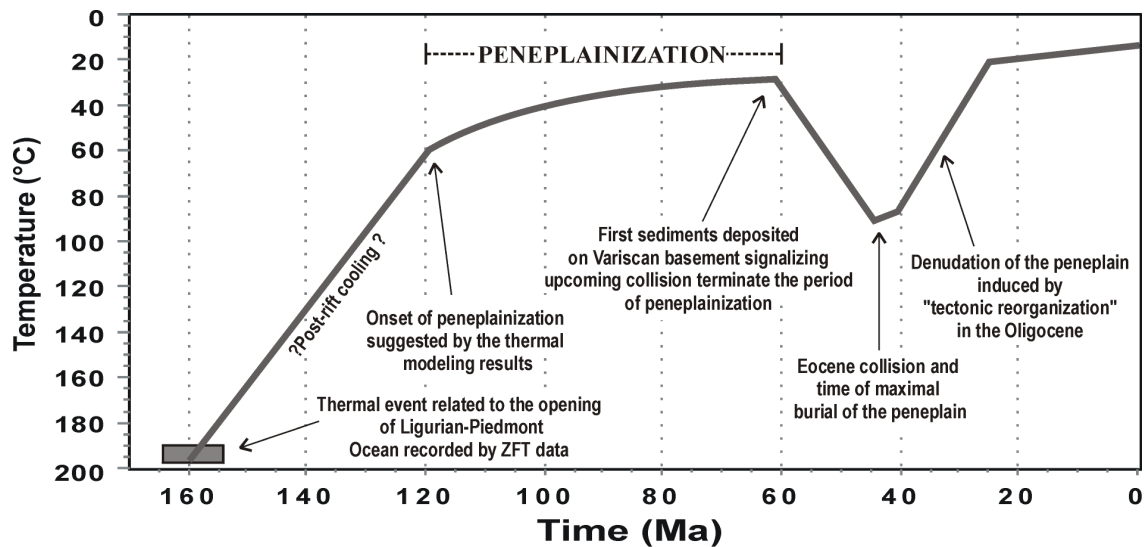


**Fig. 7-3-2:** Schematic time-temperature evolution of the Variscan basement in Corsica drawn from AFT, ZFT and (U-Th)/He data and regional geological considerations. Cooling path is redrawn after best fit curve of the sample XC-2 (southern Corsica); period of peneplainization is bracketed between ~120 and 60 Ma.

Alpine nappes (Rossi et al., 1980). The period from that time to the Early Paleocene is characterized by thermal stagnation and can therefore be regarded as a period of tectonic quiescence, when the topography was smoothed by erosion and the peneplain was formed. Thus the time of peneplainization can be bracketed between ~120 and 60 Ma, which is certainly long enough to smooth down the landscape. The period of peneplainization ceased prior to the Late Paleocene, because at that time the first flysch sediments were deposited on top of the Variscan basement. Until the Oligocene, the peneplain was progressively buried below the thick pile of flysch and, along its eastern part, the Alpine nappes. Since the Oligocene, Variscan Corsica was exhuming (as indicated by the FT data, see chapter 7.2.3.1) and the easily erodable pile of flysch and the Alpine nappes were removed from the top of the peneplain. As recorded by the (U-Th)He data, the exhumation of the basement lasted until the Early Miocene. The onset of peneplain destruction can be inferred from the granitic conglomerates in the Francardo Basin deposited at ~17 Ma, indicating a growing relief in Variscan Corsica and incision of first valleys into the peneplain. The arrangement of the valleys was controlled by the SW-NE trending faults, which were reactivated during the rotation of the Corsica-Sardinia block, and which segmented the peneplain to numerous blocks. During Middle to Late Miocene times, these blocks experienced several periods of differential uplift and tilting. The uplift was accompanied by valley incision at the expense of the paleosurface remnants, and it is likely that some peneplain remnants remained preserved on the top of the ridges (defined as "summit" paleosurface by Kuhlemann et al., 2005a), and some of them were downthrown along normal faults and are preserved in lower altitudes (defined as "piedmont" paleosurface by Kuhlemann et al., 2005a). In this way the ridge-and-valley pattern of Variscan Corsica evolved. Although at present the surface of Corsica is

severely eroded, relief evolution of Variscan Corsica was basically completed at ~5 Ma, although later modified by Quaternary glaciation (Kuhlemann et al., 2005a).

When looking at the present-day arrangement of the paleosurfaces in Variscan Corsica and comparing it to the new data, a sort of polarity can be observed between southern and northern regions.

In the north, paleosurface remnants are less preserved, they are smaller in size and summit remnants are at higher altitudes (up to ~2600 m). The landscape is characterized by sharp crests separated by deep gorges. AFT data yield younger ages (~25-20 Ma) and faster cooling than in the south.

In the southern areas, paleosurface remnants are more frequently preserved, they are larger and the summit remnants are located at lower altitudes (less than ~1700 m). The landscape is characterized by wide valleys and broad ridges topped by plateaus (paleosurfaces). AFT data revealed older cooling (~35-25 Ma) and the cooling rate was less rapid than in the samples from the north.

This pattern can be once again considered to be a consequence of varying thickness of the covering lid, which the Variscan basement inherited during Eocene collision. The thickness of the cover diminished roughly in a SW direction with increasing distance from the Alpine front, thus, the northern part of the basement was loaded by heavier weight than the southern part. As a consequence, during the denudation from below this cover, an isostatic rebound in the north must have been greater than in the south, resulting in the stronger uplift and formation of higher topography with steep gradients. Accordingly, the valley incision could operate much faster, cutting off the paleosurface plateaus on the top of the ridges more effectively. This process in the north often resulted in a creation of crests topped by sharp ridges at the expense of plateaus.

Conversely, in the south, due to the less heavy lid, the isostatic rebound was not that great, resulting in the weaker uplift and formation of lower topography with moderate gradients. The valley incision operated in slower rates, leaving the paleosurface remnants on top of the ridges.

### **7.3.4 Conclusions**

The paleosurfaces of Corsica are remnants of a single pre-Tertiary peneplain that was formed on the top of the crystalline basement during late Early Cretaceous to Early Paleocene times. During Alpine collision in the Eocene, it was covered by a thick flysch pile and thus preserved. In the Oligocene, the peneplain started to exhume and the cover lid was removed from its top. During the Miocene rotation, the peneplain was cut by faults, and at ~17 Ma the region was uplifted by differential block movements, creating a topographic relief and inducing valley incision. This event

can be understood as an onset of peneplain destruction that occurred mainly by fault-induced valley incision and widening.

A greater isostatic rebound in the northern areas of Variscan basement, resulting from denudation from below the heavier cover, induced stronger uplift that led to creation of higher relief with steep gradients. Consequently, due to more effective erosion, the paleosurface remnants were destroyed faster than in the south.

## 8 SYNTHESIS AND CONCLUSIONS

### 8.1 A COMPREHENSIVE MODEL

In order to summarize the main results obtained during this study and integrate them with known data, a comprehensive model consisting of several time sections is proposed. The geodynamic evolution of Corsica is reconstructed along an E-W trending profile across the island. The geomorphological evolution, focusing on the evolution of the paleosurfaces, is sketched along a N-S trending profile across the Variscan basement (Fig. 8-1).

In the **Middle to Late Jurassic (~180-145 Ma)**, the Ligurian-Piedmont Ocean opened between the African and Laurasian plates (including Iberian microplate with Corsican crystalline basement; e.g., Stampfli et al., 2002). Rifting and ocean opening was associated with increased heat flow related to mantle upwelling.

The Variscan basement of Corsica was situated in the vicinity of the rift (heat source) that led to a reheating of the rocks currently exposed on the surface to the temperatures of more than ~250°C.

This thermal event is recorded by ZFT data. The first rocks of future Alpine Corsica were formed (ophiolites) and deposited (deep-sea sediments) in the Ligurian-Piedmont Basin (e.g., ophiolites dated as  $161 \pm 3$  Ma; Ohnenstetter et al., 1981).

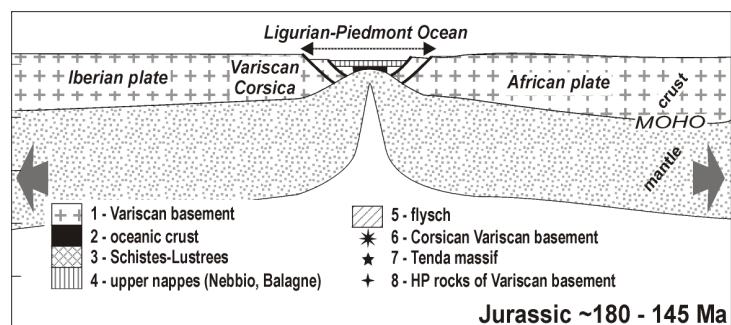
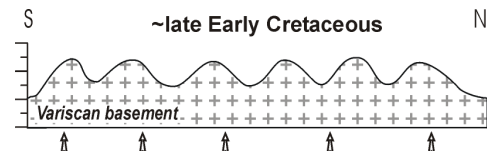
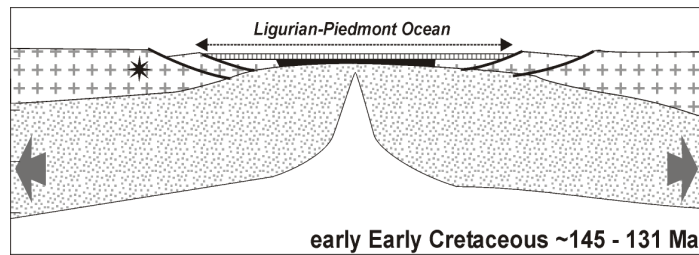


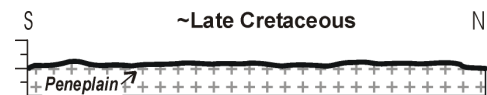
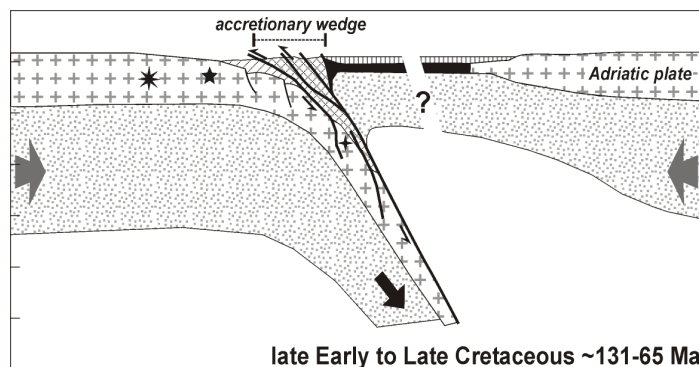
**Fig. 8-1:** Simplified evolutionary model of Corsica depicted along a E-W trending profile (left panels), and an illustration showing paleosurface evolution along a S-E profile running through the Variscan basement and crossing the major massifs (right panels); arrows indicate exhumation/uplift and burial/subsidence. The last two panels depict the real present-day situation. Figure continues to the next pages, see text for explanation.

In the early **Early Cretaceous (~145-131 Ma)**, spreading of the Ligurian-Piedmont Ocean continued, and the volume of the future Alpine rocks was increasing. The Variscan basement progressively cooled down to surface temperatures, as indicated by AFT data. The cooling is the consequence of (i) retreat of the basement from the heat source (or spreading center) in course of



continuous ocean spreading and related decrease in thermal gradient, and (ii) exhumation of the basement was exhumed in the course of rift shoulder uplift that was creating a topographic relief on the top of the basement. It is likely that at the end of the Early Cretaceous, a relief was developed in Variscan Corsica.

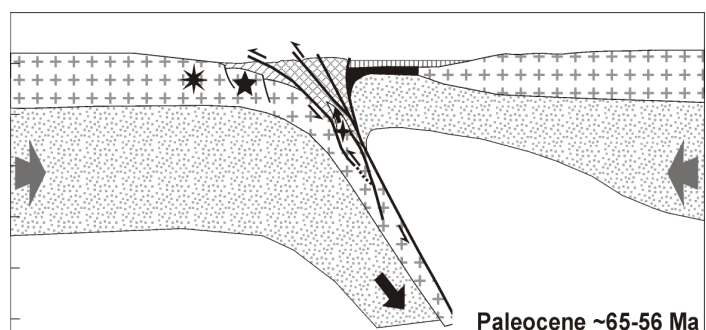
Between the late **Early** and **Late Cretaceous (~131-65 Ma)**, an eastward intraoceanic subduction zone developed in the Ligurian-Piedmont Ocean, which later led to closure of this ocean and to collision between the European and Adriatic continental plates.



During this long period, a tectonic standstill prevailed in Variscan Corsica, the basement was exposed to erosion, and the previously evolved relief was progressively smoothed to a peneplain.

The sedimentary sequences of the Alpine nappes ended up with the Upper Cretaceous flysch, indicating tectonic activity. In the Late Cretaceous, the subduction zone in the Ligurian-Piedmont Ocean was fully developed. This is evidenced by metamorphism of some tectonic units of oceanic as well as continental origin at HP/LT conditions, recorded by a Sm/Nd age of ~83.8 Ma (Lahondère and Guerrot, 1997), and a  $^{40}\text{Ar}/^{39}\text{Ar}$  age of 65 Ma (Brunet et al., 2000).

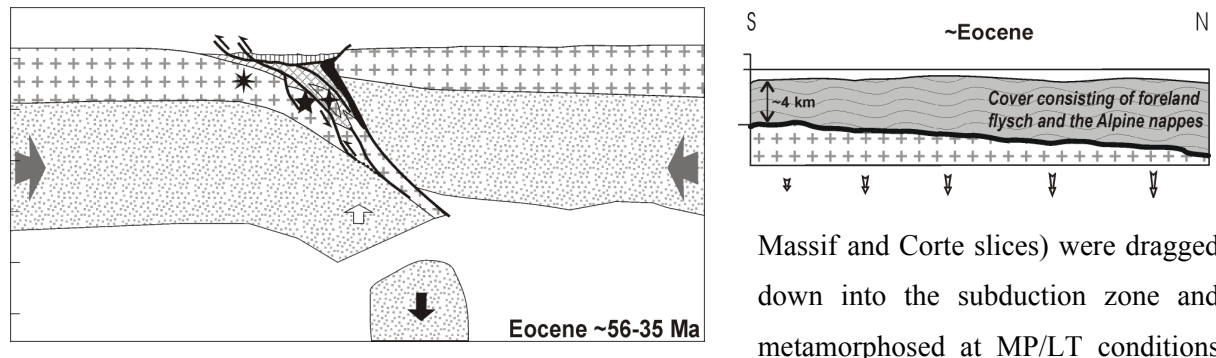
In the **Paleocene (~65-56 Ma)**, Variscan Corsica was approaching an advancing subduction zone, and finally in the Late Paleocene the first sediments of the foreland flysch trough were deposited on the basement (Egal, 1992), indicating the commencement of the Alpine collision. The peneplain was subsiding below sea-level and



progressively covered by flysch. This process can be understood as termination of the peneplainization period in Variscan Corsica.

The **Eocene (~56-35 Ma)** can be characterized by the collision between Variscan and Alpine Corsica.

According to the AFT data, the entire Variscan basement was affected by the collision: either buried below flysch or overridden by Alpine nappes. Some of its easternmost external parts (Tenda

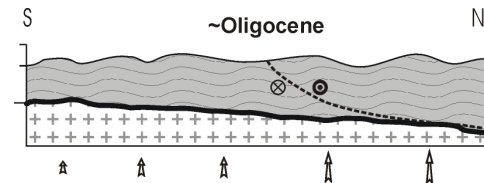
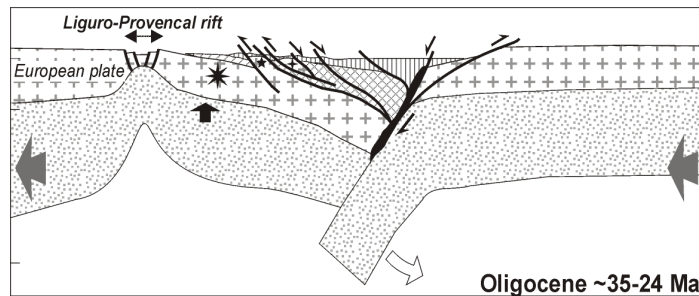


Massif and Corte slices) were dragged down into the subduction zone and metamorphosed at MP/LT conditions (blueschist facies) between ~45 and 32 Ma together with another slices of Ligurian-Piedmont origin ( $^{40}\text{Ar}/^{39}\text{Ar}$  data of Brunet et al., 2000). The major part of the Variscan basement was residing at temperature levels between 120 and 200°C, as indicated by FT data. An exception was the eastern margin, where the ZFT system was partially reset, indicating temperatures of more than ~200°C, and the southernmost part, where the AFT system was only partially annealed indicating temperatures below 100°C. At the same time (~45-33 Ma), due to buoyancy forces and shearing, the crustal slices until then residing at HP/LT conditions were detached from the downgoing slab and started to rise upwards to MP/LT levels (Malavieille et al., 1998). This stage corresponds to presence of the accretionary wedge between Variscan continental margin and the Ligurian-Piedmont oceanic domain. In the Late Eocene, closure of the remnant Ligurian-Piedmont oceanic basin resulted in a second orogenic phase with the emplacement of unmetamorphosed ophiolitic nappes (Balagne, Nebbio and Macinaggio nappes) which overthrust the previously exhumed and eroded HP belt as well as foreland deposits with Lutetian nummulites (Nardi et al., 1978; Durand-Delga, 1984; Jourdan, 1988; Malavieille et al., 1998).

During the collision, the peneplain was covered by a thick sequence of flysch that functioned as a protector. Therefore the peneplain could survive an attack of collision in major parts of Variscan Corsica.

The **Oligocene (~35-23 Ma)** can be characterized as a period of tectonic reorganization, since several tectonic events occurred contemporaneously at that time. Until ~33 Ma a thick accretionary complex was built in Corsica. At ~33 Ma the boundary conditions changed from compression to

extension and the overthickened crust started to collapse and exhume (Jolivet et al., 1990; Jolivet et al., 1998; Brunet et al., 2000). This stage of post-orogenic extension was the consequence of eastward rollback of the newly evolved Apennine subduction zone (Fournier et al., 1991; Jolivet et al., 1991; Daniel et al., 1996), and of isostatic rebound responding to the earlier slab break off in the east-dipping Alpine subduction zone (Malavieille et al., 1998).



First occurrences of synrift sediments in the Gulf of Lions indicate an inception of Ligurian-Provençal rifting between the Corsica-Sardinia micro-plate and the European mainland.

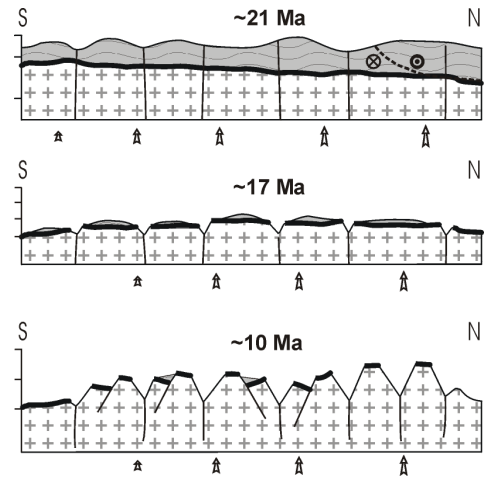
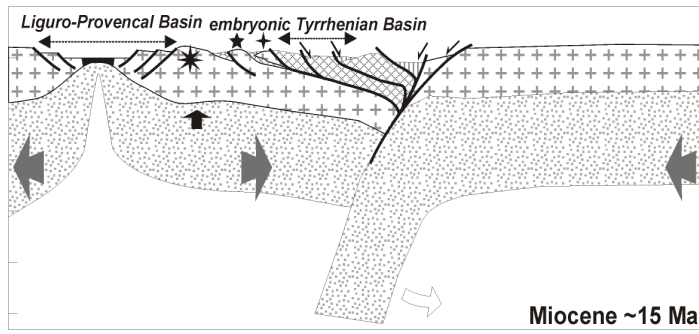
Variscan Corsica started to exhume, which led to the removal of the thick cover from the top of the basement. The removal of the cover was executed by erosional denudation in the major part of Variscan Corsica and by tectonic denudation in NE part of the island. The NW part of the basement was thermally affected by a heating in the Early Miocene related to the opening of the Ligurian-Provençal Ocean.

Variscan Corsica started to exhume, which led to the removal of the thick cover from the top of the basement. The removal of the cover was executed by erosional denudation in the major part of Variscan Corsica and by tectonic denudation in NE part of the island. The NW part of the basement was thermally affected by a heating in the Early Miocene related to the opening of the Ligurian-Provençal Ocean.

In Alpine Corsica, the Alpine thrust planes with top-to-west sense of shear were reactivated as ductile to brittle-ductile shear zones with top-to-east sense of shear (Jolivet et al., 1990; Fournier et al., 1991), leading to exhumation of formerly buried HP and MP metamorphic rocks (e.g. Tenda Massif) along extensional detachments (Jolivet et al., 1990; Fournier et al., 1991).

It is likely that during rifting and passive margin uplift of Variscan Corsica, new relief formed in Corsica. As recorded by the AFT data, the peneplain (or paleosurface) was cooling through the PAZ in moderate fashion, and the covering pile of flysch and Alpine nappes was removed from its top.

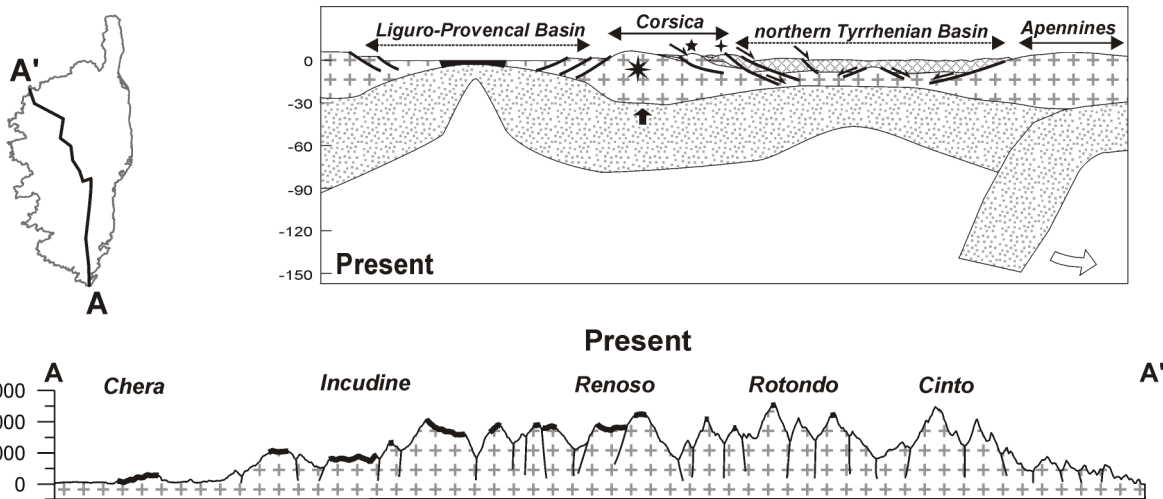
In the **Miocene (~24-5 Ma)**, extension still continued due to the eastward retreating Apennine subduction zone. Consequently, at ~18 Ma rifting of the Tyrrhenian Basin started east of Corsica. Between ~21 and 16 Ma the Corsica-Sardinia block rotated counter-clockwise close to its present position, and oceanic crust formed in the Ligurian-Provençal Basin (Vigliotti and Langheim, 1995). During rotation, Variscan Corsica was cut by sub-vertical faults, which predefined later block boundaries and orientation of the valleys. Exhumation still continued, removing the cover from the top of the basement. The peneplain, segmented into several pieces, cooled through the HePRZ. At ~17 Ma, the relief in Corsica reached at least several hundred meters, providing material to local basins. Some blocks with paleosurface remnants were already on the surface progressively destroyed by



valley incision. At ~10 Ma, an uplift affected all of Corsica (Kuhlemann et al., 2005a), inducing block tilting, the valleys were widening at the expense of the paleosurface remnants.

At **present**, Corsica is a part of a micro-continent surrounded by two oceanic basins in back-arc position to the eastward retreating Apennine subduction zone.

The Variscan basement is characterized by a ridge-and-valley pattern, where some paleosurface remnants remained preserved on the top of the ridges, and some of them were downfaulted and are preserved on the foothills. The paleosurface remnants in the north were, due to greater isostatic rebound, uplifted to higher altitudes, and cut off by incising valleys more rapidly, and therefore destroyed more effectively than in the south. Hence, there are less paleosurface remnants preserved in the north than in the south.



## 8.2 FINAL CONCLUSIONS

1. In the Late Jurassic, the Variscan basement of Corsica was affected by a thermal event related to the opening of the Ligurian-Piedmont Ocean, which is recorded by ZFT data.
2. After the Jurassic thermal event, the basement was cooling to near-surface conditions where it remained until the Early Paleocene. Since the Late Paleocene, the basement was progressively buried below sediments of the foreland basin, and later during Eocene collision it was partly covered by Alpine nappes.
3. At the end of the Eocene, all of Variscan Corsica was covered by a thick pile of rocks, leading to a total reset of the AFT system in the major part of the basement and to total a reset of all Eocene flysch sediments.
4. In the Oligocene, after tectonic reorganization, the basement started to exhume, which led to the removal of the thick cover from the top of the basement. The removal of the cover occurred by erosional denudation in the major part of Variscan Corsica, as well as by tectonic denudation in the NE part of the island.
5. AFT ages from the NW part of Variscan Corsica record an Early Miocene thermal event associated with the opening of the Ligurian-Provençal Ocean.
6. All paleosurface remnants in Corsica have their origin in one single paleosurface.
7. The age of the paleosurface formation is bracketed between ~120 and 60 Ma.
8. During Eocene collision, the paleosurface was buried by a thick flysch pile and was thus protected from destruction. In the Oligocene, the paleosurface started to exhume and the cover was removed. Destruction of the paleosurface started during the Miocene rotation, when it was cut by faults, and at ~17 Ma the region was uplifted by differential block movements, creating relief and inducing valley incision.

## ACKNOWLEDGEMENTS

First of all I would like to thank my supervisors, Joachim Kuhlemann and Wolfgang Frisch. Wolfgang and Achim, thank you for designing this interesting project, for giving me a chance to work on it, for inspiring advices, guidance in the field, collecting most of the samples for this project, your patience and time for discussion, and allowing me the freedom for research. Your very critical but very true and constructive reviews of earlier versions improved the text of this thesis substantially (especially at the very end). Thanks also for allowing me to participate at several conferences and workshops, for understanding the needs of having days-off and supporting any kind of travel.

The dearest thanks go to a person who without his help this thesis would probably never reach the stage where it is today: István Dunkl. István, if I had to write down all the things that you should be thanked for, several pages would surely not be enough. So just in a few sentences, thank you for proposing me as a candidate for this project, introducing me into the fission track world, your help with data acquisition and interpretation, all brainstorming discussions, endless encouragement, motivation and your inimitable sense of humor. Thank you also for ceding me the responsibly of a prominent "foster father" of our "metal baby", your 24-7 availability, your ability to share any kind of problem, and simply for being more than good friend. On this point, I also thank your family, especially your wife Judit, who helped me to organize my life and whose help made my studies in Tübingen more attractive.

I am gratefully indebted to Balázs Székely for his mental support, creative ideas regarding data handling and interpretation, for expressing his talent to analyze any kind of problem, for his provoking questions passing me "bugs of dubitation". Last but not least, thank you for teaching me the basics of GIS.

Also, I would like to thank Desmond B. Patterson, for constructing the helium extraction line for our workgroup. Des, thank you for having introduced me into the He world and for your patience in answering my endless questions. Mostly, I really had fun working with you on "the beast" (except of several Friday late evenings when you usually got a sudden desire to do something very necessary), and I will never forget your extremely colorful vocabulary, particularly when things were going wrong in the lab!

In the last three years in "AG-Frisch" I came across many people whom I would also like to thank: Horst and Volker, our ex-Romanian guys, who were always ready to help with and discuss anything, and for bringing an "eastern" temperament into our workgroup; Andreas and Christian, our "Kreuzeck" guys, for their assistance in the laboratory work, discussions dealing not necessarily with geology and help with an abstract and references; Monika and Bertram for their help and having a great time during fieldwork in Corsica; Igor, my Slovakian ex-roommate, for sharing his software and help with any kind of computer problems; Paul for help with the structural data; to the rest, Ines, Rajeev, Heiko, Martina, Caro, Tamás, Daniel, Cornelia, Ingrid, thank you for creating a pleasant atmosphere in the workgroup. Forgive me if I have forgotten anyone.

The help of many at the Tübingen University is greatly appreciated. The ladies from the separation lab (Kost, Höckh, Mühlbayer-Renner) and our "HiWi's" (Thomas, Florentina, Jan and Klaus), thanks for their help with the mineral separation. Mr. Stumpf and Mr. Kurz, without their reparation skills and their elegant inventions the helium line would probably never spit out any data.

Many thanks go to SUERC group in East Kilbride (Fin Stuart, Cristina Persano, Kate Dobson, Jurgen Foeken, Rob Ellam, Nadine Olive) for great cooperation, for sharing their knowledge in the field of (U-Th)/He method, and mainly for conducting U and Th analyses. Cristina and Kate thank you so much, and my apologies for all the troubles you had with my capsules. To Jurgen, I owe many thanks for discussion concerning error calculation, and for conducting thermal modeling.

A special thank-you to Ken Farley and Noreen Evans for carrying out the U-Th measurements free of charge, for helpful advice on the error calculation procedure and for helpful suggestions on the He dating technique.

Peter van der Beek is acknowledged for providing corrected coordinates of the samples of Mrs. Zarki-Jakni, and supplying otherwise inaccessible literature.

Gábor Timár and Gábor Molnár are thanked for their help with rectification and conversion of coordinates.

I cannot forget to thank Laura Niven, for careful revision of most of my manuscripts and abstracts, for being a good friend and for having good times in sometimes "gloomy" Tübingen (I will never forget your burritos!).

Except many relationships arising from the professional life at the University, there were several other friendships, which helped me to relax a little and reminded me that there is a life outside of Corsica, fission track and helium. Farky, thanks for taking me away from Tübingen, and enabling me to relieve my stress when skiing in the Alps, climbing on some crags, or roaming in the cities. When I came to Tübingen I almost forgot that sport used to be an important part of my life. Fortunately, I could again find my place in goal of a local handball club, where I found many friends (e.g., Miro, Jörg, Marco, Daniel, "Siggy", "Häger", "Grabo", to name few of them), whom I also want to thank.

V neposlednom rade by som chcel poďakovať svojim rodičom za lásku, podporu a porozumenie počas rokov môjho štúdia.

At the very end I would like to express my "massive respect" and a "big fanks" to my best friend Zuzana. Zuzi, you insisted on wasting not too many words on you at this place. So, just very simply, THANK YOU for being here with me and for being who you are.

## REFERENCES

- Abreu, V.S., and Anderson, J.B., 1998. Glacial eustasy during the Cenozoic: Sequence stratigraphic implications. *AAPG Bulletin*, 82, 1385-1400.
- Amaudric du Chaffaut, S., and Saliot, P., 1979. La région de Corte: secteur clé pour la compréhension du métamorphisme alpin en Corse. *Bull. Soc. Géol. France*, 7/21, 149-154.
- Amaudric du Chaffaut, S., 1982. Les unités alpines à la marge orientale du massif cristallin corse. *Trav. Lab. Géol.*, 15, ENS, Paris, 133 pp.
- Balestrieri, M.L., Stuart, F.M., Persano, C., Abbate, E., and Bigazzi, G., 2005. Geomorphic development of the escarpment of the Eritrean margin, southern Red sea, from combined apatite fission-track and (U-Th)/He thermochronometry. *Earth and Planetary Science Letters*, 231, 97-110.
- Barbarand, J., Hurford, T., and Carter, A., 2003. Variation in apatite fission-track length measurement: implications for thermal history modelling. *Chem. Geol.*, 198, 77-106.
- Bellaiche, G., Irr, F., and Labarbarie, M., 1976. Découverte de sédiments marins fini oligocène-aquitainien au large du Massif des Maures (Canyon des Stoechades). *C. R. Acad. Sci. Paris*, 283, 319-322.
- Bellon, H., 1976. Séries magmatique néogènes et quaternaires du pourtour de la méditerranée occidentale, comparées dans leur cadre géochronométrique: implications géodynamiques, doctoral dissertation, Univ. de Paris-Sud Centre D'Orsay.
- Bergman, S.C., and Corrigan, J., 1996. Compositional variation of natural apatites subjected to fission track analysis. *8th Int. Workshop Fission-Track Dating*, Gent. 7.
- Bézert, P., and Caby, R., 1988. Sur l'âge post-bartonien des événements tectono-étamorphiques alpins en bordure orientale de la Corse cristalline (Nord de Corte). *Bull. Soc. Géol. France*, 6, 965-971.
- Bézert, P., and Caby, R., 1989. La déformation progressive de l'éocène de la région de Corte: nouvelles données pétrostructurales et conséquences pour la tectogénèse alpine en Corse. *C. R. Acad. Sci. Paris*, 95-101.
- Boccaletti, M., Elter, P., and Guazzone, G., 1971. Polarità strutturali delle Alpi e dell'Appennino Settentrionale in rapporto all'inversione di una zona di subduzione nord-tirrenica. *Mem. Soc. geol. It.*, 10, 371-378.
- Borel, G., 1995. Préalpes médianes romandes: courbes de subsidence et implications géodynamiques. *Bulletin de la Société vaudoise des Sciences naturelles*. 83(4), 293-315.
- Braun, J., 2002. Quantifying the Effect of Recent Relief Changes on Age-Elevation Relationships. *Earth and Planetary Science Letters*, 200, 331-343.
- Brown, R.W., Summerfield, M.A., and Gleadow, A.J.W., 1994. Apatite Fission Track Analysis: Its Potential for the Estimation of Denudation Rates and Implications for Models of Long-term Landscape Development. In: *Process Models and Theoretical Geomorphology*, (Kirkby, M.J., ed.), pp. 23-53.
- Brunet, C., Monié, P., and Jolivet, L., 1997. Geodynamic evolution of the Alpine Corsica based on new <sup>40</sup>Ar/<sup>39</sup>Ar data. *Terra Abstracts*, 9, 493.
- Brunet, C., Monié, P., Jolivet, L., and Cadet, J.P., 2000. Migration of compression and extension in the Tyrrhenian Sea, insights from <sup>40</sup>Ar/<sup>39</sup>Ar ages on micas along a transect from Corsica to Tuscany. *Tectonophysics*, 321, 127-155.
- Burtner, R.L., Nigrini, A., and Donelick, R.A., 1994. Thermochronology of Lower Cretaceous source rocks in the Idaho-Wyoming thrust belt. *Am. Assoc. Petrol. Geol. Bull.*, 78(10), 1613-1636.
- Carlson, W.D., 1990. Mechanisms and kinetics of apatite fission track annealing. *Am. Mineral.*, 75, 1120-1139.

- Carlson, W.D., Donelick, R.A., and Ketcham, R.A., 1999. Variability of apatite fission-track annealing kinetics: Experimental results, *Am. Mineral.*, 84, 1213–1223.
- Carmignani, L., Decandia, F.A., Disperati, L., Fantozzi, P.L., Lazzarotto, A., Liotta, D., and Oggiano, G., 1995. Relationship between the Tertiary structural evolution of the Sardinia-Corsica-Provençal Domain and the Northern Apennines. *Terra Nova*, 7, 128-137.
- Caron, J.M., 1977. Lithostratigraphie et tectonique des schistes lustrés dans les Alpes cottiennes septentrionales et en Corse orientale. *Sci. géol. Mém.*, 48, Strasbourg, 326 pp.
- Caron, J.M., Kiénast, J.R., and Triboulet, C., 1981. High-pressure-low-temperature metamorphism and polyphase alpine deformation at Sant'Andrea di cotone (eastern corsica, france). *Tectonophysics*, 78, 419-451.
- Carpéna, J., Mailhé, D., Naeser, C.W., and Poupeau, G., 1979. Sur la datation par traces de fission d'une phase tectonique d'age Eocène supérieur en Corse. *C.R. Acad. Sci. Paris*, 289. 829-832.
- Cavazza, W., Zattin, M., Ventura, B., and Zuffa, G.G., 2001. Apatite fission-track analysis of Neogene exhumation in northern Corsica (France). *Terra Nova*, 13, 51-57.
- Chamot-Rooke, N., Gaulier, J.M., and Jestin, F., 1999. Constraints on Moho depth and crustal thickness in the Liguro-Provençal basin from a 3D gravity inversion: Geodynamic implications, In: *The Mediterranean basins: Tertiary extension within the Alpine Orogen*: (Durand, B., et al., eds.). pp. 37-61. Geological Society, London.
- Cherchi, A., and Montadert L., 1982. Oligo-Miocene rift of Sardinia and the early history of the western Mediterranean basin, *Nature*, 298, 736-739.
- Cocherie, A., Rossi, P., and Le Bel, L., 1984. The Variscan calc-alkalic plutonism of Western Corsica: Mineralogy and major and trace element geochemistry. *Phys. Earth Planet. Inter.*, 35, 145-178.
- Coulon, C., 1977. Le volcanisme calco-alkalin cénozoïque de Sardaigne (Italie): Pétrologie, géochimie et genèse des laves andésitiques et des ignimbrites: Signification géodynamique, doctoral dissertation, Univ. d'Aix-Marseille III, Aix en Provence, France.
- Crowley, K.D., Cameron, M., and Schaeffer, R.L., 1991. Experimental studies of annealing of etched fission tracks in fluorapatite. *Geochimica et Cosmochimica Acta*, 55, 1449-1465.
- Daniel, J.M., Jolivet, L., Goffe, B., and Poinssot, C., 1996. Crustal-scale strain partitioning: Footwall deformation below the Alpine Oligo-Miocene detachment of Corsica. *J. Struct. Geol.*, 18, 41-59.
- Davis, W.M., 1905. Complications of the geographical cycle. *Report of the Eighth Geographical Congress*, Washington, pp. 50-163.
- Dewey, J.F., Helman, M.L., Turco, E., Hutton, D.H.W., and Knott, S.D., 1989. Kinematics of the western Mediterranean. In: *Alpine Tectonics*. (Coward, M.P., Dietrich, D., and Park, R.G., eds.). Geol. Soc. Spec. Pub., 45; 265-283.
- Dodson, M., 1973. Closure Temperature in Cooling Geochronological and Petrological Systems. *Contrib. Min. Petrol.*, 40; 259-274.
- Dogliani, C., Gueguen, E., Harabaglia, P., and Mongelli, F., 1999. On the origin of west-directed subduction zones and applications to the western Mediterranean. In: *The Mediterranean basins: Tertiary extension within the Alpine Orogen* (Durand, B., Jolivet, L., Horvath, F., and Seranne, M., eds.), pp. 541-570. Geological Society Special Publications, vol. 156.
- Donelick, R.A., 1991. Crystallographic orientation dependence of mean etchable fission track length in apatite: An empirical model and experimental observations. *Am. Mineral.*, 76, 83 - 91.
- Donelick, R.A., Roden, M.K., Mooers, J.D., Carpenter, B.S., and Miller, D.S., 1990. Etchable track length reduction of induced fission tracks in apatite at room temperature (~23°C): crystallographic orientation effects and 'initial' mean lengths. *Nucl. Tracks Radiat. Meas.*, 17, 261-265.

- Donelick, R.A., Ketcham, R.A., and Carlson, W.D., 1999. Variability of apatite fission track annealing kinetics II: Crystallographic orientation effects. *Am. Mineral.*, 84, 1224-1234.
- Dumitru, T.A., 1993. A new computer automated microscope stage system for fission-track analysis. *Nucl. Tracks Radiat. Meas.*, 21, 575-580.
- Dunkl, I., 2002. TRACKKEY: A windows program for calculation and graphical presentation of fission track data. *Computers and Geosciences*, 28(1), 3-12.
- Durand-Delga, M., 1978. *Corse-Guides géologiques régionaux*. Masson éd. Paris, 208 pp.
- Durand-Delga, M., 1984. Principaux trait de la Corse Alpine et corrélation avec les Alpes ligures. *Mem. Soc. Geol. Ital.*, 28, 285-329.
- Egal, E., 1992. Structures and tectonic evolution of the external zone of Alpine Corsica. *J. Struct. Geol.*, 14(10), 1215-1228.
- Ehlers, T.A., and Farley, K.A., 2003. Apatite (U-Th)/He Thermochronometry: methods and applications to problems in tectonics and surface processes. *Earth and Planetary Science Letters-Frontiers*, 206, 1-14.
- England, P., and Molnar, P., 1990. Surface uplift, uplift of rocks, and exhumation of rocks. *Geology* 18, 1173-1177.
- Farley, K.A., 2000. Helium diffusion from apatite: General behavior as illustrated by Durango fluorapatite. *J. Geophys. Res.*, 105(B2), 2903-2914.
- Farley K.A., 2002. (U-Th)/He dating: Techniques, calibrations, and applications. *Mineral. Soc. Am. Rev. Mineral. Geochem.* 47, 819-844.
- Farley, K.A., Wolf, R.A., and Silver, L.T., 1996. The effects of long alpha-stopping distances on (U-Th)/He ages. *Geochimica and Cosmochimica Acta*, 60(21), 4223-4229.
- Fellin, M.G., 2003. Neogene to quaternary Thermo-Tectonic Evolution of North-Eastern Corsica (France). Doctoral dissertation, University of Bologna, 90pp.
- Fellin, M.G., Picotti, V., and Zattin, M., 2005. Neogene to Quaternary multiple rifting and inversion in north-eastern Corsica: retreat and collision in the Western Mediterranean. *Tectonics*, 24, TC1011, 29pp.
- Ferrandini, A., and Loÿe-Pilot, M.D., 1992. Tectonique en distension et décrochement au Burdigalian-Tortonian en Corse: l'exemple du bassin Francardo-Ponte-Leccia (Corse Centrale). *Géologie Alpine, sér. spéc.*, Résumés de colloques 1, 30-31.
- Ferrandini, M., Ferrandini, J., Loÿe-Pilot, M.D., Butterlin, J., Cravatte, E, J., and Janin, M.C., 1998. Le Miocène du bassin de Saint-Florent (Corse); modalités de la transgression du Burdigalien supérieur et mise en évidence du Serravallien. – *Geobios* 31(1), 125-137.
- Ferrandini, L., Rossi, P., Ferrandini, M., Farjanel, G., Ginsburg, L., Schuler, M., and Geissert, F., 1999. La Formation conglomératique du Vazzino près d'Ajaccio (Corse-du-Sud), un témoin des dépôts du Chattien supérieur continental synrift en méditerranée occidentale. *C. R. Acad. Sci. (Paris), Série II, Sciences de la Terre et des Planètes* 329(4), 271-278.
- Ferrandini, J., Gattacceca, J., Ferrandini, M., Deino, A., and Janin, M.C., 2003. Chronostratigraphy and paleomagnetism of Oligo-Miocene deposits of Corsica (France): geodynamic implications for the liguro-provençal basin spreading. *Bull. Soc. Géol. France*, 174(4), 357-371.
- Fitzgerald, P.G., and Gleadow, A.J.W., 1988. Fission track geochronology, tectonics and structure of the Transantarctic Mountains in Northern Victoria Land, Antarctica, *Isotope Geoscience*, 73, 169-198.
- Fitzgerald, P.G., Sorkhabi, R.B., Redfield, T.F., and Stump, E., 1995. Uplift and denudation of the central Alaska Range: A case study in the use of apatite fission-track thermochronology to determine absolute uplift parameters. *J. Geophys. Res.*, 100, 20175-20191.
- Fleischer, R.L., Price, P.B., Symes, E.M., and Miller, D.S., 1964. Fission track ages and track-annealing behaviour of some micas. *Science* 143, 349-151.

- Fleischer, R.L., Price, P.B., and Walker, R.M., 1965. Effects of temperature, pressure, and ionization on the formation and stability of fission tracks in minerals and glasses. *J. Geophys. Res.*, 70, 1497-1502.
- Fleischer, R.L., Price, P.B., and Walker, R.M., 1975. *Nuclear Tracks in Solids*. University of California Press, 605 pp.
- Foeken, J.P.T., 2004. Tectono-morphology of the Ligurian Alps and adjacent basins (NW Italy). Doctoral dissertation, Vrije Universiteit Amsterdam, The Netherlands, 192 pp.
- Foeken, J.P.T., Dunai, T.J., Bertotti, G., and Andriessen, P.A.M., 2003. Late Miocene to present exhumation in the Ligurian Alps (Southwest Alps) with evidence for accelerated denudation during the Messinian salinity crisis *Geology*, 31(9), 797-800.
- Fournier, M., Jolivet, L., and Goffé, B., 1991. Alpine Corsica metamorphic core complex, *Tectonics*, 10, 1173-1186.
- Frisch, W., 1981. Plate motions in the Alpine region and their correlation to the opening of the Atlantic ocean. *Geol. Rundschau*, 70, 402-411.
- Frisch, W., and Meschede, M., 2005. *Plattentektonik*. Darmstadt, Primus Verlag, 196pp.
- Galbraith, R.F., 1981. On Statistical Models for Fission Track Counts. *Math. Geol.*, 13(6), 471-478.
- Galbraith, R.F., and Laslett, G.M., 1993. Statistical models for mixed fission track ages. *Nucl. Tracks Radiat Meas.*, 21, 459-470.
- Gallagher, K., and Brown, R.W., 1997. The onshore record of passive margin evolution. *J. Geol. Soc. London*, 154, 451-457.
- Gallagher, K., Brown, R., and Johnson, C., 1998. Fission track analysis and its applications to geological problems. *Ann. Rev. Earth Planet. Sci.*, 26, 519-572.
- Gibbons, W., and Horák, J., 1984. Alpine metamorphism of Hercynian hornblende granodiorite beneath the blueschists facies Schistes Lustrés nappe of NE Corsica. *J. Metamorph. Geol.*, 2, 95-113.
- Gleadow, A.J.W., 1981. Fission-track dating methods: what are the real alternatives? *Nucl. Tracks*, 5, 3-14.
- Gleadow, A.J.W., and Duddy, I.R., 1981. A natural long-term track annealing experiment for apatite. *Nucl. Tracks*, 5, 169-174.
- Gleadow, A.J.W., Duddy, I.R., and Green, P.F., 1986a. Fission track lengths in the apatite annealing zone and the interpretation of mixed ages. *Earth Planet. Sci. Lett.*, 78, 245-254.
- Gleadow, A.J.W., Duddy, I.R., and Green, P.F., 1986b. Confined fission track lengths in apatite: a diagnostic tool for thermal history analysis. *Contrib. Min. Pet.*, 94, 405-415.
- Gorini, C., Le Marrec, A., and Mauffret, A., 1993. Contribution to the structural and sedimentary history of the Gulf of Lions, (Western Mediterranean) from ECORS profiles, industrial seismic profiles and well data. *Bull. Soc. Géol. France*, 164, 353-363.
- Green, P.F., 1981. A new look at statistics in Fission-Track dating. *Nuclear Tracks*, 5(1/2), 77-86.
- Green, P.F., 1985. Comparison of zeta calibration baselines for fission track dating of apatite, zircon and sphene. *Chem. Geol.*, 58, 1-22.
- Green, P.F., 1988. The relationship between track shortening and fission track age reduction in apatite: combined influences of inherent instability, annealing anisotropy, length bias and system calibration. *Earth and Planetary Science Letters*, 89, 335-352.
- Green, P.F., Duddy, I.R., Gleadow, A.J.W., Tingate, P.R., and Laslett, G.M., 1986. Thermal annealing of fission tracks in apatite 1. A qualitative description, *Chem. Geol.*, 59, 237-253.
- Green, P.F., and Duddy, I.R., 1989. Some comments on paleotemperature estimation from apatite fission track analysis. *J. Petrol. Geol.*, 12, 111-114.
- Gueguen, E., Doglioni, C., and M. Fernandez, M., 1998. On the post-25 Ma geodynamic evolution of the western Mediterranean, *Tectonophysics*, 298, 259-269.

- Harris, L., 1984. Déformations et déplacements dans les chaînes Rendus de l'Académie des Sciences, Série II, 10, 453-458.
- Hasebe, N., Tagami, T., and Nishimura, S., 1994. Towards zircon fission-track thermochronology; reference framework for confined track length measurements. *Chem. Geol.*, 112, 169-178.
- Hendriks, B., 2003. Cooling and denudation of the Norwegian and Barents Sea margins, Northern Scandinavia. Constrained by apatite fission track and (U-Th)/He thermochronometry, doctoral dissertation, Vrije Universiteit, Amsterdam, The Netherlands, 177 pp.
- House, M.A., Wernicke, B.P., Farley, K.A., and Dumitru, T.A., 1997. Cenozoic thermal evolution of the central Sierra Nevada, California, from (U-Th)/He thermochronometry. *Earth and Planetary Science Letters*, 151, 167-179.
- House, M.A., Farley, K.A., and Stockli, D., 2000. Helium chronometry of apatite and titanite using Nd-YAG laser heating. *Earth and Planetary Science Letters*, 183, 365-368.
- House, M.A., Wernicke, B.P., and Farley, K.A., 2001. Paleo-geomorphology of the Sierra Nevada, California, from (U-Th)/He ages in apatite. *Am. J. Sc.*, 301, 77-102.
- Hurfurd, A.J., 1986. Standardization of fission track dating calibration; results of questionnaire distributed by International Union of Geological Sciences Subcommittee on Geochronology. *Nucl. Tracks Rad. Meas.*, 11, 329-333.
- Hurfurd, A.J., 1990a. Standardization of fission track dating calibration: Recommendation by the Fission Track Working Group of the I. U. G. S. Subcommittee on Geochronology, *Chem. Geol.*, 80, 171-178.
- Hurfurd, A.J., 1990b. International Union of Geological Sciences Subcommittee of Geochronology recommendation for the standardization of fission track dating calibration and data reporting. *Nucl. Tracks Rad. Meas.*, 17, 233-236.
- Hurfurd, A.J., and Green, P.F., 1983. The zeta age calibration of fission-track dating. *Chem. Geol.*, 41, 285-312.
- Hurfurd, A.J., and Hammerschmidt, K., 1985.  $^{40}\text{Ar}$ - $^{39}\text{Ar}$  and K-Ar dating of the Bishop and Fish Canyon tuffs: calibration ages for fission track dating standard. *Chem. Geol.*, 58, 23-32.
- Hurley, P.M., 1954. The helium age method and the distribution and migration of helium in rocks, In: *Nuclear Geology*, (Faul, H., ed.) New York, John Wiley and Sons, pp. 301-329.
- Jakni, B., 2000. Thermochronologie par traces de fission des marges conjuguées du bassin Liguro-Provençal: La Corse et le massif des Maures-Tanneron, doctoral dissertation, Univ. Joseph Fourier, Grenoble, France. 344 pp.
- Jakni, B., Poupeau, G., Sosson, M., Rossi, P., Ferrandini, J., and Guennoc, P., 2000. Dénudations cénozoïques en Corse: Une analyse thermochronologique par traces de fission sur apatites. *C. R. Acad. Sci. Paris*, 331, 775-782.
- Jolivet, L., Dubois, R., Fournier, M., Goffé, B., Michard, A., and Jourdan, C., 1990. Ductile extension in Alpine Corsica, *Geology*, 18, 1007-1010.
- Jolivet, L., Daniel, J.M., and Fournier, M., 1991. Geometry and kinematics of ductile extension in Alpine Corsica, *Earth Planet. Sci. Lett.*, 104, 278-291.
- Jolivet, L., Faccenna, C., Goffé, B., Mattei, M., Rosseti, F., Brunet, C., Storti, F., Funiciello, R., Cadet, J.P., d'Agostino, N., and Parra, T., 1998. Midcrustal shear zones in postorogenic extension: example from the Tyrrhenian Sea. *Journal of Geophys. Res.* 103, 12123-12160.
- Jolivet, L., and Faccenna, C., 2000. Mediterranean extension and the Africa-Eurasia collision, *Tectonics*, 19, 1095-1106.
- Jonckheere, R., Mars, M., Van den haute, P., Rebetez, M., and Chambaudet, A., 1993. L'apatite de Durango (Mexique): Analyse d'un minéral standard pour la datation par traces de fission: *Chem. Geol.*, 103, 141-154.

- Jourdan, C., 1988. Balagne orientale et massif du Tende (Corse septentrionale): Etude structurale, interprétation des accidents et des déformations, reconstitutions géodynamiques, doctoral dissertation, Univ. de Paris Sud, Orsay, France.
- Ketcham, R.A., Donelick, R.A., and Carlson, W.D., 1999. Variability of apatite fission-track annealing kinetics: III. Extrapolation to geological time scales. *Am. Mineral.*, 84, 1235-1255.
- Ketcham et al., in press: <ftp://ctlab.geo.utexas.edu/ketcham/ft/HeFTy/>
- Klaer, W., 1956. Verwitterungsformen im Granit auf Korsika. – *Petermanns Geograph. Mitt. Ergänzungsheft* 261, 146 pp.
- Kuhlemann, J., Székely, B., Frisch, W., Danišík, M., Dunkl, I., Molnár, G., and Timár, G., 2005a. DEM analysis of mountainous relief in a crystalline basement block: Cenozoic relief generations in Corsica (France). *Z. für Geomorph.*, 49, 1-21.
- Kuhlemann, J., Van der Borg, K., Danišík, M., and Frisch, W., 2005b. Erosion rates on subalpine paleosurfaces in the western Mediterranean by in-situ <sup>10</sup>Be concentrations in granites: implications for surface processes and long-term landscape evolution In: *EGU meeting*, Vienna, Austria, Geophysical Research Abstracts, Vol. 7, 00373.
- Lacombe, O., and Jolivet, L., 2005. Structural and kinematic relationships between Corsica and the Pyrenees-Provence domain at the time of the Pyrenean orogeny. *Tectonics*, 24(1), TC1003, 10.1029/2004TC001673
- Lahondère, D., 1988. Le métamorphisme écolitique dans les orthogneiss, et les metabasites ophiolitiques de la région de Farinole (Corse). *Bulletin de la Société Géologique de France*, 4, 579-585.
- Lahondère, D., 1991. Les schistes bleus et les écolites à lawsonite des unités continentales et océanique de la Corse alpine: Nouvelles données pétrologiques et structurales. Thèses de 3ème cycle, Université Montpellier II, France.
- Lahondère, D., and Guerrot, C., 1997. Datation Nd-Sm du métamorphisme écolitique en Corse alpine: un argument pour l'existence, au Crétacé supérieur, d'une zone de subduction active localisée le long du bloc corso-sarde. *Géologie de la France*, 3, 3-11.
- Laslett, G.M., P.F. Green, I.R. Duddy, and Gleadow, A.J.W., 1987. Thermal annealing of fission tracks in apatite 2. A quantitative analysis, *Chem. Geol.*, 65, 1-13.
- Lippolt, H.J., and Weigel, E., 1988. <sup>4</sup>He diffusion in <sup>40</sup>Ar retentive minerals. *Geochim. Cosmochim. Acta*, 52, 1449-1458.
- Lippolt, H.J., Leitz, M., Wernicke, R.S., and Hagedorn, B., 1994. (U-Th)/He dating of apatite: experience with samples from different geochemical environments. *Chem. Geol.*, 112, 179-191.
- Loup, B., 1992. Mesozoic subsidence and stretching models of the lithosphere in Switzerland (Jura, Swiss Plateau and Helvetic realm). *Ecl. Geol. Helv.*, 85(3), 541-572.
- Loÿe-Pilot, M.D., and Magné, J., 1978. La formation de Peri (plaine orientale corse): Formation continentale à paléosols d'âge post-tortonien, *C. R. Acad. Sci. Paris, Ser. D*, 287, 1175-1178.
- Loÿe-Pilot, M.D., and Magné, J., 1989. Excursion du Groupe Français d'étude du Neogene en Corse, Livret - guide de l'itinéraire plaine orientale.
- Lucazeau, F., and Mailhé, D., 1986. Heat flow, heat production and fission track data from the Hercynian basement around the Provençal Basin (western Mediterranean). *Tectonophysics*, 128, 335-356.
- Luo, X., Rehkämper, M., Lee, D., and Halliday, A.N., 1997. High precision <sup>230</sup>Th/<sup>232</sup>Th and <sup>234</sup>U/<sup>238</sup>U measurements using energy-filtered ICP magnetic sector multiple collector mass spectrometry. *International Journal of Mass Spectrometry and Ion Processes*, 171, 105-117.
- Mailhé, D., 1982. Application des méthodes de datation <sup>40</sup>Ar-<sup>39</sup>Ar et traces de fission de l'uranium à l'étude du déroulement de l'orogénèse alpine en Corse. Thèse 3ème cycle, USTL, Montpellier.

- Mailhé, D., Lucazeau, F., and Vasseur, G., 1986. Uplift history of thrust belts: An approach based on fission track data and thermal modelization. *Tectonophysics*, 124, 177-191.
- Malavieille, J., 1983. Étude tectonique et microtectonique de la nappe de socle de Centuri (zone des Schistes Lustrés de Corse), Conséquence pour la géométrie de la chaîne alpine. *Bull. Soc. Géol. France*, 25, 195-204.
- Malavieille, J., Chemenda, A., and Larroque, C., 1998. Evolutionary model for Alpine Corsica: Mechanism for ophiolite emplacement and exhumation of highpressure rocks, *Terra Nova*, 10, 317-322.
- Maluski, H., 1977. Application de la méthode  $^{40}\text{Ar}$ - $^{39}\text{Ar}$  aux minéraux des roches cristallines perturbées par des événements thermiques et tectoniques en Corse. *Bull. Soc. Géol. France*, 19(4), 849-855.
- Mancktelow, N.S., and Grasemann, B., 1997. Time-dependent effects of heat advection and topography on cooling histories during erosion. *Tectonophysics*, 270, 167-195.
- Mattauer, M., and Proust, F., 1976. Sur quelques problèmes généraux de la chaîne alpine en Corse. *Compte Rendu de l'Académie de Science*, Paris, 18(5), 1249-1251.
- Mattauer, M., Faure, M., and Malavieille, J., 1981. Transverse lineation and large scale structures related to Alpine obduction in Corsica, *J. Struct. Geol.*, 3, 401-409.
- Mauffret A., Contrucci I., and Brunet, C., 1999. Structural evolution of the northern Tyrrhenian sea from new seismic data. *Marine and Petroleum Geology*, 16(5), 381-407.
- McDowell, F.W., and Keizer, R.P., 1977. Timing of mid-Tertiary volcanism in the Sierra Madre Occidental between Durango City and Mazatlan, Mexico. *Geol. Soc. Amer. Bull.*, 88, 1479-1487.
- Meesters, A.G.C.A., and Dunai, T.J., 2002a. Solving the production- diffusion equation for finite diffusion domains of the various shapes, part 1; implications for low temperature (U-Th) /He thermochronology. *Chem. Geol.*, 186(3-4), 333-344.
- Meesters, A.G.C.A., and Dunai, T.J., 2002b. Solving the production -diffusion equation for finite diffusion domains of various shapes part 2, Application to cases with Alpha ejection and non-homogeneous distribution of the source. *Chem. Geol.*, 186(3-4), 345-363.
- Mitchell, S.G., and Reiners, P.W., 2003. Influence of wildfires on apatite and zircon (U-Th)/He ages, *Geology*, 31, 1025-1028.
- Montigny, R., Edel, J.B., and Thuizat, R., 1981. Oligo-Miocene rotation of Sardinia: K-Ar ages and paleomagnetic data of Tertiary volcanics, *Earth Planet. Sci. Lett.*, 54, 261-271.
- Nardi, R., Puccinelli, A., and Verani, M., 1978. Carta geologica della Balagne "sedimentaria" (Corsica) alla scala 1:25.000 e note illustrative, *Boll. Soc. Geol. Ital.*, 97, 11-30.
- Naeser, C.W., 1967. The use of apatite and sphene for fission track age determination. *Bull. Geol. Soc. Am.*, 78, 1523-1526.
- Naeser, N.D., 1992. Miocene cooling in the southwestern Powder River Basin, Wyoming - Preliminary evidence from apatite fission-track analysis: *U.S. Geological Survey Bulletin* 1917-O, 17 pp.
- Naeser, C.W., and Fleischer, R.L., 1975. Age of the apatite at Cerro de Mercado, Mexico: A problem for fission-track annealing corrections. *Geophys. Res. Lett.* 2(2), 67-70.
- Ohnenstetter, M., Ohnenstetter, D., Vidal, Ph., Cornichet, J., Hermitte, D., and Mace, J., 1981. Crystallization and age of zircon from Corsican ophiolitic albitites: consequences for oceanic expansion in Jurassic times. *Earth Planet. Sci. Lett.*, 54, 397-408.
- Olive, V., Ellam, R.M., and Wilson, L., 2001. A protocol for the determination of the rare earth elements at picomole level in rocks by ICP-MS: Results on geological reference materials USGS PCC-1 and DTS-1. *Geostandards Newsletter-the Journal of Geostandards and Geoanalysis* 25(2-3), 219-228.
- Olivet, J.-L., 1996. La cinématique de la plaque Ibérique: *Bulletin des Centres de Recherches Exploration-Production Elf-Aquitaine*, 20, 131-195.

- Orszag-Sperber, F., 1978. Le Néogène de la Corse et ses relations avec la géodynamique de la Méditerranée occidentale, doctoral dissertation, Univ. Paris-Sud Centre d'Orsay, Paris, France.
- Orszag-Sperber, F., and Pilot, M.-D., 1976. Grands traits du Néogène de Corse. *Bull. Soc. Géol. France*, 18 (5), 1183-1187.
- O'Sullivan, P.B., and Parrish, R.R., 1995. The importance of apatite composition and single-grain ages when interpreting fission track data from plutonic rocks: a case study from the Coast Ranges, British Columbia. *Earth Planet. Sci. Lett.*, 132, 213-224.
- Pecerillo, A., 2003. Plio-Quaternary magmatism in Italy. *Episodes*, 26(3), 222-226.
- Persano, C., Stuart, F.M., Bishop, P., and Barfod, D., 2002. Apatite (U-Th)/He age constraints on the development of the Great Escarpment on the southeastern Australian passive margin. *Earth Planet. Sci. Lett.*, 200, 79-90.
- Persano, C., 2003. A combination of apatite fission track and (U-Th)/He thermochronometers to constrain the escarpment evolution in south eastern Australia: a case study of a high elevation passive margin. Doctoral dissertation, University of Glasgow, Scotland.
- Price, P.B., and Walker, R.M., 1962. Chemical etching of charged-particle tracks in solids. *J. Appl. Phys.*, 33, 3407-3412.
- Price, P.B., and Walker, R.M., 1963. Fossil tracks of charged particles in mica and the age of minerals. *J. Geophys. Res.*, 68, 4847-4862.
- Prone, A., and Rousset, C., 1981. Les quartz des rhyolites permiennees comme marqueurs de la rupture paléogéographique médio-crétacé dans le sud est de la France. *Bull. Soc. Géol. France*, 7, 487-492.
- Ravenhurst, C., Roden, M.K., Willet, S.D., and Miller, D.S., 1992. Dependence of fission track annealing on apatite crystal chemistry. 7th Int. Workshop Fission-Track Thermochronology, Philadelphia. 11 (Abstr.).
- Réhault, J.-P., Boillot, G., and Mauffret, A., 1984. The western Mediterranean basin geological evolution, *Mar. Geol.*, 55, 447-477.
- Ring, U., Brandon, M.T., Lister, G.S., and Willett, S., 1999. Exhumation processes.- In: *Exhumation Processes: Normal faulting, ductile flow and erosion*, (Ring, U., Brandon, M.T., Lister, G.S., and Willett, S. eds.)- Special Publications of the Geological Society London, 154, 1-28.
- Rollet, N., Déverchère, J., Beslier, M.O., Guennoc, P., Réhault, J.P., Sosson, M., and Truffert, C., 2002. Back arc extension, tectonic inheritance, and volcanism in the Ligurian Sea, western Mediterranean, *Tectonics*, 21(3), 1015. doi:10.1029/2001TC900027.
- Rondeau, A., 1961. *Recherches géomorphologiques en Corse (la part de la tectonique et de l'érosion différentielle dans le relief de l'île)*. Monographie, 586 pp.
- Rosenbaum, G., Regenauer-Lieb, K., and Weinberg, R., 2005. Continental extension: from core complexes to rigid block faulting, *Geology*, 33, 609-612.
- Rossi, P., Rouire, J., and Durand-Delga, M., 1980. Carte Géologique de la France, A 1/250 000, Corse, sheet 44/45, Notice explicative de la feuille, BRGM, Orléans, 80 pp.
- Rutherford, E., 1905. Present problems in radioactivity. *Popular Science*, May: 1-34.
- Seidl, G., 1974. Über die morphologischen Auswirkungen jünger Hebungen in den Schists Lustrés östlich Ponte Leccia (Korsika). *N. Jahrb. Geol. Paläont. Mh.* 8, 479-497.
- Sérrane, M., 1999. The Gulf of Lion continental margin (NW Mediterranean) revisited by IBS: an overview. In: *The Mediterranean basins: Tertiary extension within the Alpine Orogen*. (Durand, B., Jolivet, L., Horváth, F., and Sérrane, M., eds.), pp. 15-36. Geological Society Special Publications, vol. 156.
- Stampfli, G.M., Borel, G., Marchant, R., and Mosar, J., 2002. Western Alps geological constraints on western Tethyan reconstructions. *Journal of Virtual Explorer* 8, 77-106.

- Stockli, D., Farley, K., and Dumitri, T., 2000. Calibration of the (U-Th)/He thermochronometer on an exhumed fault block in the White Mountains, eastern California and western Nevada. *Geology*, 28(11), 983-986.
- Strutt, R., 1905. On the radio-active minerals. *Roy. Soc. London Proc.*, 76, 88-101.
- Strutt, R., 1908. The accumulation of helium in geologic time. *Roy. Soc. London Proc.*, 81(A), 272-277.
- Strutt, R., 1909. The leakage of helium from radioactive minerals. *Roy. Soc. London Proc.*, 82(A), 166-169.
- Stüwe K., 2002. *Geodynamics of the Lithosphere*. An Introduction. Berlin, Springer Verlag, 450pp.
- Stüwe, K., White, L., and Brown, R., 1994. The influence of eroding topography on steady-state isotherms. Application to fission track analysis. *Earth Planet. Sci. Lett.*, 124, 63-74.
- Stüwe, K., and Hintermüller, M., 2000. Topography and isotherms revisited: the influence of laterally migrating drainage divides. *Earth Planet. Sci. Lett.*, 184, 287-303.
- Summerfield, M.A., 1991. Sub-aerial denudation of passive margins: regional elevation versus local relief models. *Earth Planet. Sci. Lett.*, 102, 460-469.
- Summerfield, M.A., and Brown, R.W., 1998. Geomorphic factors in the interpretation of fission-track data. In: *Advances in Fission - Track Geochronology*, (Van den Haute, P., and De Corte, F., eds.), Kluwer Academic Publishers, pp. 269-284.
- Tagami, T., Galbraith, R. F., Yamada, R., and Laslett, G.M., 1998. Revised annealing kinetics of fission tracks in zircon and geological implications, In: *Advances in fission-track geochronology*. (Van den haute, P., and De Corte, F., eds.), Kluwer academic publishers, Dordrecht, The Netherlands, pp. 99-112.
- Turcotte, D. L., and Schubert, G., 2002. *Geodynamics*. 2nd edition, Cambridge UP, Cambridge, 456 pp.
- Vance, J., 1999. Zircon fission track evidence for a Jurassic (Tethyan) thermal event in the Western Alps. *Mem. Sci. Geol. Padova*, 51(2), 473-476.
- Van der Beek, P., 1995. *Tectonic evolution of continental rifts - inferences from numerical modelling and fission track thermochronology*. Doctoral dissertation, Vrije Universiteit Amsterdam, the Netherlands, 232 pp.
- Van der Voo, R., 1993. *Paleomagnetism of the Atlantic, Tethys and Iapetus Oceans*. Cambridge University Press, 411 pp.
- Vigliotti, L., and Kent, D.V., 1990. Paleomagnetic results of Tertiary sediments from Corsica: Evidence of post-Eocene rotation. *Physics of the Earth and Planetary Interiors*, 62, 97-108.
- Vigliotti, L., Alvarez, W., and McWilliams, M., 1990. No relative motion detected between Corsica and Sardinia. *Earth Planet. Sci. Lett.*, 98, 313-318.
- Vigliotti, L., and Langenheim, V.E., 1995. When did Sardinia stop rotating? New paleomagnetic results. *Terra Nova*, 7, 424-435.
- Wagner, G.A., 1968. Fission track dating of apatites. *Earth Planet. Sci. Lett.*, 4, 411-415.
- Wagner, G. A., 1979. Correction and interpretation of fission track ages. In: *Lectures in Isotope Geology* (Jäger, E., and Hunziker, J.C., eds.), Springer Verlag Berlin, 170-177.
- Wagner, G.A., and Reimer, G.M., 1972. Fission track tectonics: the tectonic interpretation of fission track apatite ages. *Earth Planet. Sci. Lett.*, 14, 263-268.
- Wagner, G., Reimer, G.M., and Jäger, E., 1977. Cooling ages derived by apatite fission-track, mica Rb-Sr and K-Ar dating: the uplift and cooling history of the Central Alps. *Mem. Instit. Geol. Miner. Univers. Padova*, 30, 1-27.
- Wagner, G.A., and Van den haute, P., 1992. *Fission-Track Dating*. Enke Verlag, Stuttgart, 285 pp.
- Warburton, J., 1986. The ophiolite-bearing Schistes Lustrés Nappe in Alpine Corsica: A model for the emplacement of ophiolites that have suffered HP/LT metamorphism. *Mem. Geol. Soc. Am.*, 164, 313-331.

- Warnock, A.C., Zeitler, P.K., Wolf, R.A., and Bergman, S.C., 1997. An evaluation of low-temperature apatite (U-Th)/He thermochronometry. *Geochim. Cosmochim. Acta*, 61(24), 5371-5377.
- Wendt, A.S., Vidal, O., and Chadderton, L.T., 2002. Experimental evidence for the pressure dependence of fission track annealing in apatite; intimidating implications? *Earth Planet. Sci. Lett.*, 201, 593-607.
- Wernicke, R.S., and Lippolt, H.J., 1992. Botryoidal hematite from the Schwarzwald (Germany): heterogeneous uranium distributions and their bearing on the helium dating method. *Earth Planet. Sci. Lett.*, 114, 287-300.
- Wernicke, R.S., and Lippolt, H.J., 1994. Dating of vien Specularite using internal (U+Th)<sup>4</sup>He isochrons. *Geophys. Res. Lett.*, 21, 345-347.
- Wolf, R.A., Farley, K.A., and Silver, L.T., 1996a. Helium diffusion and low-temperature thermochronometry of apatite. *Geochim. Cosmochim. Acta*, 60(21), 4231-4240.
- Wolf, R., Farley, K., and Silver, L., 1996b. Assessment of (U-Th)/He thermochronometry: the low-temperature history of the San Jacinto Mountains, California: *Geology*, 25, 65-68.
- Wolf, R.A., Farley, K.A., and Kass, D.M., 1998. Modeling of the temperature sensitivity of the apatite (U-Th)/He thermochronometer. *Chem. Geol.*, 148, 105-114.
- Yamada, R., Tagami, T., Nishimura, S., and Ito, H., 1995a. Annealing kinetics of fission tracks in zircon: an experimental study. *Chem. Geol.*, 119, 293-306.
- Yamada, R., T. Tagami, S. Nishimura, and H. Ito, 1995b, Annealing kinetics of fission tracks in zircon: an experimental study. *Chem. Geol.*, 122, 249-258.
- Young, E., Myers, A., Munson, E., and Conklin, N., 1969. Mineralogy and geochemistry of fluorapatite from Cerro de Mercado, Durango, Mexico. *U.S. Geol. Surv. Prof. Paper*, 650-D, D84-D93.
- Zarki-Jakni, B., Van der Beek, P., Poupeau, G., Sosson, M., Labrin, E., Rossi, P., and Ferrandini, J., 2004. Cenozoic denudation of Corsica in response to Ligurian and Tyrrhenian extension: results from apatite fission-track thermochronology. *Tectonics*, 23, TC1003.
- Zattin, M., Fellin, M.G., Cavazza, W., Picotti, V., Vance, J.A., and Zuffa, G.G., 2001. Exhumation of northern Corsica (France), *Geophys. Res. Abstr.*, 3, 531.
- Zeck, H.P., 1999. Alpine plate kinematics in the western Mediterranean; a westward-directed subduction regime followed by slab roll-back and slab detachment. In: *The Mediterranean basins; Tertiary extension within the Alpine Orogen*. (Durand, B., Jolivet, L., Horváth, F., and Séranne, M., eds.), Geological Society Special Publications, 156, 109-120.
- Zeitler, P.K., Herczig, A.L., McDougall, I., and Honda, M., 1987. U-Th-He dating of apatite: a potential thermochronometer. *Geochim. Cosmochim. Acta*, 51, 2865-2868.
- Ziegler, J.F., 1977. Helium: stopping powers and ranges in all elemental matter. New York, Pergamon, 367 pp.

## APPENDIX A

### MINERAL SEPARATION

In order to recover apatite and zircon concentrates from the rock samples, the following mineral separation procedure was used: rock samples of ~4-8 kg were crushed by rock splitter and jaw-crusher BB-51, sieved over 250  $\mu\text{m}$  mesh; the fraction  $<250 \mu\text{m}$  was passed through a Holman-Wilfley shaking table collecting the heaviest fraction (SW-1), which was dried in an oven at temperatures below 40°C. The obtained concentrate was further treated by heavy liquid separation (Na-polytungstate,  $\rho = 2.9 \text{ g.cm}^{-3}$ ) collecting heavy fraction, washed by distilled water and dried at room temperature. The next step was the magnetic separation with Frantz magnet (front angle 20°, side angle 10°), collecting non-magnetic, and 1.2-1.7 mA magnetic fraction since it has been recognized that some samples contain slightly "magnetic" apatites (owing probably to a contamination). In the samples containing apatites and zircons, another heavy liquid separation was applied (using diiodomethane,  $\rho = 3.3 \text{ g.cm}^{-3}$ ) in order to separate both minerals of interest.

## APPENDIX B

### FISSION TRACK METHODOLOGY

#### Preparation for FT dating and irradiation

Apatite concentrates were embedded in epoxy (1:5 mixture of Hardener HY 956 and Araldite D). Several samples were poor in apatite therefore the apatite grains were first handpicked (at least 40 grains) under binocular microscope and then embedded. Zircons were embedded in PFA Teflon™. Prepared mounts with grains were polished to  $4\pi$  geometry using 9  $\mu\text{m}$ , 3  $\mu\text{m}$  and 1  $\mu\text{m}$  oil based diamond suspension and Texmet™ polishing cloth. Spontaneous tracks in apatites were revealed by etching with 5.5 M  $\text{HNO}_3$  solution for 20 seconds at 21°C (Donelick et al., 1999). Zircons were etched in an eutectic mixture of KOH and NaOH at 215°C for 20 to 80 hours.

In this study the external detector method was used (Gleadow and Duddy, 1981): prior to irradiation, etched samples were covered by low-uranium muscovite sheets and packed together with the age standards and 2-3 dosimeter glasses (CN-5 for apatites and CN-2 for zircons) into a package. The dosimeter glasses (with known uranium content: CN-5 - 12 ppm U and CN-2 - 38 ppm U; Hurford and Green, 1983) served to monitor the neutron fluence. The package (prepared by so called "Dumitru's technique") is then enclosed to the plastic container and send to nuclear reactor in order to induce a fission of  $^{235}\text{U}$  ("induced fission tracks"). In this study, the samples were irradiated in TRIGA nuclear reactor at Oregon State University (Oregon, USA). Requested neutron flux for apatite samples was  $4.5 \times 10^{15} \text{ n/cm}^2$  and  $1.5 \times 10^{15} \text{ n/cm}^2$  for zircon samples. Dosimeter glasses CN-5, containing 12 ppm natural uranium, were used to determine neutron fluence. After irradiation, induced tracks in mica detectors were revealed by etching with 40% HF for 30 minutes at 21°C. Finally, the mounts with corresponding micas were attached side by side on a glass slide, ready for counting.

#### Age determination

Tracks were counted under a Zeiss Axioskop 2, equipped with a digitizing tablet, LED cursor, drawing tube attachment, and controlled by the computer program FT Stage version 3.11 developed by

Dumitru (1993). Tracks in apatites and mica-detectors were counted with 1250x magnification using dry objective, tracks in zircons were counted under same condition but using oil objective (Cargille oil type B,  $n = 1.515$ ). For counting only the grains with well polished surface were used, an orientation parallel to the crystallographic c-axis, homogenous uranium distribution, without fractures and without inclusions. Fission tracks were distinguished from other objects with respect to following criteria: the maximal length of tracks less than 20  $\mu\text{m}$ , conical or pipe-like shape, and random orientation of tracks. All grains of acceptable quality were counted regardless of presence or absence of fission tracks. Those grains were avoided, on which it was impossible to discriminate tracks from dislocations. To determine more accurate results, at least 21 grains from each sample were counted, in some cases more according to quality of mount. Lengths of horizontal confined tracks and  $D_{\text{pars}}$  in apatites were measured only on grains oriented parallel to the crystallographic c-axis, using the same device (Zeiss Axioskop 2). A minimum of 43 horizontal confined tracks was measured in the samples in order to obtain representative and statistically robust distribution.

Age determination of the samples was carried out with program TRACKKEY version 4.1 (Dunkl, 2002). For determination of the  $\zeta$  factor (zeta factor), the following age standards were measured: Fish Canyon Tuff apatite and zircon ( $27.8 \pm 0.7$  Ma; Colorado, USA), Durango apatite ( $31.4 \pm 0.5$  Ma; Cerro de Mercado, Mexico), and Tardree Rhyolite zircon ( $58.7 \pm 1.1$  Ma; Northern Ireland, UK; McDowell and Keizer, 1977; Hurford and Green, 1983; Green, 1985; Hurford and Hammerschmidt, 1985). The  $\zeta$  personal value was calculated as a weighted mean and standard error

**Table B-1** Calibration of zeta factor for apatite and zircon.

Age Standard	N	$N_s$	$N_i$	$\rho_d$	$N_d$	Zeta	$\pm 1\sigma$
Durango	25	697	1938	5.110	4911	339.38	16.65
Fisch Canyon	25	403	1357	5.110	4911	357.63	21.88
Fisch Canyon	25	353	1202	5.456	8081	340.51	21.83
Fisch Canyon	27	403	1370	5.257	5126	351.07	21.43
Durango	25	274	880	5.750	4936	339.98	24.62
Fisch Canyon	25	269	914	5.780	4936	307.15	22.44
Durango	25	466	1346	5.849	5647	311.05	17.92
Fisch Canyon	25	241	782	5.823	5647	311.82	24.00
Fisch Canyon	25	329	1056	5.714	5647	309.72	20.74
Fisch Canyon	40	517	1503	5.461	5193	297.66	16.61
<b>Calibration of <math>\zeta</math> value for apatite:</b>				<b>Wiegthed mean <math>\pm 1\sigma</math>:</b>		<b>324.93 <math>\pm</math> 6.46</b>	
Age Standard	N	$N_s$	$N_i$	$\rho_d$	$N_d$	Zeta	$\pm 1\sigma$
Tardree Rhyolite	19	562	407	5.820	5592	142.91	9.87
Fisch Canyon	30	1511	2039	5.820	5592	130.20	5.29
Fisch Canyon	25	1303	1864	7.228	6973	111.16	4.67
Fisch Canyon	26	1434	2531	7.973	6193	123.70	4.91
Fisch Canyon	24	1110	1786	6.842	2675	131.40	6.10
<b>Calibration of <math>\zeta</math>eta value for zircon:</b>				<b>Wiegthed mean <math>\pm 1\sigma</math>:</b>		<b>123.92 <math>\pm</math> 2.53</b>	

from measured values of  $\zeta$  and their grain-only standard errors (representing only uncertainties associated with the fission track method) and total standard errors (including also additional uncertainty associated with age of the age standard) by ZETAMEAN program of M. Brandon. The value of  $\zeta$  factor was  $324.93 \pm 6.46$  for apatite and  $123.92 \pm 2.53$  for zircon (Table A-1).

### **Thermal history modeling based on AFT data**

Thermal history was modeled by using the HeFTy Beta Release 1a modeling program (Ketcham et al., in press), which is dedicated for modeling of low-temperature thermochronometric systems, including apatite fission track, (U-Th)/He, and vitrinite reflectance. In principle, the program does two types of modeling – forward and inverse modeling. Forward modeling is the process of predicting a data (FT age, track length distribution, or He age) from a tT path defined by the user. The output data are then compared to data gained from a real sample. If modeled and measured results match, the modeled tT path may be representative for real thermal history of the sample. Inverse modeling is a process of reconstructing thermal histories based on input of measured data such as FT age, track length distribution, or He age. The program generates a large number (several thousands) of tT paths, which are tested with respect to input data. The fitting of the measured input data and modeled output data is statistically evaluated and characterized by value of the “Age GOF” (age goodness of fit). A “good” result corresponds to value 0.5 or higher, “the best” result corresponds to value 1 for both indicators. Results are presented in form of tT envelopes that contain all paths, passing statistical criteria and conforming to user-entered constraints, that best reproduces the measured data. It has to be kept in mind that even a perfectly fitting and statistically proved model of thermal history must not necessarily correspond to the real history of a sample. To avoid misinterpretation it is essential to incorporate all known geological data (e.g., vitrinite reflectance data, stratigraphic age of a sample, data obtained by other thermochronometers, etc.) into a model before the meaning of the measured ages and tT paths are evaluated. Second important point is that resolution of a thermochronometer is limited to the certain temperature range (AFT system to the range of PAZ - ~60 to 120°C; (U-Th)/He on apatite to the range of PRZ - ~40 to 75°C), therefore the parts of tT envelope defined for the zones out of this range are not necessarily representative for the real thermal evolution of a sample.

In this study, the following setting has been used: inverse modeling with Monte Carlo algorithm with minimum of 10 000 iterations; the end of the tT path was set to 13°C according to present-day mean surface temperature;

*AFT modeling:* input parameters: central FT age with 1 sigma error, track length distribution, Dpar values as kinetic parameter; multi-kinetic annealing model of Ketcham et al. (1999); initial track

length of 15.5  $\mu\text{m}$ . Known geological information (such as stratigraphic age, ZFT data) was converted into time-temperature constraints in form of boxes for the modeling.

*(U-Th)/He modeling:* input parameters: row (U-Th)/He age with 1 sigma error, radius of apatite crystal prism, prism radius; activation energy 32.9 kcal/mol; calibration after Farley (2000); other parameters - default.

## APPENDIX C

### DESCRIPTION OF HE EXTRACTION LINE

Helium Extraction Line at TU was constructed by Patterson Instruments Ltd.<sup>©</sup> in 2003 and it is a fifth "clone" of the system employed in Ken Farley's laboratory at CalTech. The system is composed of the following principal components (Fig. A-1): an in-vacuum extraction furnace for He extraction; an all-metal extraction line equipped with automatic and manual valves, and pumped by pumps; a precise volume aliquot system for spiking sample gas with <sup>3</sup>He for isotope dilution; a precise volume aliquot system for delivering a <sup>4</sup>He standard to monitor <sup>4</sup>He tank depletion; a gas purification system of getters; a quadrupole mass spectrometer for measuring <sup>3</sup>He/<sup>4</sup>He ratios. The extraction line components and valves are interfaced with a central computer and are fully automated using LabView<sup>©</sup> software.

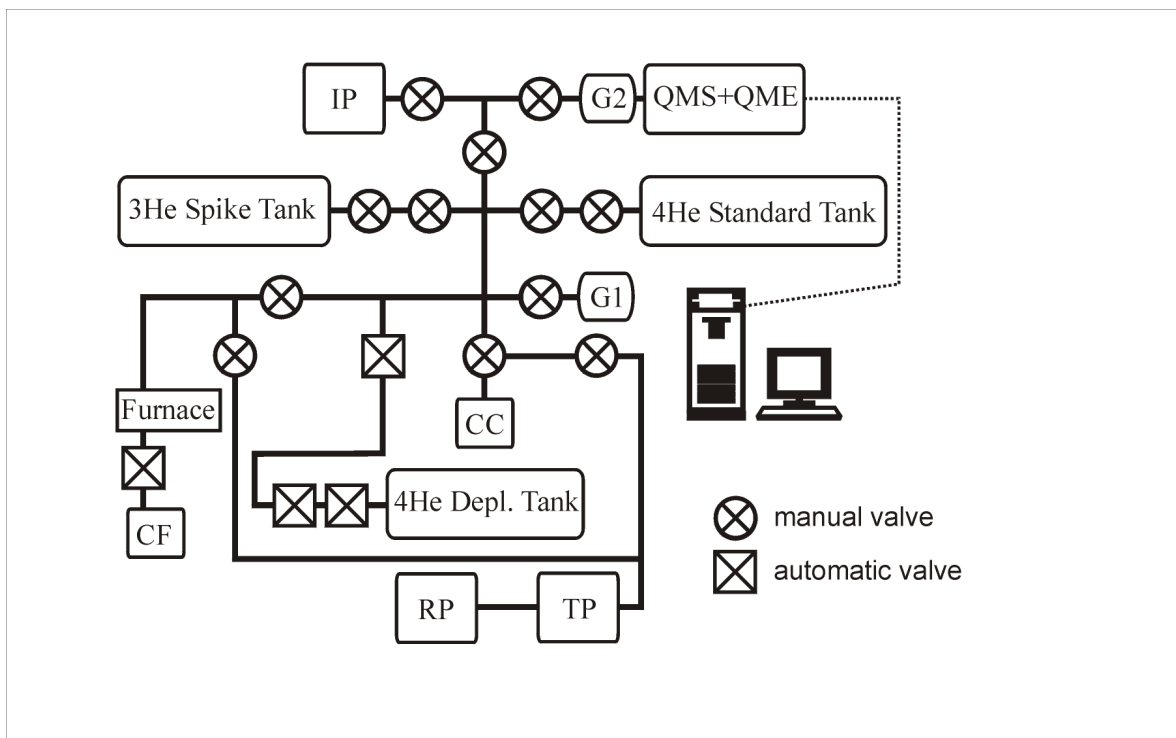


**Fig. C-1:** Schematic design of helium extraction line at TU (Patterson Instruments Ltd.<sup>©</sup>). IP - ion pump; QMS - quadrupole mass spectrometer; quadrupole electronics unit; G1, G2 - getters; CF - cold finger; TP - turbo-pump; RP - rough-pump; CC - cold cathode.

## Tubulation

The extraction line is constructed of stainless steel tubulation connected via VCR and Conflat flange fittings with Cu-gaskets, and “Quickfit” viton O-rings and Al clamps. The valves used are “B series” in-line automatic and manual valves manufactured by Nupro. Automatic valves are actuated by compressed air and controlled via the Labview 6.1 software; the manual valves are open and closed using a torque wrench.

## Pumping system

The pumping system can be divided into high vacuum and low vacuum. High vacuum is generated by the ion pump (Varian VacIon Plus 20) and the turbomolecular drag pump (Pfeiffer model TMU071P with a dedicated power supply and controller) units. Low vacuum is generated by the mechanical rough pump (Pfeiffer DuoLine 2.5A/AC rotary vane pump). Pressures in the line were monitored via three vacuum gauges - cold cathode gauge, Hi-Vac Pirani gauge, and Low-Vac Convector gauge. Typical operating pressures in high vacuum part were in the range of  $10^{-8}$  mbar.

## Getters

The term “getter” refers to any device that is designed to remove chemically active gases (such as  $H_2O$ , OH,  $N_2$ ,  $H_2$ , H, HD,  $SO_2$ ,  $O_2$ ,  $CO_2$ , CO, and the  $C_MH_N$  family such as  $^{12}C$ , CH,  $CH_2$ ,  $CH_3$ ,  $CH_4$ ,  $C_2H_6$ , etc.) from the system. The Tübingen system uses two SAES AP10N Mk3 getters, consisting of Zr-Al alloy (ST101) foil, and a metal finger, containing approximately 1 g of surface activated charcoal held at liquid nitrogen temperature to condense  $CO_2$ ,  $H_2O$ , Ar, Kr, Xe and the remaining active gases. One SEAS getter (Line Getter) is in the extraction system and is maintained at a temperature of about  $350^\circ C$ , the other one (Quad Getter) is mounted directly inside the quadrupole chamber close to the ionization source, and is kept at room temperature.

## Standard tanks, spike tank, and gas pipettes

The system includes three tanks with associated gas pipettes. The tanks serve two purposes – to deliver aliquots of an accurately known amount of  $^4He$  as the gas standard against which real samples (and blanks) are determined, and to deliver aliquots of the  $^3He$  spike used.

The original calibration was done on first principles from the Ideal Gas Law  $PV = nRT$  (P - pressure; V - volume; n - number of moles; R - universal gas constant =  $8.3145 J/mol K$ ; T -

temperature). Effectively a tank of precisely known internal volume (determined from filling with water using standard volumetric glassware) was used, combined with a high accuracy pressure gauge (a MKS brand capacitance manometer at the University of Syracuse NY was used to perform the original primary calibration) to calibrate the amount of gas delivered from a Tank and Pipette in the Syracuse University Noble Gas Isotope Research Laboratory (SUNGIRL). The Tübingen Primary  $^4\text{He}$  Gas Standard was then filled and cross-calibrated against the SUNGIRL Tank before being shipped.

### ***PRIMARY $^4\text{He}$ GAS STANDARD – DEPLETION TANK***

The primary  $^4\text{He}$  gas standard, or depletion tank (D-tank), is the primary standard for calibrating the system, and is used to monitor and calibrate the secondary  $^4\text{He}$  tank.

#### *Tank Details:*

Tank Volume:  $5\,800 \pm 10 \text{ cm}^3$

Pipette Volume:  $0.2037 \pm 0.0020 \text{ cm}^3$

### ***SECONDARY $^4\text{He}$ GAS STANDARD – THE Q-TANK***

The secondary  $^4\text{He}$  standard tank (or Q-tank) provides the isotopically pure  $^4\text{He}$  that is used as the daily working gas standard.

#### *Tank Details:*

Tank Volume:  $5\,800 \pm 10 \text{ cm}^3$

Pipette Volume:  $0.2287 \pm 0.0023 \text{ cm}^3$

Over time, the large number of aliquots taken from the Q-tank causes detectable depletion. This is corrected for using the depletion factor, and by periodically re-calibrating the Q-tank against the D-tank. Cross calibration between the two  $^4\text{He}$  tanks is made every after about 400 aliquots are taken from the secondary  $^4\text{He}$  standard tank.

### ***$^3\text{He}$ SPIKE TANK***

The Spike tank contains isotopically pure  $^3\text{He}$ . The exact amount of  $^3\text{He}$  delivered per aliquot is not (and need not be) precisely known – provided that the amount of  $^3\text{He}$  delivered is constant for standards and samples on a day-by-day basis.

## **Extraction furnace**

The in-vacuum extraction furnace is used to diffusively extract helium from apatite samples at ~950°C. It is a relatively simple single vacuum furnace using a resistively heated tungsten heater element coiled around an Al<sub>2</sub>O<sub>3</sub> ceramic crucible. Reusable stainless steel capsules with apatite crystals are placed in holes in a metal rod connected to a linear motion feedthrough. This sample holder is then placed in the arm of the “Xmas tree” on top of the furnace, and samples are sequentially dropped into the crucible by sliding them forward using the linear motion feedthrough. The furnace is driven by a power supply consisting of a Eurotherm 2408 temperature controller, a Eurotherm 125A phase-angle fired thyristor, and a secondary step-down transformer. Temperature within the crucible is monitored using a C-type thermocouple (W-Re alloy). The furnace chamber is cooled using a total of five 24VDC fans.

## **The <sup>4</sup>He mass-spectrometer**

<sup>4</sup>He analyses on Helium Extraction Line at TU were conducted using a quadrupole mass spectrometer (Pfeiffer Prisma QMS-200, Asslach, Germany) that is operated using Quadstar QS422 software. The mass spectrometer is equipped with a dual filament electron bombardment ionization source and both Faraday and Channeltron (or Secondary Electron Multiplier – SEM) ion detectors. At the time of this study, the following operating parameters were used: detector type: Channeltron (SEM); voltage of SEM – 1000V; emission current - 2 mA.



EBERHARD KARLS UNIVERSITÄT TÜBINGEN  
Zentrum für Geowissenschaften (IFG)  
Sigwartstr. 10  
72076 Tübingen  
<http://www.uni-tuebingen.de/geo/ifg/>